ROLE OF BUBBLE-BASED NANOSYSTEMS IN CHEMO-IMMUNOTHERAPY OF COLON CANCER

By

JOSHUA PAUL VANOSDOL

Bachelor of Science in Biology
Fairmont State University
Fairmont, West Virginia
2012

Submitted to the Faculty of the
Graduate College of the
Oklahoma State University
in partial fulfillment of
the requirements for
the Degree of
DOCTOR OF PHILOSOPHY
May, 2020

ROLE OF BUBBLE-BASED NANOSYSTEMS IN

CHEMO-IMMUNOTHERAPY OF COLON CANCER

Dissertation Approved:

Dr. Ashish Ranjan

Dissertation Adviser

Dr. Jerry Malayer

Dr. Myron Hinsdale

Dr. Carey Pope

Dr. Daqing Piao

Name: Joshua Paul VanOsdol

Date of Degree: MAY, 2020

Title of Study: ROLE OF BUBBLE-BASED NANOSYSTEMS IN CHEMO-IMMUNOTHERAPY OF COLON CANCER

Major Field: COMPARATIVE BIOMEDICAL SCIENCES

Abstract: Colorectal cancer is one of the most commonly diagnosed forms of cancer with over 4% of both men and women developing it sometime during their life. Currently, surgical excision of large tumor masses followed by chemotherapy is the preferred method of treatment. However, the large inoperable masses can be difficulty to resect with wide margins, and adjunctive chemotherapeutics do not penetrate uniformly in advanced stage tumors. Additionally, a drug's cytostatic or cytotoxic effect may not be sufficient to eliminate both the targeted tumor and developing metastases located far from the primary treated regions. To address these issues, we hypothesized that the use of High Intensity Focused Ultrasound (HIFU) in combination with a Doxorubicin (Dox) loaded Echogenic Low Temperature Sensitive Liposome (E-LTSL) would deliver sufficient drug to solid tumor masses and promote immunomodulatory effects against distant metastasis in a murine colon cancer model. To test this hypothesis we 1) developed an E-LTSL that allowed precisely controlled penetration of Dox into colon tumors under image guidance, 2) characterized the acoustic and therapeutic effects of E-LTSL nanobubbles with HIFU in an immunocompromised mice, and 3) determined the efficacy of HIFU+E-LTSL in an immunocompetent bilateral mouse colon model. The data generated from these aims indicated that HIFU+E-LTSL enhanced local drug delivery and penetration compared to traditional chemotherapeutic approaches. Interestingly, while the Dox permeation into tumor from vasculature was enhanced with HIFU+ELTSL compared to other treatments, it didn't translate into significantly improved efficacy in an immunocompromised mouse model with multiple treatments. However, in an immunocompetent mouse model, both local treatment and systemic effects were comparatively more effective with the combined treatment at reduced treatment frequencies. In conclusion, HIFU+E-LTSL increased the requisite Dox delivery to colorectal cancer and also augmented systemic anti-tumor immune response rates.

TABLE OF CONTENTS

LIST OF TABLES

Table Page

LIST OF FIGURES

Figure Page

CHAPTER I

REVIEW OF LITERATURE

Abstract

Conventional chemotherapeutic approaches result in variable outcomes in colon cancer patients for a number of reasons including the lack of homogenous drug penetration into solid tumors, inadequate drug extravasation, and presence of stromal cell mediated chemo-resistance. To overcome these barriers, nanomedicines are being currently developed to improve outcomes relative to conventional chemotherapy. This review focuses on established and novel approaches that enhance drug concentration in tumors as well as promote immunomodulation of host cells with the use of focused ultrasound and nanomedicines. Preclinical data suggest that the proposed combinatorial approach has the potential to drastically improve survival outcomes in patients. The measured success of combination therapies is linked not only to tumor control in the treated site, but also to prevention of tumor recurrence and progression of metastasis.

Introduction

According to Siegel et al. [1], colorectal cancer was the third most commonly diagnosed form of cancer in both men and women in the United States in 2019. The percentage of deaths attributed to colon cancer according to these projections rested at 9% (27,640 deaths) for men and 8% (23,380 deaths) for women [1]. Similarly, in 2018, nearly 1.1 million cases of colon cancer were diagnosed worldwide while 550,000 died from the disease [2]. Current treatment approaches for advanced stage colon cancer includes surgery plus adjunctive radiation, and chemotherapy. Additionally, immunotherapy is fast emerging as the 4^{th} modality for treatment in patients. Despite this, the response rates vary based on the tumor microenvironments, resulting in modest outcomes in patients. This literature review primarily focuses on ways to address these clinical limitations by leveraging the advances in High intensity focused ultrasound (HIFU) mediated nanomedicine therapy in conjunction with chemotherapy.

Principles of HIFU therapy

HIFU is minimally invasive, safe, and reliable [3]. Ultrasound and more specifically, HIFU has several characteristics that affect how it interacts with tissue. Ultrasound can be achieved with a transducer that emits sound at a frequency above the human audible range of 20 kHz. When used for imaging, increasing the frequency yields a higher spatial resolution, but at the cost of increasing attenuation, and thus, decreasing the potential imaging depth. HIFU, however, tends to utilize lower frequencies to ensure greater depth of penetration and focuses the sonic energy into a single spot. This focal point experiences mechanical and thermal effects sufficient to cause a noticeable biological

effect compared to an imaging ultrasound. HIFU can be aimed at an unlimited depth from the body surface, and its intensity in tissue can be modulated by modifying the treatment parameters. Since HIFU has the added benefit of heating deep-seated tissue, this property can be leveraged to enhance drug release locally from nanoparticles (e.g. in colon cancer) and immune effects from cancer cells in the local region. Towards this goal, in this dissertation, we focused on how HIFU heating and its mechanical effect impact anti-tumor outcomes. It may be noted that in addition to HIFU, a variety of other methodologies can also be utilized for tumor heating. For example, a water bath can heat a region of tissue locally with some accuracy, but it can still be challenging to generate precise heating without indiscriminately warming adjoining tissue. Likewise, invasive catheters for tumor heating required surgical procedures, that at times may be technically challenging. In contrast, HIFU heating maintains a steady, elevated temperature with precise spatial control in tissue [4-6]. Previous studies have shown that mild and ablative heating with HIFU improved chemotherapy delivery in vivo [5, 7], ex vivo [8], and in vitro [4, 5] compared to free drug or non-heated encapsulated drug studies. The proposed mechanism of drug delivery enhancement in interstitial spaces was via. by the modification of perfusion and interstitial fluid pressure [9].

As noted above, HIFU can expose tissues to a range of energy ranges, thereby generating moderate to high heating and bio-effects. For instance, mild hyperthermia (40–45°C) is fundamentally distinct from hyperthermia-based ablative technologies (> 55°C) that are intended to destroy tumor tissue by heating [10], and thus for various bio-effects, tissue temperatures must be delicately balanced and precisely controlled [11, 12]. The most commonly used method for performing absolute thermometry is based on temperature-

dependent chemical shift changes in proton resonance relative to that of a reference resonance under magnetic resonance imaging (MRI)[13]. However, the use of MRI is expensive, requires large dedicated facilities, and has technical limitations (e.g., interference by target tissue movement), and the agents that are required to create tumor imageability (e.g., gadolinium) may alter the chemical shift, thereby disrupting the fidelity of temperature measurement and drug delivery [14, 15]. Thus, developing novel liposomal nanoparticles that encapsulate temperature sensitive contrast agents that can be imaged with less-expensive ultrasound can be clinically relevant [16]. *Towards this goal, the objective of this project was to assess the role of perfluoropentane or PFP (~30 ^{o}C) in tumor imaging, and sonoporation. PFP can be injected in the form of liquid droplets dispersed in an aqueous medium that then are converted to echogenic bubbles upon warming to body temperature for ultrasound imaging* [17]. We hypothesized that this method of enhancement of the extravasation and penetration of systemically administered chemotherapeutics, and ability to provide thermometry control under US guidance can be highly significant for treatment of deep-seated colon tumors away from the body surface.

In addition to precise temperature elevations, HIFU can also induce cavitation effects with perfluorocarbon-based bubble agents for chemo-immune responses. When first looking at the innate immune response, prior research has shown that tumor cells exposed to mild hyperthermia for 2 h expressed shock proteins such as HSP72 which promoted natural killer (NK) cell proliferation and cytotoxic activity [18-20]. Hyperthermia also enhanced immune responses directly from immune cells. For example, natural killer cells directly heated for several hours at a temperature of 39.5ºC demonstrated higher NKG2D clustering, allowing superior lytic function [21]. Other leukocytes, when

directly heated such as dendritic cells [22, 23], macrophages [24, 25], and CD8+ T [26] have also shown the upregulation of immunogenic markers with HIFU. Similarly, ablative treatments with HIFU have shown to replace surgical approaches for unresectable tumors [27], providing the added benefit of flooding the local area with tumor antigen for immune cell recruitment [28]. While direct destruction of tumors with HIFU heating is interesting to some extent, the heating ranges drastically impact immune activations. For example, one study found that tumor cells killed with HIFU heating <55ºC had more dendritic cell (DC) maturation than cells destroyed by <80ºC temperature ranges[29]. Furthermore, Xing et al. showed that mice receiving HIFU treatment two days prior to surgical amputation demonstrate reduced metastasis [30]. Studies that have analyzed immunomodulatory effects of focused ultrasound can be found in Table 1.1. For therapeutic optimization, here we mainly focused on mild-hyperthermia ranges, and how they impact outcomes in colon cancers in combination with nanomedicines.

Physical and Bioeffects of Nanomedicines

Synthesized nanoparticles (NPs) based nanomedicines containing chemotherapeutic agents have been widely reported for increasing the circulatory half-life of the drugs, and reducing toxic side-effects. Here, we focus on liposomal NPs. Liposomes are made up of a phospholipid bilayer containing hydrophilic lumen, and can load therapeutics into the bilayer or the aqueous core[31]. Liposome NPs primarily rely on enhanced permeability and retention (EPR) for drug delivery to tumors [32-35]. In EPR, NPs passively accumulates in the tumor by utilizing its disorganized vasculatures [36, 37]. For instance, Doxil, the first FDA approved liposome, encapsulating doxorubicin or Dox (a commonly

used drug that treats a wide range of different malignancies) leveraged EPR, increasing the drug delivery by 10-20 fold compared to Dox alone in tumors [38-40]. This approach also minimized the off-target effects and limited cardio-toxic effects [38, 41-48]. While EPR is effective in early stage tumors, large inoperable tumor masses with avascular and necrotic tissues show sub-optimal responses to liposome NPs. These are also compounded by the low rates of perfusion and high interstitial fluid pressure [49]. So, liposome NP may be of little use in advanced tumors, resulting in modest outcomes [50-54]. Attempts to address this by increasing dose and frequency of administration often causes intense side effects [55]; all of which often results in tumor recurrence and metastasis. *Thus, a key critical barrier that this dissertation is aiming to address is to develop methodologies suitable for reliable drug (e.g. Dox) penetration into whole tumor.*

Towards this aim, we evaluated the role of HIFU heating with heat sensitive liposomal NP therapies, allowed for rapid delivery of chemotherapies to neoplastic sites compared to Dox, even in the absence of EPR effects [5, 56-58]. Low temperature sensitive liposomes (LTSLs) preferentially release their drug payload once they pass through a warm region (~40°C), and thus, it can dramatically improve drug delivery relative to conventional therapy [59]. In addition, innovations in nanoformulation compositions by incorporating gaseous contrast agents that rupture or burst under HIFU mediated sonic stress, can offer unique benefits to improve homogeneous tumor bioeffects [60, 61]. Further, the long-term efficacy following surgical removal of large, identifiable tumor masses via immune activation of tumor microenvironment can prevent recurrence and metastatic growth [62-65]. Thus, these led to our interest in the dual-mode therapy with HIFU and LTSLs especially in the context of activating the adaptive immune response in

patients [66-68]. Below we discuss the proposed chemo-immunotherapy mechanisms that can be activated with HIFU heating and LTSL-based nanoformulations.

Colon cancer biology, and the role for chemo-immunotherapy with HIFU and LTSLs

Despite known and proposed advances in drug delivery modalities, there are several known mechanisms by which cancer cells develop chemo-resistance. These include modifications of drug targets, drug inactivation, increases in drug efflux pumps, DNA damage repair, cell death inhibition, and cancer epithelial/mesenchymal transition, leading to a more aggressive cancer subtypes [69]. The two factors that are covered in this review are drug efflux pumps and cancer stem cells, which are of importance when considering treatments with Dox in colon cancer models. ATP-binding cassette (ABC) transporters proteins are often responsible for multidrug resistance in cancer, since they actively regulate intracellular concentrations of chemotherapeutics by actively pumping them out of the cell. P-glycoprotein, a well-known membrane protein, which is regulated by the Abcb1 gene, is normally used to help remove toxicants from the cell, but it can also aid chemotherapeutic resistance where it is overexpressed [70-73]. Other proteins regulated by Abcg2 and Abcc1 have been shown to function similarly [74-76]. In addition to efflux pumps, cancer cells expressing stem markers, such as Aldh1a1, Notch2, and Gata6 are more resistant to chemotherapeutics. The Aldh1a1 gene encodes for an aldehyde oxidizing enzyme, and has been correlated to poor survival in patients with colorectal cancer [77]. When overexpressed in cancer stem cells, it protects against reactive oxygen species often associated with chemotherapeutic cytotoxic effect, increasing the likelihood of tumor metastasis [78]. Other markers tend to be more cancer

specific. For example, Notch2 expression correlated to suppression of colorectal cancer [76]. In contrast, Gata6 overexpression can cause mixed results, with aggressive metastatic tumor growth in some cases [79, 80] and tumor suppression in others [81]. Thus, understanding the roles of these multidrug resistance genes can potentially help delineate the chemotherapeutic effects of various agents.

Cancer cells rapidly mutate to alter drug targets and influence therapeutic response [82]. Also, as tumors grow, they induce an immunosuppressive tumor microenvironment, augmenting metastatic and aggressive phenotypes, while also preventing the phagocytic clearance by the immune cells [83, 84]. For example, resistance to pharmacologic agents used in chemotherapy (e.g. gemcitabine, doxorubicin) in solid tumors has been linked to tumor-associated macrophages (TAMs)[85, 86]. TAMs induce upregulation of cytidine deaminase (CDA), the enzyme that metabolizes drugs like gemcitabine following its transport into the cell[87]. TAMS can enhance tumor proliferation by secreting high amounts of vascular epithelial growth factor, Il-10, or TGF-β [88, 89]. Shree et al. showed that TAMS were able to inhibit doxorubicin efficacy by limiting Taxol-induced tumor cell death via cathespin expression [90]. TAMs can be categorized into M1 (classical activated) and M2 (alternative activated pro-tumor) phenotype. In the case of immunosuppressive cancer, TAMs demonstrate an M2-like phenotype, thereby contributing to drug resistance and cancer stem cell like phenotype[91]. Importantly, the activation and recruitment of M1 macrophage has shown to enhance efficacy of chemotherapeutics by stroma depletion and drug resistance in pancreatic tumors[92]. Tumors also produce cytokines that induce the proliferation of CD4+ T regulatory cells, and this phenomenon can enhance malignancy [93, 94] Likewise, dendritic cells altered

by TME produce inadequate activation of cytotoxic cells [95]. *Based on this premise, we hypothesize that successful reactivation and reprogramming of an immune competent profile with nanomedicines and HIFU heating can improve chemosensitivity and allow development of dual-mode chemo-immunotherapy protocols for more effective outcomes in colon cancer*.

To achieve this goal, in this project we characterized the role of LTSLs that were loaded with PFP agents with HIFU heating. As described previously**,** liquid chemical agents can transition into a gaseous state upon specific ultrasonic activation. The gaseous component is often referred to as an ultrasound contrast agent (UCA) since it provides a stark echogenic signal during ultrasound imaging relative to the surrounding tissue. Examples of UCAs include octafluoropropane and perfluoropentane, and these have been incorporated into the liposome [8] by sonication [16], or are co-injected during treatment without direct integration into the liposome [60]. For instance, Suslick et al. used an ultrasonic horn to sonicate a solution to generate protein shelled microbubbles[96]. Freeze-drying is another method of microbubble synthesis in which a continuous aqueous phase with a stabilizer is used to disperse a liquid with the use of high-shear-flow emulsification [97].

In addition to serving as contrast agents, bubbles also increase the cavitation nuclei in the HIFU field when exposed to alternating high- and low-pressure acoustic waves. Stable or non-inertial cavitation occurs if the less intense HIFU pulses match the cavitation nuclei's resonant frequency and bubble oscillation. In contrast, inertial cavitation occurs when the pressure waves from HIFU cannot sustain a steady volumetric change of the cavitation nuclei and it collapse (and destruction) in a non-uniform fashion. The collapse forms a

microjet which can puncture holes in a cell membrane [98]. In general, the point at which stable or inertial cavitation occurs from ultrasonic contrast agents is heavily dependent on the frequency and peak pressure of HIFU [99]. For driving drug penetration in tumors, inertial cavitation is preferred since it is capable of causing sonoporation [100]. Cavitation based sonoporation also opens phospholipids bilayer of cells to assist a greater nuclear localization of encapsulated agents [101, 102]. In addition, bubble mediated sonoporation can improve the immunogenic gene expressions by gene delivery [103]. Liu et al. showed microbubble immunomodulation in CT26 tumors with HIFU. Mice that received both HIFU and microbubbles compared to HIFU only, demonstrated reduced tumor growth rates and an increased infiltration of CD8+ and CD4+ cells into the tumor [104]. Although promising, current bubble and HIFU mediated cavitation of tumors has limitations. Typically, microbubble-based agents have a short half-life, and are not good for local drug delivery applications. Approaches to address by co-loading microbubbles and drug into the liposome, or encapsulation of bubble agents into a polymer shell and then conjugates them to the liposomes showed to improve the systemic circulation and drug loading efficiency [105]. To further improve response rate, in this project, we developed LTSL-based echogenic nanobubbles (E-LTSLs). E-LTSLs are composed of a phospholipid bilayer, and co-encapsulate drug cargo and the ultrasound contrast agent (UCA) perfluoropentane (PFP) [16]. Specific lipid components include: 1,2-Dipalmitoylsn-glycero-3-phosphocholine (DPPC), 1,2-distearoyl-sn-glycero-3-phosphoethanolamine-N-[methoxy (Polyethylene glycol)2000] (DSPE-mPEG2000), and monostearoyl-2-hydroxy-sn-glycero-3-phosphocholine (MSPC). DSPE-mPEG helps the liposome evade the reticuloendothelial system since it lowers the accumulation of serum

protein on the lipid bilayer, which can increase the clearance rate of particle [106]. Similarly, monostearoyl-2-hydroxy-sn-glycero-3-phosphocholine (MSPC) solid to liquid transition (39.5-42ºC) allows rapid drug release. Thus, our lipid combination can allow the E-LTSLs to release Dox in heated tissue while simultaneously providing imageability when the PFP transitions to a gas state. Additionally, we proposed that our approach can induce bubble mediated sonoporation to enhance immune effects [107]. Thus, the novel integrated platform of ultrasound guided nanotechnology platform that incorporates multiple components with established advantages of mechanical and thermal effects can aid rapid translation for cancer therapy. We also posit that even if cavitation doesn't play a huge role in drug penetration, the amount of energy absorbed by the bubbles in presence of HIFU would aid rapid temperature increase and immunological effect, indirectly assisting the immunotherapeutic outcomes [108]. Furthermore, it would allow us to monitor local drug release, positioning them truly as a theranostic agent.

Several interesting image guided approaches have been described in literatures for monitoring local drug delivery and responses. For example 2D passive acoustic mapping of cavitation using Sonovue microbubbles with ultrasound activation was correlated with bioluminescence from liposomal release of luciferin and subsequent interaction with a luciferase expressing murine tumor cell line. [109]. A key limitation of cavitation imaging correlation is that stable and inertial cavitation does not occur until nearly 80% of echogenicity is lost [110]. Another common way to report the liposomal release is by using magnetic resonance imaging (MRI). MRI tracks LTSLs via the encapsulated [Gd(HPDO3A)(H2O)] contrast agent [6, 10]. In contrast to MRI, ultrasound imaging can provide the benefits of imaging and also aid drug and immune activations [111, 112].

Using a fluorescent drug or chemical in conjunction with the bubble based LTSL agents can allow image guided therapy during HIFU [108, 113]. Thus, the use of micro/nanoobubbles based LTSL can intimately connect drug release and bubble associated cavitation in tumors [60]. Ultrasound imaging makes them a very useful theranostic agent since bubble creation and visualization can help monitor drug release in real time as the liposomes become unstable with external trigger [109, 114].. When exposed to HIFU hyperthermia, PFP bubbles can exert additional stress on tumor cells to induce immunological activation. Table 1.2 shows a list of bubble-based therapies and imaging modalities pertaining to use in colorectal cancer models. Based on this, the proposed hypothesis and aims are described below.

Dissertation Hypothesis

HIFU induced Dox release and acoustic activation from echogenic low temperature sensitive liposomes (E-LTSL) will promote superior cytotoxicity and immune effects against murine colon cancer model.

Aim 1: Synthesis of E-LTSL, characterization & assessment of drug penetration in colon tumors

Hypothesis: Echogenic liposomes with HIFU hyperthermia (40–42°C) can acoustically modulate the tumor microenvironment to result in improved drug penetration relative to liposomes alone.

1. Synthesize and characterized long-circulating echogenic nanobubble encapsulated LTSLs (E-LTSLs) and NTSLs (E-NTSLs)

2. Evaluation of in vivo drug release following short duration (~20min each) HIFU treatments administered sequentially over an hour in a large volume of mouse xenograft colon tumor

3. Determination of the impact of the HIFU/nanobubble combination on intratumoral drug distribution.

Aim 2: Determine impact of E-LTSL nanobubbles in an immunocompromised murine colon carcinoma model

Hypothesis: Systemic E-LTSL and HIFU will improve survival in immunodeficient mice

1. Characterize extravasation of systemically administered Dox in solid tumor mass in presence of echogenic low temperature sensitive liposomes (E-LTSL) with high intensity focused ultrasound (HIFU)

2. Test E-LTSL efficacy in immunocompromised C26 colon carcinoma mouse model

3. Characterize tumor microenvironment changes linked to multidrug resistance.

Aim 3: Determine impact of E-LTSL nanobubbles on chemo-immunotherapy outcomes in murine colon carcinoma model

Hypothesis: E-LTSL/HIFU would inhibit tumor growth by reprogramming tumor microenvironment

1. Determine the tumor growth rate reduction in treated and untreated (abscopal) tumor with HIFU combined LTSL and E-LTSL

2. Analyze the immune profile in treated and untreated CT26 tumors

3. Determine immune tolerance mechanisms of HIFU activated LTSLs

Author (et al.)	Year	Summarized Findings
Chapelon [117]	1992	Rats with treated adenocarcinomas had reduced rates of metastasis
Hu [118]	2007	Mechanical and thermal HIFU both increased Dendritic cell accumulation in tumor draining lymph nodes but antitumor effects were superior for mechanical based HIFU,
Chida [119]	2009	HIFU treatment increased CD4+ and CD8+ T cell tumor infiltration
Deng [120]	2010	Tumor lysate generated from HIFU ablation was loaded into dendritic cells increased CTL activity against hepatocellular carcinoma
Huang [121]	2012	Surgical resection of tumor post HIFU inhibited tumor re-challenge
Xia [122]	2012	HIFU ablation of hepatocellular carcinoma increased tumor specific CTLs with increased levels of IFN-γ and TNF-α secretion.
Bandyopadhyay [123]	2016	Low intensity focused ultrasound in B16 tumors increased tumor antigen and when combined with ablative radiation therapy reduced primary tumor growth, recurrence, and metastasis rates.

Skalina [124]	2019	Low intensity focused ultrasound induced localization of HSP on cell surface 4T1 breast cancer and prostate adenocarcinoma, priming immune response prior to radiotherapy ablation of tumor.
Aydin [125]	2019	Non ablative HIFU in B16 and 4T1 cell lines induced increased calreticulin, increased proinflammatory cytokines, and decreased anti-inflammatory cytokines from tumors.
Cohen [126]	2020	Non-ablative pulsed HIFU promoted innate and adaptive immune response in B16 melanoma and 4T1 breast cancer tumors. Tumor growth rate was reduced 24 hours after the HIFU Treatment.

Table 1.1. List of HIFU tumor immunomodulation studies.

Author (et al.)	Year	Summarized Findings
Xu [127]	2010	Dual mode targeting and imaging demonstrated in LS174T human colon cancer cell line. Texas red labeled nanobubbles were fluorescently quantified and correlated to echogenic signal.
Lin [128]	2010	HIFU combined with microbubbles enhances lipid coated quantum dots concentration in CT26 colon carcinoma tumor of BALB/c mice
Lin [129]	2012	HIFU combined with Sonovue microbubbles enhances Dox concentration in CT26 colon carcinoma using liposomal Dox carrier.
Wu [130]	2013	Nanobubbles demonstrate high echogenicity and half-life relative to Definity microbubbles in colorectal adenocarcinoma (LS174T).
Zhang [131]	2014	Tumor angiogenesis was hindered with HIFU and endostain microbubbles.
Sta Maria [132]	2015	Using a mouse xenograft human colorectal adenocarcinoma model, low dose focused ultrasound with microbubbles increased NK cell accumulation at tumor 24h after treatment.

Perera [133]	2017	Fluorescence imaging and ultrasound imaging confirmed that lipid/surfactant stabilized perfluorpentane nanobubbles maintained echogenicity longer than microbubble formulation *in vivo.*
Bulner [134]	2019	Enhanced anti tumor effect observed with the use of anti PD-1 and HIFU stimulated microbubbles. Projected T-cell dependent mechanism not observed.

Table 1.2. List of bubble enhanced colon cancer therapy studies.

CHAPTER II

SEQUENTIAL HIFU HEATING AND NANOBUBBLE ENCAPSULATION PROVIDE EFFICIENT DRUG PENETRATION FROM STEALTH LIPOSOMES IN COLON CANCER

Abstract

Mild hyperthermia generated using high intensity focused ultrasound (HIFU) and microbubbles (MBs) can improve tumor drug delivery from non-thermosensitive liposomes (NTSLs) and low temperature sensitive liposomes (LTSLs). However, MB and HIFU are limited by the half-life of the contrast agent and challenges in accurate control of large volume tumor hyperthermia for longer duration (>30min.). The objectives of this study were to: 1) synthesize and characterize long-circulating echogenic nanobubble encapsulated LTSLs (E-LTSLs) and NTSLs (E-NTSLs), 2) evaluate in vivo drug release following short duration (~20 min each) HIFU treatments administered sequentially over an hour in a large volume of mouse xenograft colon tumor, and 3) determine the impact of the HIFU/nanobubble combination on intratumoral drug distribution. LTSLs and NTSLs containing doxorubicin (Dox) were co-loaded with a nanobubble contrast agent (perfluoropentane, PFP) using a one-step sonoporation method to create E-LTSLs and

E-NTSLs, which then were characterized for size, release in a physiological buffer, and ability to encapsulate PFP. For the HIFU group, mild hyperthermia (40-42°C) was completed within 90 min after liposome infusion administered sequentially in three regions of the tumor. Fluorescence microscopy and high performance liquid chromatography analysis were performed to determine the spatial distribution and concentration of Dox in the treated regions. PFP encapsulation within E-LTSLs and E-NTSLs did not impact size or caused premature drug release in physiological buffer. As time progressed, the delivery of Dox decreased in HIFU-treated tumors with E-LTSLs, but this phenomenon was absent in the LTSL, NTSL, and E-NTSL groups. Most importantly, PFP encapsulation improved Dox penetration in the tumor periphery and core and did not impact the distribution of Dox in non-tumor organs/tissues. Data from this study suggest that short duration and sequential HIFU treatment could have significant benefits and that its action can be potentiated by nanobubble agents to result in improved drug penetration.

Introduction

To improve cancer chemotherapy delivery and survival outcomes, particularly in difficult cancers (e.g. ovarian, pancreas, primary liver tumor etc.), a key current direction is use of nanomedicine such as liposomes. These range in type from long-circulating non-thermosensitive liposomes (NTSL; e.g. Doxil, Onivyde, etc.) and low temperature sensitive liposomes (LTSL) that release drug above 40 °C (e.g. Thermodox) [10, 56, 133-135]. These liposomes are also being combined with high intensity focused ultrasound (HIFU) and microbubbles (MBs) to leverage precisely selected and dynamic modulation of biological, physiological, and mass transport properties of the tumor

microenvironment [59, 136-139]. These are promising advancements, but they are associated with several limitations. For example, MBs have short half-lives (within a few minutes) and limited drug payload capacity [140], and additional innovations are needed in formulation approaches to improve their use for image guided drug delivery (IGDD) [141]. Administering mild hyperthermia (40–45 °C) with HIFU to the entire volume of a deep seated tumor for long duration (~ 30 min–1 h) is associated with technical challenges related to spatiotemporal control, thereby reducing its feasibility for clinical use [142]. Thus, developing new approaches for administration of HIFU treatment for desired drug release from liposomes in tumors is needed.

Theoretically, liposomes offer the key advantage of ferrying both imaging and therapeutic agents that can potentially be utilized to measure/monitor the temporal and spatial patterns of solid tumor IGDD. However, such capability is limited by multiple factors, including target tissue movement, low spatial resolution (in positron emission tomography (PET), off-target radiation exposure (in PET or computed tomography (CT)), and inability to accurately define regions of interest (ROIs) at certain tissue depths (in fluorescence and luminescence modalities). Unlike these IGDD modalities, US imaging is safe, portable, widely-accessible and provides unlimited field of view at large distances from the body surface for routine clinical use. In prior research, the encapsulation of a perfluoropentane (PFP)-based nanobubble contrast agent enabled it to stay in liquid form in the liposome core because of Laplace pressure, thereby allowing PFP to attain gas bubble state and echogenicity slowly at body temperature [143]. This phenomenon resulted in longer circulatory life and stable ultrasound imageability [144]. A variety of methodologies have been reported for PFP encapsulation in liposomes. Recently, we

adapted the PFP emulsification encapsulation technology reported previously by Ibsen et al. and others [145-147] to synthesize nanobubble encapsulated echogenic LTSLs (E-LTSLs) and E-NTSLs. Our central hypothesis is that interaction of long circulating echogenic liposomes with HIFU hyperthermia (~ 40–42 °C) can acoustically modulate the tumor microenvironment to result in improved drug penetration relative to liposomes alone. The motivation to this idea stems from our previous studies where increased liposomal drug penetration by reducing interstitial fluid pressure [59, 148] and improving tumor perfusion was noted [149, 150]. We believe that by incorporating PFP in liposomes and its combination with short bursts of HIFU treatment, the drug release and liposome transport in tumor blood vessels within the first hour of injection can be further improved drastically, followed by transport of doxorubicin across the endothelial barrier and cellular uptake in tumor by bubble mediated sonoporation [149, 150].

The current approach in liposome mediated drug delivery is to apply HIFU homogeneously in a small volume of target region for ~ 30–60 min. This is promising, but for effective therapeutic outcome and realize the full potential of liposome and HIFU combination in clinic, a large volume of tumor must be treated within the first hour of injection. In this regard, we hypothesized that in contrast to focal heating of small volumes for long duration, zonal heating of a tumor covering the entire volume for shorter durations upon echogenic liposome injection can be an elegant way to increase extravasation of the released drug from NTSLs or LTSLs (see schematic illustration), however this has not heretofore been adapted to cancer drug delivery. The objective of this study was to apply E-LTSLs and E-NTSLs in a mouse model and determine their impact on drug delivery following zonal hyperthermia of a large volume of colon tumor.

Additionally, the influence of tumor transit time of LTSLs/NTSLs and the synergistic benefits of thermally induced drug release as opposed to ultrasound induced inertial cavitation for modulation of the tumor microenvironment and extracellular matrix for tumor drug penetration was assessed.

Materials & Methods

Materials

PFP (99%, Exfluor Research Corporation, Round Rock, TX, USA) was used as the US contrast agent. Monostearoyl-2-hydroxy-sn-glycero-3-phosphocholine (MSPC), 1,2-dipalmitoylsn-glycero-3-phosphocholine (DPPC), and 1,2-distearoyl-sn-glycero-3-phosphoethanolamine-N-[methoxy (Polyethylene glycol)2000] (DSPE-mPEG2000) were obtained from Corden Pharma Corporation (Boulder, CO, USA). 1,2-Dihexadecanoyl-sn-Glycero-3-Phosphoethanolamine, Triethylammonium Salt (Lissamine™ Rhodamine B) was obtained from Thermo Fisher Scientific Inc., and PKH67 Green Fluorescent Cell Linker was obtained from Sigma Aldrich (Milwaukee WI, USA). Dox was obtained from LC Laboratory (Woburn, MA, USA). Acetonitrile (high performance liquid chromatography (HPLC) grade) was obtained from Pharmco-AAPER (Brookfield, CT, USA). Ethylene glycol (99%, spectrophotometric grade), phenylboronic acid (98%), and 2,2-dimethoxypropane (98%) were purchased from Alpha Aesar (Ward Hill, MA, USA). The PD-10 column was obtained from GE Healthcare Life Sciences, (Buckinghamshire, United Kingdom, UK). C26 colon cancer cells were kindly provided by the National Cancer Institute.

Synthesis of E-LTSLs and E-NTSLs

LTSLs (lipid composition: DPPC, MSPC, and DSPE-mPEG2000 molar ratio of 85.3:9.7:5.0) and NTSLs (DPPC, cholesterol, and DSPE-mPEG2000 in the molar ratio of 58.1:36.8:5.07) were prepared by hydration of a lipid film followed by the extrusion method as described previously [16, 151, 152]. Briefly, lipid mixtures were dissolved in chloroform. The solvent was evaporated and the resulting lipid film was hydrated in citrate buffer (pH 4.0) mixed with 1,3-propanediol (1, 3-PD) (0.65 M, for PFP emulsification) at 55 °C for 30 min and extruded five times through double stacked 200 nm polycarbonate filters to yield a final lipid concentration of 50 mg lipid/mL (80.8 mM for LTSLs and 70.3 mM NTSLs). A PD-10 size-exclusion column equilibrated with 5–10 column volumes of 1 × phosphate buffered saline (PBS) was used to remove free 1,3-PD from the outside of the liposomes.

Encapsulation of Dox into the LTSLs and NTSLs was carried out using the pH-gradient loading protocol described by Mayer et al.. [150]. In general, the outside of the E-LTSLs was adjusted (by column) to about pH 7.4 using PBS, whereas the inside remained acidic at pH 4. Dox was loaded at 2 mg/100 mg lipid concentration at 37 °C for 1 h. PFP-loaded E-LTSLs and E-NTSLs were prepared using a one-step sonoporation method. Briefly, 2 mL of the liposomal formulations were incubated under continuous sonication (~ 20 kHz) in 3 mL vials along with PFP (boiling point 30 °C; 20 μL/100 mg lipid) for 1–2 min. PFP and LTSLs were kept cold prior to being combined, and the sonication bath was kept at 4 °C to minimize PFP vaporization. This method was repeated at least in triplicate (n = 3) for evaluation. Free Dox and PFP were removed using a PD-10 column. For all in vitro characterizations, LTSLs were used as a positive control. LTSL synthesis was carried out using our previously published procedure [152].

Confirmation of PFP encapsulation in liposomes E-LTSLs using a fluorescence technique

To confirm PFP loading in LTSLs, a fluorescent methodology was developed. Briefly, a thin film of LTSLs (lipid composition: DPPC, MSPC, DSPE-mPEG2000, and Lissamine™ Rhodamine B at a molar ratio of 84.3:9.7:5:1) was prepared as described in Section 2.2 and hydrated with 1 mL of water for 15–30 min at 55 °C. Next, 9 μL of PFP and 1 μL of PKH67 were transferred in a 0.5 mL tube and sonicated for 5 min at 4 °C, and 5 μL of PKH-67 labeled PFP then were sonicated with 1 mL of LTSLs and directly imaged on a mattek well plate under an Olympus IX81 confocal microscope using a 2 ms exposure time with the Tetramethylrhodamine (TRITC, ex/em of 545/600 filter) and a 100 ms exposure time with the green fluorescent protein (GFP, ex/em of 480/530) filter at 60 × APO.

To measure PFP stability as a function of temperature (25–42 °C), E-LTSLs (50 mg lipid/mL) were diluted 300 fold in PBS, and 3 mL of sample were placed in a quartz cuvette equipped with a stopper and magnetic stirrer. Fluorescence of the released PKH67 labeled PFP was recorded at an excitation wavelength of 490 nm and fluorescence emission was measured at 502 nm using a Cary Eclipse Fluorescence Spectrometer (Agilent Technologies, Santa Clara, CA, USA) equipped with an inbuilt temperature control system. The temperature was set to steadily increase from 25.5 to 42.5 °C. A fluorescent reading was recorded at every 0.5 °C increment. 10 × triton was used to lyse the E-LTSLs after the temperature increase to allow complete release of PFP. Empty LTSL signal was used as a blank.

Characterization of E-LTSLs and E-NTSLs

E-LTSLs and E-NTSLs were characterized for size (z-average) using dynamic light scattering (DLS) with a 90 plus PALS Nanobrook device (Brookhaven Instruments, Holtsville, NY, USA). Briefly, 10–20 μL of E-LTSLs or E-NTSLs were added to 2 mL of PBS in a cuvette, and DLS measurements were recorded at room temperature. For each liposomal formulation an average of five measurements were taken, and the mean size and standard deviation were calculated for the E-LTSL and E-NTSL samples. Zeta potentials were measured using water rather than PBS with the same equipment and lipids.

Dox release from E-LTSLs and E-NTSLs

Stability was assessed by measuring release of encapsulated Dox from E-LTSLs and E-NTSLs as a function of temperature (25–42 °C) in PBS. E-LTSLs (50 mg lipid/mL) and E-NTSLs (50 mg lipid/mL) were diluted 300 fold in PBS, and 3 mL of sample were placed in a quartz cuvette equipped with a stopper and magnetic stirrer. Fluorescence of the released Dox was recorded at an excitation wavelength of 480 nm and fluorescence emission was measured at 590 nm using a Cary Eclipse Fluorescence Spectrometer (Agilent Technologies, Santa Clara, CA, USA) equipped with an inbuilt temperature control system. The temperature was set to steadily increase from 25.5 to 42.5 °C. A fluorescent reading was recorded at every 0.5 °C increment.

Drug release based on fluorescence quantification as a function of change in temperature was determined using the following equation:

$$\% \text{ Dox release} = [(It - Io)/(Im - Io)] \times 100$$

where Io represents the initial fluorescence intensity of E-LTSLs and E-NTSLs in suspension at 25 °C, It is the intensity of the same sample at a predetermined temperature, and Im represents is the fluorescence intensity of completely released Dox from E-LTSLs at 45 °C or from E-NTSLs post-lysis of the liposomes with 10 × triton.

In vivo drug delivery study

Study design

Athymic nude mice bearing C26 mouse adenocarcinoma cell tumors were divided into nine treatment groups designed using a combination of four different liposome formulations with or without HIFU: NTSLs ± HIFU, E-NTSLs ± HIFU, LTSLs ± HIFU, E-LTSLs ± HIFU, and free Dox only. In all groups (n = 5–6 mice), 5 mg Dox/kg body weight were administered intravenously.

Establishment of mouse model of colon cancer

All animal-related procedures were approved and carried out under the regulations and guidelines of the Oklahoma State University Animal Care and Use Committee. C26 cells were grown as a monolayer to 80–90% confluence in RPMI supplemented with 10% v/v fetal bovine serum (FBS) and 1% v/v streptomycin/penicillin. Confluent cells were harvested, washed, and diluted with sterile cold PBS to generate 0.5 × 105 cells/50 μL. Next, 50 μL of cell inoculum was injected per mouse in the thigh region of the mouse hind leg using a 25-gauge needle (BD, Franklin Lakes, NJ, USA). Mice were monitored and tumor growth was measured by serial caliper measurements (General Tools Fraction + ™, New York, NY, USA). Tumor volumes were calculated using the formula (length × width2)/2, where length is the largest dimension and width is the smallest dimension

perpendicular to length. Tumors were allowed to grow to a volume of 300–400 mm3 prior to initiating studies, and treated at 5 mg Dox/kg Body weight IV.

Segmental hyperthermia generation in mouse tumors

An integrated ultrasound-HIFU alpinion system was used for tumor identification, sonication, and treatment characterization. The HIFU transducer has 1.0 MHz central frequency, 45 mm radius, and 64 mm aperture diameter with a central opening 40 mm in diameter. For HIFU treatments, each tumor was divided into two halves (top and bottom). The top half was further divided into three fragments along the y-axis: F1, F2, and F3, where F1 was on top, F2 in the middle, and F3 on the bottom (Fig. 2.2a). A 3 × 3 raster pattern of focal points (A, B, C) along the x axis was used to generate a mild-hyperthermia gradient of 40–42 °C for ~ 20 min in each fragment (Fig. 2.2b). Each focal point (~ 5.23 mm3) with dimensions of 1x1x10mm in x, y and z, axis, respectively was heated sequentially for 7 min. Thus, this methodology covered ~ 25mm3 of each fragment for a 20 min hyperthermia session (Fig. 2.2b). Since the transducer footprint (10 mm) was aligned along the z axis, adjacent muscle and bone tissue were also heated during sequential heating.

HIFU treatment set-up and methodology

Mice were anesthetized with 2–5% isoflurane and restrained in custom built mouse holders attached to a 3D positioning stage. The tumor bearing flank region was dipped in degassed water maintained at 37 °C for coupling with the HIFU transducer. Using real time ultrasound guidance, the tumors were positioned so that the target was in the center of the focal zone of the transducer. Prior to actual drug delivery studies, we calibrated the

instrument to a temperature of 42 °C in tumor bearing mice by optimizing the HIFU parameters (duty cycle, pulse repetitive frequency, total acoustic power, and time) as described previously [5, 153]. Furthermore, a temperature gradient was established by inserting a thermocouple inside of the mouse tumor and taking readings at and up to 2 mm away from the focus. This was done to ascertain the effective diameter over which sufficient heating for Dox release could be achieved (Fig. 2.2b). Tumors were allowed to equilibrate for 3 min before commencing the treatment. For hyperthermia treatment, the center of the tumor was aligned with the HIFU focus at a fixed focal depth for efficient coverage, and VIFU-2000 software was used to define the target boundary and slice distance in X, Y, and Z directions for automatic rastering of the transducer. HIFU treatment parameters used were as follows: HIFU treatment parameters used were as follows: 5 Hz frequency, 50% duty cycle, 10 W acoustic power, and a peak positive/negative pressure of 6.15/− 4.41 MPa to achieve a mean target temperature of 40–42.5 °C at the focus.

Post HIFU treatment tissue harvesting procedures

Upon completion of treatment, mice were euthanized. To clear the vasculature of drug/liposomes, transcardiac perfusion was performed immediately by opening the chest cavity and intracardially injecting 10 mL of PBS. Tumor and tissue samples from liver, spleen, lung, heart, kidney, skin, and muscle both adjacent and contralateral to the heated tumor were excised, weighed, snap-frozen over liquid nitrogen, and stored at − 80 °C until Dox analysis.

Quantification of Dox by HPLC

Tissue homogenization and sample preparation for HPLC were carried out using previously published methods [16, 59]. Briefly, samples were homogenized, and Dox was extracted and quantified with HPLC using daunorubicin as the internal standard. The HPLC detection system consisted of fluorescence detectors, and detection was performed at ex/em of 498/593 nm. Data were acquired using Shimadzu LC solution software. Concentrations of the analyte in tissues were determined using peak-area ratios of the sample analyte to the internal standard from the calibration curve.

Histology

A single whole tumor tissue sample from each HIFU group as well as the free drug group was selected prior to homogenization to be saved for histology. Histological analysis of NTSL and LTSL alone treated tumors were not performed since they do not demonstrate Dox penetration in the absence of HIFU. To analyze Dox distribution, 8 μm sections of frozen tumors were prepared, and two serial sections were mounted per slide. Fluorescently-labeled tissues were mounted with mounting medium containing DAPI (Vector Laboratories) to visualize cell nuclei at an exposure time of 10 ms (ex/em of 365/440), and Dox was imaged at an exposure 100 ms (ex/em of 480/590). Image acquisition and display parameters were constant for different treatments to allow for qualitative comparison. Whole-section digital histological scans were acquired using a 10 × objective on an Olympus ZDC2 IX81 fluorescence microscope equipped with a color CCD camera, cooled monochrome CCD camera, motorized scanning stage, and Metamorph mosaic stitching software. Cell density, and cavitation were assessed in hematoxylin- and eosin- (H&E) stained sections using an Aperio ScanScope at 20 ×.

Statistical analysis

Treatment groups were compared for differences in mean tumor Dox concentration using analysis of variance (ANOVA) followed by Tukey's multiple comparison post-hoc test. All analyses were performed using GraphPad Prism 5.0 (GraphPad Software Inc.). All p-values were two-sided, and $p < 0.05$ was taken to indicate statistical significance. Values were reported as mean ± standard error of the mean (SEM).

Results

Fluorescence analysis of PFP encapsulation in liposomes

Confocal microscopy confirmed the presence of the PKH-labeled PFP emulsion within the liposome aqueous core at 25 °C (Fig. 2.3a-c). Its presence was indicated by distinct yellow-to-orange spots formed by co-localization of red LTSLs with green PFP following sonication. PFP remained stable inside the E-LTSL from 25 to 43 °C, and a more intense signal indicative of release was noticed following triton (Fig. 2.3d).

Characterization of E-LTSLs and E-NTSLs

Active loading of Dox by transmembrane pH gradient yielded an encapsulation efficiency of ~ 95% and ~ 65% for E-LTSLs and E-NTSLs, respectively. Following PFP loading by one-step sonoporation, E-LTSLs and E-NTSLs retained about 70–80% of the encapsulated drug. Table 2.1 shows the hydrodynamic diameter, polydispersity index, and zeta potential values of E-LTSLs and E-NTSLs at room temperature (25 °C), and these were fairly similar among various groups following PFP loading.

Dox release from E-LTSLs and E-NTSLs in physiological buffer

Percent Dox release from E-LTSL and LTSL alike in PBS by its fluorescence dequenching was minimal (< 5%) at 25–39 °C (Fig. 2.4); was followed by a more gradual release at 40 °C (~ 20%), and was rapid and complete (> 95%) near the temperature giving maximum release rate (~ 41–42 °C). In 10% FBS, Dox release from E-LTSL and LTSL was ~ 20% at 37 °C, and ~ 90% at 40 °C. Greater than 95% release was attained at 41–42 °C. In contrast, release from NTSL and E-NTSL was alike in serum/PBS, and was < 5% at all the temperatures tested (Fig. 2.4).

Biodistribution of Dox

Whole tumor

Tumor Dox concentrations were 1.2 ± 0.2, 1.6 ± 0.1, 0.9 ± 0.1, 2.8 ± 0.7, 1.6 ± 0.1, 2.1 ± 0.3, 5.2 ± 0.5, and 3.8 ± 0.1 μg Dox/g tissue for free Dox, NTSLs, LTSLs, E-LTSLs, E-NTSLs, E-NTSLs + HIFU, E-LTSLs + HIFU, and LTSLs + HIFU, respectively. Drug delivery to both heated LTSL and E-LTSL treated tumors exceeded free Dox delivery by ~ 4- and ~ 5-fold, respectively, and was significantly higher than all other treatment groups. Compared to the LTSLs + HIFU treatment, heated tumors treated with E-LTSLs achieved ~ 1.5-fold greater drug delivery. In addition, the unheated E-LTSLs had twice the Dox concentration compared to LTSL (Fig. 2.5 and Table 2.2).

Tumor fragments

Dox delivery in the E-LTSLs + HIFU treated tumor resulted in a general trend of decreasing concentration starting from the F1 fragment to the bottom (2.6 and Table 2.3). E-LTSL - HIFU tumor fragment doxorubicin concentrations were 6.4 ± 1.3, 5.4 ± 0.5, 4.7 ± 0.9 and 2.8 ± 0.4 for F1, F2, F3, and bottom respectively. In contrast, F1, F2, and F3

demonstrated similar drug delivery for LTSLs, NTSLs, and or E-NTSLs in all heated and unheated fragments.

Organ biodistribution

Treatment with NTSLs and E-NTSLs alone resulted in significantly higher Dox concentrations in spleen than the other groups. Adding HIFU to LTSL and E-LTSL treatment resulted in significantly greater Dox concentrations in heated muscle compared to the Dox group. Dox levels in, the heart, the kidney, and liver were comparable between various groups (Fig. 2.7, Table 2.2).

Ratio of Dox in heated tumor adjoining muscle and unheated contralateral muscle

Because HIFU treatment also heated the muscles adjoining the tumor, the Dox concentration was significantly greater relative to contralateral unheated muscle by 4- to 5-fold for E-LTSL and LTSL (Table 2.2). Additionally, E-LTSLs achieved ~ 1.2-fold greater drug uptake compared to LTSLs alone in the heated muscle relative to contralateral unheated muscle (Fig. 2.8). Drug delivery attained by NTSL and E-NTSL were similar in heated muscle compared to the unheated contralateral muscles with slightly greater uptake of Dox for NTSLs.

Histological examination of whole tumors

H&E images did not reveal any cavitation-like effect following HIFU and E-LTSL treatment. Moderate to high Dox delivery along the periphery of the tumor was evident in all HIFU treated tumors. In the E-LTSL and E-NTSL treated tumors and to a lesser extent the LTSL treated tumors, drug penetration into the tumor core was more evident (Fig.

2.9). The LTSL treatment resulted in some brighter areas along the periphery to the core on the bottom and top of tumor, whereas both the E-NTSL and E-LTSL groups had a much more uniform distribution of Dox throughout the whole tumor. Unlike HPLC data, the fluorescence images for E-LTSLs + HIFU treatment did not demonstrate an apparent drug gradient decrease from top to bottom of the tumor.

Discussion

Improving the ability to target liposomes and release drugs in real time at sufficient levels with enhanced penetration in a solid tumor is an important clinical need. The objective of this study was to understand the mechanisms of focal drug delivery from liposomes and HIFU in a mouse model and ways we can optimize this technology for clinical use.

Previously, MBs encapsulated in a solid lipid or polymeric shell have been utilized for controlled drug delivery in tumors [154, 155]. Such treatments are limited by the short half-life of MBs, which is caused by quick destruction by the reticulo-endothelial system due to their large size, and instability upon systemic administration. In contrast to MBs, nanosized echogenic liposomes encapsulating PFP theoretically should have increased stability and half-life [156]. To confirm that bubble encapsulation inside E-LTSLs is indeed possible, we loaded optically labeled PFP into LTSLs. Confocal microscopy clearly showed that the process of PFP emulsification achieved effective encapsulation in liposomes, rather simply forming an admixture with the lipids (Fig. 2.3.). To rule out alteration in liposome integrity and to investigate the role of PFP permeability through the liposomal membrane, the thermal stability of E-LTSL and E-NTSLs was explored in vitro (Fig. 2.4). Our data suggest that PFP encapsulation has no impact on Dox release in

physiological buffer. Additional investigations in mouse colon tumors indicated that both LTSL + HIFU and E-LTSL + HIFU treatments resulted in 4- to 5-fold greater Dox delivery at 42 °C than the LTSL and Dox groups at body temperature. Also, drug delivery attained by E-LTSLs was slightly greater (~ 1.5-fold) than that of LTSLs, which suggests that bubble formation during HIFU treatment may provide an additive response (Fig. 2.5). As in tumors, in adjoining heated muscle tissues we observed relatively higher Dox concentration for the E-LTSLs + HIFU treatment, which reinforces the role of bubble agents in improved cellular uptake (Fig. 2.7). Recently, Theek et al.. reported that sonoporation using MBs enhanced the extravasation and penetration of relatively large liposomal nanocarriers out of the blood vessels into the tumor interstitium by a variety of mechanisms, including perfusion modulation, mechanical disruption, and pore formation in tumor vessels [157]. It is currently not known whether or not similar mechanisms drive drug delivery and uptake in presence of nanobubbles. Although the data for thermally sensitive E-LTSLs are in line with Theek et al. studies, we observed that NTSLs and E-NTSLs were relatively less effective in achieving such outcomes. We believe that the presence of liposomal components (cholesterol, PEG) in NTSLs that resist triggered release of a drug at hyperthermic temperatures and support liposome accumulation in tumors relative to non-tumor tissue through the enhanced permeation and retention effect could be responsible for slow stromal transport of chemotherapeutic agents [158]. Thus, we propose that enhanced uptake of chemotherapeutics in a tumor from thermally and non-thermally sensitive carriers in presence of nanobubbles is an interplay among a rapid drug release rate, enhanced diffusion from blood vessels, and reduced resistance to drug transport upon nanobubble and hyperthermia treatment. For NTSLs and E-NTSLs, the

apparent lack of such a phenomenon suggests that the lipid components are the rate limiting factors. Future studies, especially those focused on the roles of intravascular versus interstitial transport of released drug from NTSLs + HIFU, would shed more light on these processes.

In a previous study, the plasma pharmacokinetics of Dox in a LTSL formulation was evaluated after intravenous administration. In contrast to Dox, which demonstrates a rapid initial clearance of > 95% in ~ 5 min, the LTSL formulation decreased ~ 90% over a 4 h time period [59]. Thus, currently HIFU treatments are generally performed over the first hour so that the maximal amount of drug is released at the peak plasma LTSL concentration. However, achieving spatially and temporally controlled homogeneous heating of deep seated tumors for long durations (30 min to an hour) is not always easy with HIFU due to target motion and if the treatment cell area (focal spot) has a large volume [142]. Thus, a gap between LTSL injection and HIFU hyperthermia treatment can impact drug delivery, which highlights the importance of mean transit time and quick intravascular heating of tumors [159, 160]. To assess such impacts and devise alternative methodologies of tumor heating following liposome injection, we chose three regions in our tumor model and sequentially heated them for durations of 21 min each. Our data suggest that segmental heating of tumors does not impact LTSL drug delivery when the plasma concentration of LTSLs is > 75% of Cmax over the first hour, and it achieves a similar level of drug in the chosen regions even when heated for shorter duration. However, relative to LTSLs, the sustained presence of PFP nanobubbles in the tumor microenvironment from E-LTSLs has a positive influence on maintaining high concentrations of Dox in the tumor. It may be noted that in case of MBs, ultrasound

contrast agents acoustically shield the beam from the underlying tissue resulting in temperatures higher than the target temperature [161]. However, encapsulated PFC emulsions in echogenic liposomes tend to be incompressible when in a liquid state [162], and produce poor oscillation and backscatter in the US, and thus instead of generating unusually high temperature, they most likely cause sonoporation and reduced resistance to drug transport upon combination with mild hyperthermia. Thus, we propose that zonal hyperthermia using HIFU for shorter durations (15–20 min) with nanobubble liposome provides larger drug coverage when administered sequentially, without adversely impacting net drug delivery compared to single point larger duration heating (~ 1 h), and thus this approach may be useful for treating deep seated tumors, and should be an investigation of future studies.

Successfully implementing a drug delivery system that permits selective anatomic delivery from passively accumulated NTSLs in tumors faces additional challenges, such as lack of enhanced intratumoral drug distribution [163]. Previously, the MB and HIFU combination has been shown to modulate microvascular permeability within a tumor [104]. In other studies, NTSLs that contained echo-contrast PFP gas enhanced gene and siRNA delivery in vitro and in vivo [164-166]. For MBs, the mechanism governing enhanced penetration was reported to be impulsive pressures exerted by the collapse of gaseous agents and formation of subsequent cavitation bubbles, resulting in improved transmembrane permeability [167]. Although a direct cavitation response was not detected in our H&E images following nanobubble treatment, E-NTSLs positively impacted the intratumoral penetration of Dox. Fluorescence analysis of E-LTSLs + HIFU treated tumors also revealed significantly improved intratumoral Dox delivery compared

to treatments with Dox or NTSLs (Fig. 2.9). Prior research has shown that the extravascular transport distances of 70-nm nanoparticles were 40 and 10 μm in tumors with high and low permeability, respectively [168]. Thus, if acoustic pressure, pulse resonance frequency, and sonication rates are synergistically optimized with nanobubbles, out data suggest that this can improve intratumoral penetration relative to nanoparticle or hyperthermia alone even for non-thermosensitive liposomes. While the degree of permeability produced by HIFU hyperthermia or bubbles needs to be studied in greater detail, our initial data suggest that nanobubble action is potentiated in the presence of hyperthermia to cause greater transport of drug to the tumor core and thus this may serve as a suitable alternative to MBs.

In conclusion, the results of our study suggest that zonal administration of HIFU sequentially for short duration is a promising method for improving drug delivery into solid tumors from LTSLs. Intravenous administration of PFP encapsulated in LTSLs or NTSLs allowed Dox to reach the tumor core, and the mechanisms governing such transport involve the interplay of hyperthermia and reduced tissue barriers. This approach might prevent tumor recurrence in deep seated tumors and should be the subject of future investigations.

Acknowledgements

Research reported in this publication was supported by the Center for Veterinary Health Sciences Seed Support, National Cancer Institute of the National Institutes of Health under Award Number R15CA179369 & 3R15CA179369-01A1S1; the Oklahoma Center for Advancement in Science and Technology (OCAST: HR13-217), and the Oklahoma

State University (OSU) Kerr Endowed chair support and Technology Business Development Program grant. The content is solely the responsibility of the authors and does not necessarily represent the official views of the National Institutes of Health or OCAST. The liposomes (mentioned herein) is based on research and is not commercially available. Its future availability cannot be guaranteed due to regulatory issues.

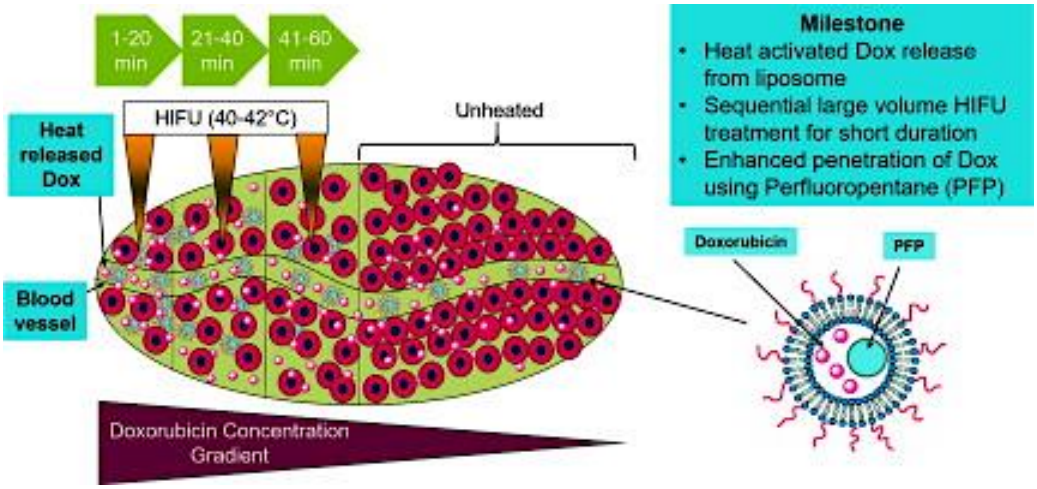

Fig. 2.1. Schematic illustration of Doxorubicin (dox) delivery regulated by zonal administration of High Intensity Focused Ultrasound (HIFU) across mouse colon tumor.

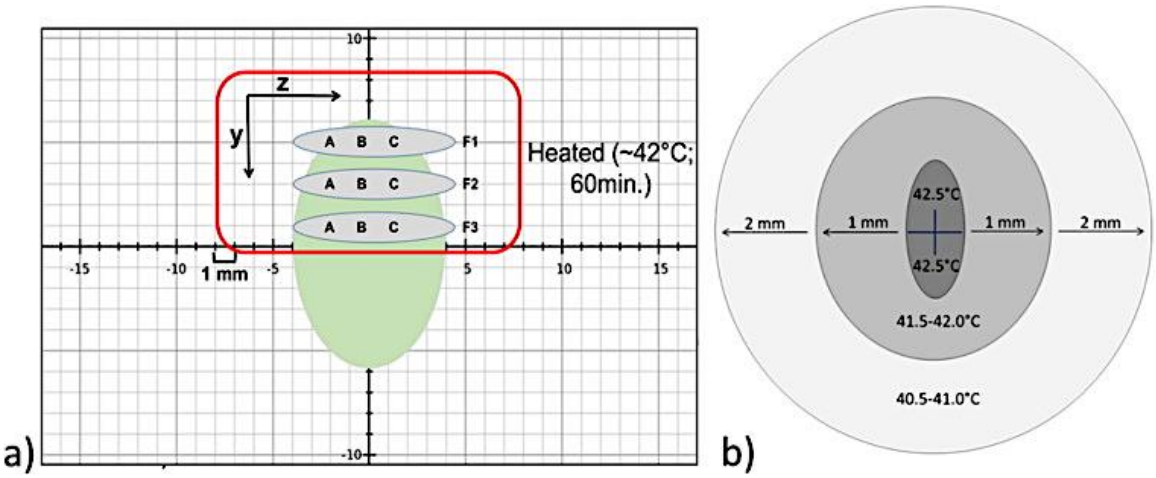

Fig. 2.2. a) The tumor was divided into a top half consisting of three sequentially heated fragments and a bottom unheated half. Before injection, fragment 1 (F1) was heated for 3 min. During injection, starting at F1, a 1 min heating regime was applied to point A, followed by B, and finally C. This process was repeated seven times to ensure that F1 was heated between 40 and 42 °C for a total of 21 min. F2 and F3 were heated in the same way to achieve a cumulative heating of ~ 60 min.; b) Illustration of the thermal gradient in the mouse tumor model up to 2 mm away from the HIFU focus. Temperature was measured throughout the tumor by moving the HIFU focus over a thermocouple inserted into the tumor. Any area within the 1 × 1 × 10 mm focus volume and up to 3 mm radius could be heated for 40–42 °C.

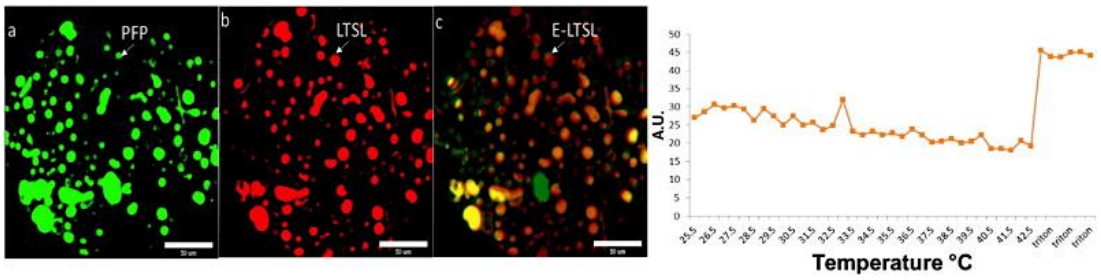

Fig. 2.3. Confocal microscopy showing PFP (green) encapsulated in the lipid bilayer (red) at 25 °C; d) Thermal scan for E-LTSL loaded with PKH67 labeled PFP. Increase in fluorescence signal is observed post lysis of E-LTSL with triton, due to de-quenching of PKH67 PFP from the liposomes. LTSL were used as control for the baseline fluorescence from liposomes (data not shown).

Liposomes	Size (nm)		Polydispersity index		Zeta Potential (mv)	
	Mean	**SEM**	**Mean**	**SEM**	**Mean**	**SEM**
NTSL	190.1	1.9	0.1	0.01	-26.8	3.6
ENTSL	193.8	1.2	0.11	0.04	-43.8	0.6
LTSL	176.8	0.5	0.11	0.01	-48	1.7
ELTSL	171.6	0.5	0.12	0.01	-28.3	1.1

Table 2.1. Size, polydispersity and zeta potential of NTSL, E-NTSL, LTSL and E-LTSL at 25°C

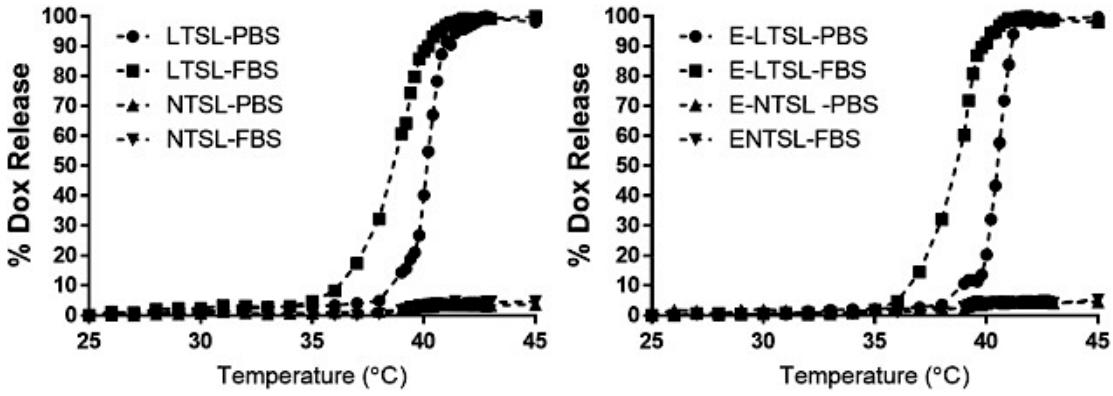

Fig. 2.4. Percent release of doxorubicin (Dox) in PBS and FBS between 25 and 42.5 °C for NTSLs, E-NTSLs, LTSLs, and E-LTSLs.

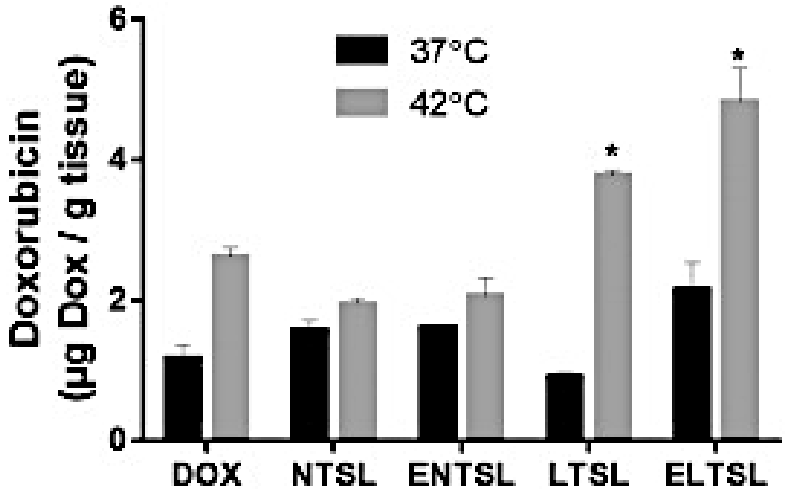

Fig. 2.5. Doxorubicin (Dox) concentrations in tumors at body temperature (37 °C) as well as HIFU treated tumors for free Dox, NTSLs, E-NTSLs, LTSLs, and E-LTSLs for all liposome formulations following a 5 mg/kg Dox injection. Data are shown as mean Dox concentration ± standard error of mean ($n = 3 - 6$), ($F_{8,28}$=23.63, *$p < 0.05$, Tukey's multiple comparison); *Indicates significant differences from the unheated internal control.

Organs	Dox	LTSL	LTSL HIFU	NTSL	NTSL HIFU	E-LTSL	E-LTSL HIFU	E-NTSL	E-NTSL HIFU
Spleen	7.2 (1.9)	7.8 (1.0)	7.3 (0.7)	27 (1.7)	16 (3.9)	8.0 (0.8)	6.5 (0.9)	29 (3.9)	16.3 (2.7)
Heart	4.1 (0.7)	3.9 (0.5)	3.8 (0.3)	2.4 (0.4)	1.2 (0.1)	3.4 (0.3)	5.1 (1.2)	2.0 (0.3)	1.1 (0.1)
Kidney	15.1 (0.5)	22.5 (4.5)	10.5 (1.5)	6.3 (0.6)	2.3 (0.5)	23.6 (3.6)	12 (2.0)	6.0 (1.2)	1.6 (0.1)
Lung	1.7 (0.1)	3.0 (0.5)	2.6 (0.5)	1.6 (0.4)	2.4 (0.6)	1.1 (0.3)	3.5 (0.2)	1.3 (0.1)	1.0 (0.2)
Liver	18.7 (1.3)	14 (1.1)	11 (2.7)	4.9 (0.9)	4.2 (1.6)	15.8 (0.9)	12 (2.1)	7.2 (0.9)	6.0 (1.2)
Muscle	2.5 (0.1)	1.9 (0.2)	8.1 (1.3)	0.9 (0.2)	1.4 (0.2)	1.5 (0.1)	9.9 (0.4)	0.9 (0.1)	1.1 (0.2)
Tumor	1.2 (0.2)	0.9 (0.1)	3.8 (0.1)	1.6 (0.1)	1.9 (0.1)	2.1 (0.4)	5.1 (0.4)	1.6 (0.1)	2.1 (0.3)

Table 2.2 Average Dox delivery in various organs with and without HIFU for various liposome groups. (Data are expressed as μg Dox/g of tissue; (mean ± SEM)

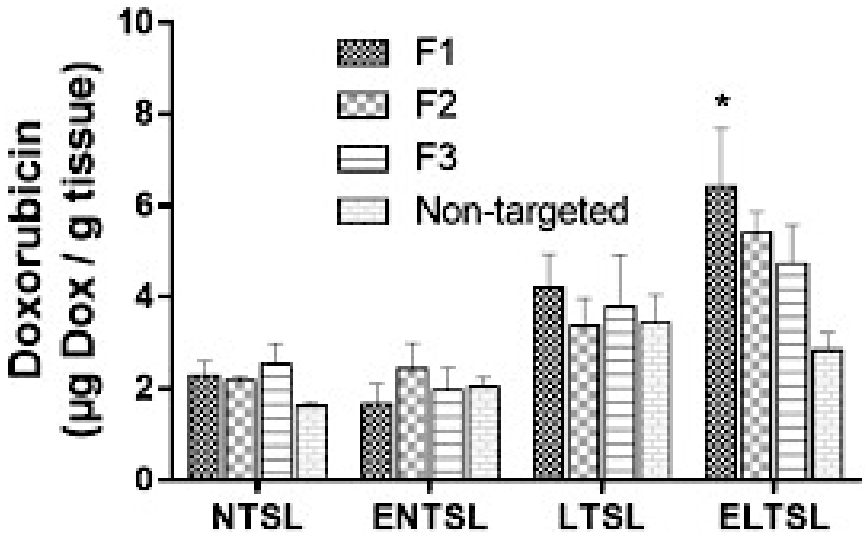

Fig. 2.6. Doxorubicin (Dox) concentrations in HIFU treated tumor fragments (F1, F2, and F3) for NTSLs, E-NTSLs, LTSLs, and E-LTSLs following a 5 mg/kg Dox injection. Data are shown as mean Dox concentration ± standard error of mean (n: 3 − 6). E-LTSL F1* is significantly different from unheated bottom fragment ($p < 0.05$, pair wise comparison).

Liposome	F1	F2	F3	Unheated fraction
NTSL/HIFU	2.3 (0.3)	2.2 (0.1)	2.5 (0.4)	1.6 (0.1)
E-NTSL HIFU	1.7 (0.4)	2.4 (0.5)	2.0 (0.5)	2.0 (0.2)
LTSL/HIFU	4.2 (0.8)	3.4 (0.6)	3.8 (1.1)	3.4 (0.6)
E-LTSL/HIFU	6.4 (1.3)	5.4 (0.5)	4.7 (0.9)	2.8 (0.4)

Table 2.3. Average Dox delivery in heated fragments (F1, F2 and F3), and unheated fraction of colon tumor, (data are expressed as μg Dox/g of tissue; (mean ± SEM)).

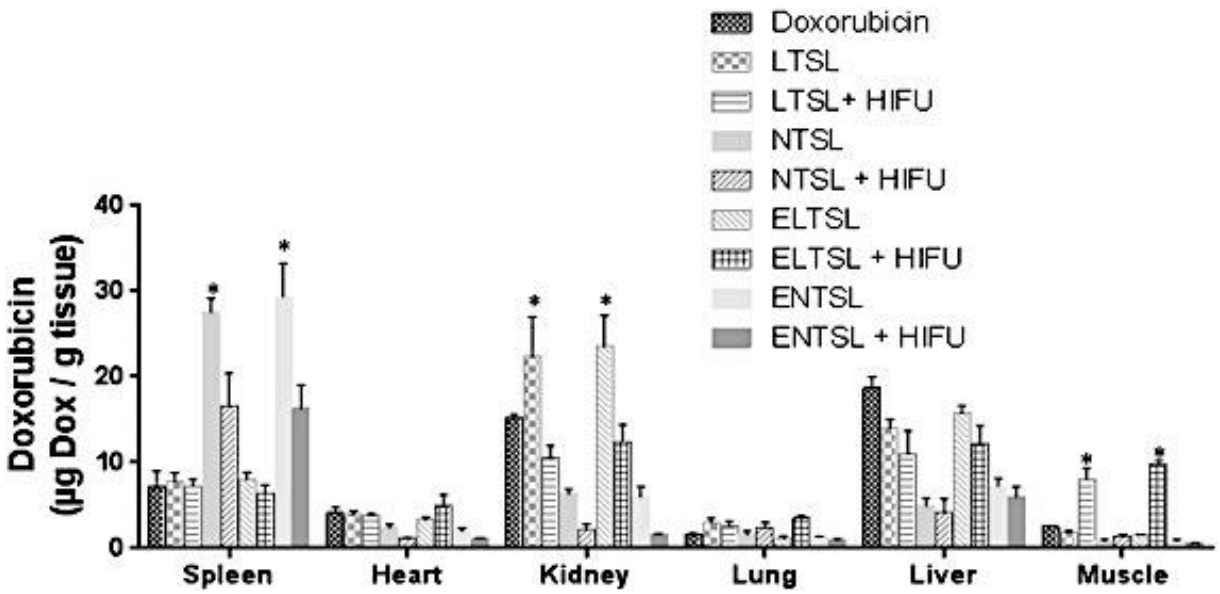

Fig. 2.7. Doxorubicin (Dox) concentrations in µg Dox/g of tissue for organs and muscle distal to tumors in a 37 °C water bath for Dox, NTSLs, E-NTSLs, LTSLs, and E-LTSLs as well as HIFU treated tumors for all liposome formulations following a 5 mg/kg Dox injection. Data are shown as mean Dox concentration ± standard error of mean (n = 5–6) (*$p < 0.05$, Tukey's multiple comparison); *Indicates significant difference with Dox treatment group in same organ.

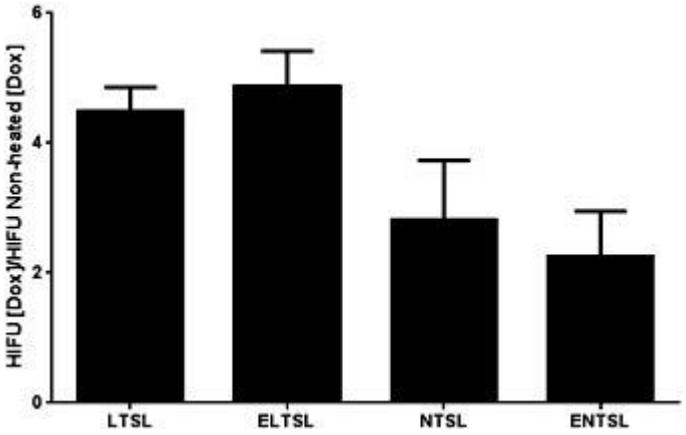

Fig. 2.8. Ratio of doxorubicin (Dox) in tumor adjoining muscle heated with HIFU and unheated contralateral muscle for NTSLs, E-NTSLs, LTSLs, and E-LTSLs. Data are shown as mean concentration of Dox in tissue ± standard error of mean (n = 3–6), ($F_{3,10}$=3.93, *p < 0.05, Tukey's multiple comparison).

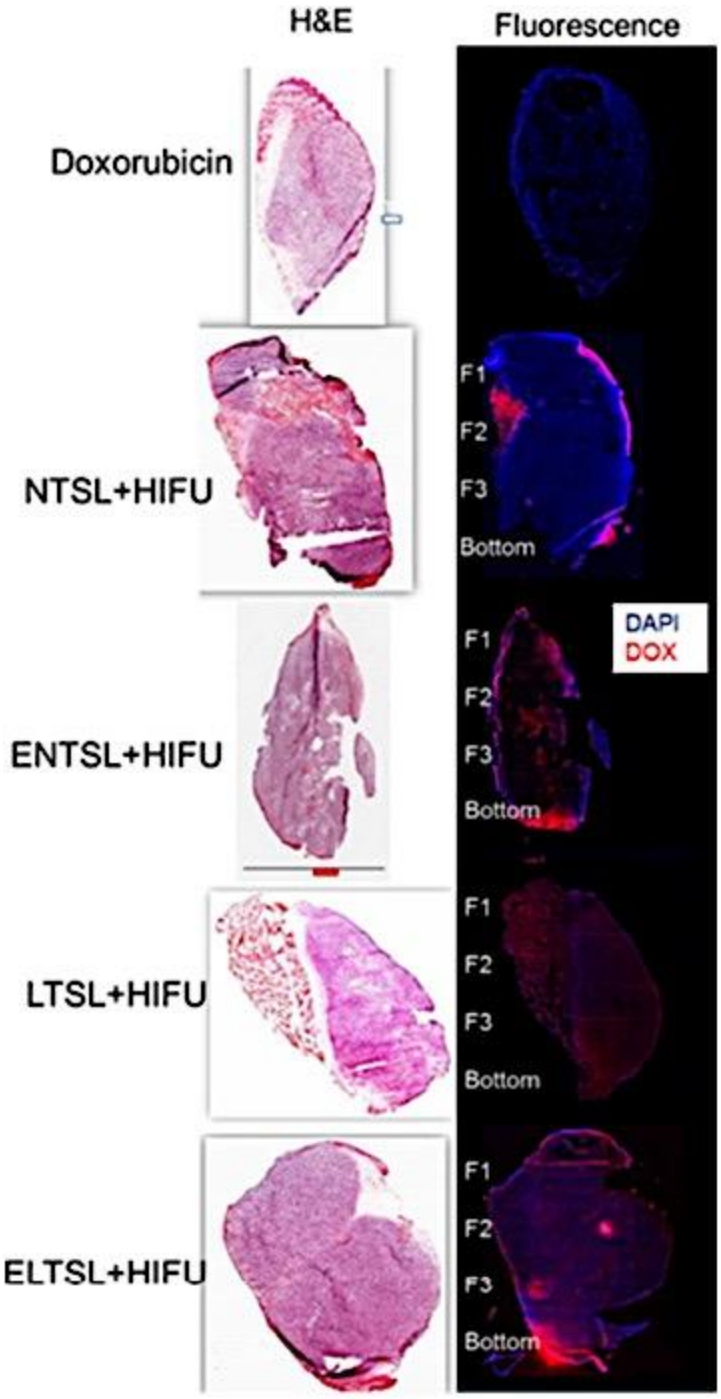

Fig. 2.9. H&E (left column) and fluorescent (right column) images of HIFU treated tumors. All tumors are oriented with the F1 fragment on top when appropriate.

CHAPTER III

THERAPEUTIC EFFICACY OF HIFU AND ECHOGENIC LTSL IN IMMUNOCOMPROMISED COLON CANCER MODEL

Abstract

A key drawback of conventional cancer chemotherapy is the inability to achieve homogeneous drug delivery to solid tumors and prevent tumor recurrence. These can be further complicated by the acquired chemo-resistance. To overcome this barrier, the objectives of this study were to 1) characterize extravasation of systemically administered doxorubicin (Dox) in solid tumor mass in presence of echogenic low temperature sensitive liposomes (E-LTSL) and high intensity focused ultrasound (HIFU) in C26 colon carcinoma mouse model, 2) evaluate E-LTSL efficacy in immunocompromised mice bearing C26 tumors, and 3) characterize multidrug resistance in the tumor microenvironment following various treatments. For drug extravasation characterization, mice bearing colon cancer received intravenous injection of Dox in the presence of HIFU +/- E-LTSLs. HIFU heating was performed in ~50% of the tumor volume, with the rest acting as an internal unheated control. HPLC was performed to ascertain Dox delivery. The net penetration depth from blood vessels was determined computationally by

analyzing fluorescent images of tumor sections. Efficacy of HIFU+E-LTSL (with encapsulated Dox) was evaluated by monitoring tumor growth after three successive treatments over a 6-day period. Data suggested that HIFU+E-LTSL treatment group resulted in significantly higher mean drug extravasation from blood vessels compared to other groups. However, the survival rates from HIFU+E-LTSL was modest compared to untreated control. Cancer stem cell markers and xenobiotic efflux pumps Aldh1a1, Notch2, Gata6, Abcc1, Abcg2, and Abcb1, which play a role in chemo resistance remain largely unchanged with HIFU/ELTSL treatment, leading us to believe that Dox E-LTSL efficacy was not dependent on these factors. In conclusion, our animal data suggest that HIFU+E-LTSL enhances tumor Dox penetration. However, the marked increased drug delivery capabilities were insufficient to improve therapeutic outcomes in immune-compromised mice bearing the colon tumors.

Introduction

Conventional chemotherapy delivers insufficient and heterogeneous drug delivery into solid tumors. This is because solid tumors have densely packed cells, abnormal vasculature support, and high interstitial fluid pressure that prevents the dispersion of drugs deep into the tumor [171-173]. Current methods of increasing chemotherapeutic drug delivery and reduce side-effects include the use of nanoparticles (NPs) to a targeted region. NPs increase drug delivery by exploiting vaso-regulatory factors and chemicals including nitric oxide [171], bradykinin [174, 175], and tumor penetrating peptides such as iRGD [176-178]. To further enhance this process, NPs can be combined with focused ultrasound for improved cavitation and stimuli-sensitive release of contents in the tumors. Although promising, tumors with poor expression of targeted ligands or with poor

vasculature networks may not achieve sufficient drug delivery. In some cases, some treatments such as those that utilize miRNAs may actually promote metastasis [179]. Additionally, multidrug resistance acquired post treatment in the form of cancer stem cell and xenobiotic efflux pump upregulation can negate the advantages of effective dosage [180, 181]. Xenobiotic efflux pumps are transmembrane proteins that actively pump endogenous and exogenous compounds out of the cell [181, 182]. Colon cancers generate resistance to chemotherapeutic drugs such as Dox by upregulating proteins from the ABC protein family which actively remove intracellular delivered agents, preventing response to treatment [183]. Long-term multidrug resistance can also be acquired by cancer stem cell activation or with changes in expression of cell regulatory proteins, causing resistance to standardized chemotherapeutic practices [184-186]. Thus, a critical need is to enhance penetration depth of anticancer drugs in the solid tumor by tackling the tumor microenvironment factors, especially in tumors that are not good for targeted therapy. We hypothesized that systemically administered NP-encapsulated doxorubicin and combination with mild hyperthermia (42 ºC) can increase therapeutic efficacy against malignant murine cancers. Prior research with hyperthermia have shown that it can boost Dox diffusion into tumors both in the free and NP-encapsulated forms [187, 188]. [189]. To further increase Dox uptake in a target region, in this study, we utilized the sonoporation effects of our NPs by systemically administering echogenic lot temperature sensitive liposomes (E-LTSL). E-LTSL are synthesized by encapsulating an ultrasound contrast agent (UCA), Perfluoropentane (PFP) in its aqueous core. E-LTSLs offer a number of advantages over more commonly used microbubbles. In contrast to microbubbles, E-LTSL have a smaller size, better stability, and an enhanced half-life.

Thus, E-LTSL can serve as an effective theranostic agent for detection of tumor vascularity in real time. Also, unlike microbubble agents, E-LTSLs cause minimal cavitation effects in the tissue due to a lack of violent inertial cavitation [112, 190]. Due to these favorable features, E-LTSL may have clinical utility for improving drug penetration in tumors. The objective of this study was to assess whether the presence of E-LTSL and HIFU measurably increase Dox delivery in the murine colon tumor model. Additionally, we determined if enhanced Dox extravasation from E-LTSL correlated with the therapeutic efficacy, and multidrug resistance pathways in the colon tumors.

Materials & Methods

Materials

PFP (99%, Exfluor Research Corporation, Round Rock, TX, USA) was used as the nanobubble contrast agent. Monostearoyl-2-hydroxy-sn-glycero-3-phosphocholine (MSPC), 1,2-dipalmitoylsn-glycero-3-phosphocholine (DPPC), and 1,2-distearoyl-sn-glycero-3-phosphoethanolamine-N-[methoxy (Polyethylene glycol)2000] (DSPE-mPEG2000) were obtained from Corden Pharma Corporation (Boulder, CO, USA). PKH67 Green Fluorescent Cell Linker was obtained from Sigma Aldrich (Milwaukee WI, USA). Dox was obtained from LC Laboratory (Woburn, MA, USA). Acetonitrile (high performance liquid chromatography (HPLC) grade) was obtained from Pharmco-AAPER (Brookfield, CT, USA). FITC Rat Anti-Mouse antibody was obtained from (BD Biosciences CA, USA) Ethylene glycol (99%, spectrophotometric grade), phenylboronic acid (98%), and 2,2-dimethoxypropane (98%) were purchased from Alpha Aesar (Ward Hill, MA, USA). The PD-10 column was obtained from GE Healthcare Life Sciences,

(Buckinghamshire, United Kingdom, UK). C26 cells were kindly provided by the National Cancer Institute.

Synthesis and characterization of E-LTSL

E-LTSL (lipid composition: DPPC, MSPC, and DSPE-mPEG2000 molar ratio of 85.3:9.7:5.0) were prepared by hydration of a lipid film followed by the extrusion method as described previously. Briefly, the lipids were dissolved in chloroform. The solvent was evaporated and the resulting lipid film was hydrated in citrate buffer (pH 4.0) mixed with 1,3-propanediol (1, 3-PD) (0.65 M, for PFP emulsification) at 55 °C for 30 min and extruded five times through double stacked 200 nm polycarbonate filters to yield a final lipid concentration of 50 mg lipid/ml. A PD-10 size-exclusion column equilibrated with 5–10 column [16, 153, 154].volumes of 1 × phosphate buffered saline (PBS) was used to remove free 1,3-PD from the outside of the liposomes. This procedure yielded low temperature sensitive liposome which is the precursor to the E-LTSL.

Loading of PFP into an LTSL (forming an E-LTSL) was performed using a one-step sonoporation method. Briefly, 2 mL of the liposomal solution was continuously sonicated (~20 khz) at 4 °C in 3 mL vials along with PFP (boiling point 30 °C; 20 μL/100 mg lipid) for 1–2 min. PFP and LTSLs were kept cold prior to being combined, and the sonication bath was kept to minimize PFP vaporization. Free 1,3-PD and PFP were removed using a PD-10 size-exclusion column equilibrated with 5–10 column volumes of 1x phosphate buffered saline (PBS).

E-LTSL were characterized for size (z-average) using dynamic light scattering (DLS) with a 90 plus PALS Nanobrook device (Brookhaven Instruments, Holtsville, NY, USA).

Briefly, 5-10 µL of E-LTSL were added to 3 ml of PBS in a cuvette, and DLS measurements were recorded at room temperature. For each liposomal formulation, an average of three measurements were taken, and the mean size and standard deviation were calculated for the E-LTSL samples. Zeta potentials were measured in de-ionised water.

Establishment of mouse model of colon cancer

All animal-related procedures were approved and carried out under the regulations and guidelines of the Oklahoma State University Animal Care and Use Committee. C26 cells were grown as a monolayer to 80–90% confluence in RPMI supplemented with 10% v/v fetal bovine serum (FBS) and 1% v/v streptomycin/penicillin. Confluent cells were harvested, washed, and diluted with sterile cold PBS to generate 0.5 x 106 cells/50 µl. Next, 50 µl of cell inoculum was injected per mouse in the thigh region of the mouse hind leg using a 25-gauge needle (BD, Franklin Lakes, NJ, USA). Mice were monitored and tumor growth was measured by serial caliper measurements (General Tools Fraction+™, New York, NY, USA). Tumor volumes were calculated using the formula (length X width2)/2, where length is the largest dimension and width is the smallest dimension perpendicular to length. Tumors were allowed to grow to a volume of 300–400 mm3 prior to initiating studies, and the mice were treated with 5mg Dox/Kg Body weight IV.

Study design

Athymic nude mice bearing C26 mouse adenocarcinoma cell tumors were divided into two treatment groups: Dox + HIFU and Dox + HIFU + E-LTSL. In both groups (n = 7 mice), Dox was co-administered at 5 mg/kg body weight intravenously along with 250µL

E-LTSL/kg body weight. Four mice from each group were used for Dox quantification with HPLC and three mice were used for tumor imaging.

Hyperthermia generation in mouse tumors with HIFU

An integrated ultrasound-HIFU alpinion platform was used for tumor identification, sonication, and treatment characterization. For hyperthermia treatment, the center of the tumor was aligned with the HIFU focus at a fixed focal depth for efficient coverage, and VIFU-2000 software was used to define the target boundary and slice distance in X, Y, and Z directions for automatic movement of the transducer. The HIFU transducer had 1.0 MHz central frequency, 45 mm radius, and 64 mm aperture diameter with a central opening 40 mm in diameter. The mouse was oriented so that its dorsal side was facing the transducer and the caudal half was lowered into a 37 ºC water bath. The path from the transducer to the tumor aligned along the z-axis as shown in Fig 3.1. For HIFU treatments, each tumor was divided into two halves; the upper half of the tumor, which received direct HIFU heating, is referred to as the Treated half and the bottom half of the tumor, which did not receive direct HIFU heating, and was referred to as the Untreated half. The HIFU focus was positioned at the top region of the tumor for heating and was repositioned along the x axis throughout time to thoroughly heat the entire area. HIFU treatment parameters used were as follows: 5 Hz frequency, 50% duty cycle, 10 W acoustic power, and a peak positive/negative pressure of 6.15/-4.41 MPa to achieve a mean target temperature of 40–42.5 ºC at the focus. The total treatment duration was 63 min with a 3 min preheating time. Groups with no HIFU heating were kept in a 37 ºC water bath for 63 min.

Post HIFU treatment tissue harvesting procedure

Following completion of HIFU, mice were euthanized. To clear the vasculature of drug/liposomes, transcardiac perfusion was performed immediately by opening the chest cavity and intracardially injecting 10 mL of PBS. Tumors were excised, weighed, snap-frozen over liquid nitrogen, and stored at −80 °C until Dox analysis.

Quantification of Dox by HPLC

Tissue homogenization and sample preparation for HPLC were carried out using previously published methods [16, 61]. Briefly, samples were homogenized, and Dox was extracted and quantified with HPLC using daunorubicin as the internal standard. The HPLC detection system consisted of fluorescence detectors, and detection was performed at ex/em of 498/593 nm. Data were acquired done using Shimadzu LC solution software. Concentrations of the analyte in tissues were determined using peak-area ratios of the sample analyte to the internal standard from the calibration curve.

Whole tumor histology by fluorescence imaging

Three mice tumor from each treatment group were selected for histology. 8 µm sections of frozen tumors were prepared, and two serial sections were mounted per slide. Cell density, and cavitation were assessed in hematoxylin- and eosin- (H&E) stained sections using an Aperio ScanScope at 20x. A nitroblue tetrazolium (NBT) stain was used to determine regions of thermal necrosis.

Blood vessels in tissue sections were Labeled with CD-31 (rat anti mouse) mouse antibodies and slides were fixed, mounted and allowed to dry for 24 h before imaging. CD-31 was imaged at an exposure 200 ms (ex/em of 490/520) and Dox was imaged at an

exposure 100 ms (ex/em of 480/590). Image acquisition and display parameters were constant for different treatments to allow for qualitative comparison. Blood vessels were imaged at top of the treated half of the tumor and thorough out the untreated half. Whole-section digital histological scans were acquired using a 10X objective on an Olympus ZDC2 IX81 fluorescence microscope equipped with a color CCD camera, cooled monochrome CCD camera, motorized scanning stage, and Metamorph mosaic stitching software.

Dox quantification analysis

CD-31 labeled blood vessels were analyzed individually for Dox penetration and migration into the surrounding tumor interstitium by selecting a large number of ROIs across each tumor used for imaging. Dox fluorescence intensity was measured along a distance extending radially from the center of the blood vessels. These values were plotted as the average fluorescence at set distances moving away from the center of blood vessels.

E-LTSL efficacy study design

C26 cells were seeded in 200uL complete RPMI with 10% fetal bovine serum and 1% streptomycin-penicillin at a density of $2x10^4$ cells/well in 96-well plates. Cells were allowed to attach and grow to a confluency of 80, and then treated with 3.125, 5, 6.25, 10, 12.5, 18, and 25 μM for 1h at 37°C and 42°C, and cell viability was assessed at 48h with MTT assay by measuring the absorbance at 540 nm. For in vivo studies, athymic nude mice bearing C26 mouse adenocarcinoma cell tumors (70 mm^3) were divided into eight treatment: Control, HIFU, Dox ± HFU, and E-LTSL ± HIFU. In all groups (n = 4-5),

mice were treated at 5 mg Dox/kg body weight administered intravenously every 3 day (day 0, 3, and 6 respectively). HIFU treatment parameters used were as follows: 5 Hz frequency, 35% duty cycle, and 6W acoustic power to achieve a mean target temperature of 40–42.5 ºC for 1h at the focus. Survival endpoints included tumor volume exceeding 2000 mm^3 or a 15% decrease in body mass.

qRT-PCR Characterization of C26 Multidrug Resistance

At the end of study, intracardiac injection of10 mL of PBS were performed, and tumors were excised, weighed, snap-frozen over liquid nitrogen, and stored at −80 °C. Total RNA from the C26 colon carcinoma tumors was extracted using TRIZOL according to the manufacturer's instructions. RNA concentration was measured using NanoDrop ND100. 5µg of total RNA was treated with DNase I according to manufacturer's protocol, and RNA was purified with phenol-chloroform. cDNA synthesis was performed using 1µg DNase I treated RNA per reaction using iScript Reverse Transcription Supermix for RT-qPCR. Real-Time RT-PCR reaction was performed with cDNA diluted 5x. Relative gene expression for Aldh1a1, Notch 2, Gata6, Abcc1, Abcg2, and Abcb1 was evaluated by qRT-PCR using SYBR green reagent using Applied Biosystem 7500 fast Real-Time PCR instrument and a 40-cycle run for target amplification. Specific primers sequences are listed in **Table 3.1**. qRT-PCR data were analyzed by the $2^{(-\Delta\Delta CT)}$ method using GAPDH as a reference gene.

Statistical Analysis

Treatment groups were compared for differences in mean tumor Dox concentration, fluorescence intensity of Dox from the center of a blood, tumor volume, survival time,

and RNA fold change respectively with ANOVA followed by Tukey's multiple comparison post-hoc test using GraphPad Prism 5.0 (GraphPad Software Inc.). All p-values were two-sided, and $p < 0.05$ was taken to indicate statistical significance. Values were reported as mean ± standard error of the mean (SEM).

Results

Characterization of E-LTSL and LTSLs

Table 3.1 shows the hydrodynamic diameter, polydispersity index, and zeta potential values of LTSLs and E-LTSL at room temperature (25 °C). Both LTSL to E-LTSL demonstrated similar physicochemical properties. LTSL and E-LTSL demonstrated a hydrodynamic diameter of 176±3.6 and 165±2.1nm, zeta-potential of 0.2±0.004 and 0.2±0.01mV, and polydispersity index of -42.6±0.7 and -28.3±1.8 respectively (Table 3.1).

Dox Tumor Biodistribution

E-LTSL nanobubbles resulted in a significant increase in Dox tumor concentrations. Whole tumor Dox concentration for the 37°C, HIFU, and HIFU+E-LTSL groups were as follows: 1.2 ± 0.2, 2.6 ± 0.1, and 3.0 ± 0.3 μg Dox/g of tissue (Fig 3.2 and Table 3.2). Dox levels in HIFU treated, HIFU + E-LTSL treated, HIFU untreated, and HIFU + E-LTSL untreated tumor group were as follows: 2.0 ± 0.1, 3.9 ± 0.7, 2.4 ± 0.1, and 1.7 ± 0.1 μg/g. While HIFU hyperthermia increased Dox payload, E-LTSL nanobubble demonstrated a substantial increase in Dox delivery relative to Dox alone.

Dox penetration depth

Fluorescence intensity measured radially from the center of blood vessels to a distance of 200 μm (Fig 3.4) showed an increased Dox signal (red) for the HIFU + E-LTSL relative to all other groups (Fig 3.5). In general, the mean fluorescence intensity in the treated regions for the HIFU+E-LTSL was > 1.5-fold compared to other groups.

Dox Whole Tumor Fluorescence Imaging

HIFU+E-LTSL showed Dox signal in the HIFU heated region (Fig. 3.6c). In contrast, HIFU treated tumors showed Dox signal only around the tumor periphery (Fig. 3). H&E staining suggested minimal tissue damage in the treated regions (Fig. 3.6d). NBT analysis that measured cellular metabolism showed an absence of cellular necrosis as indicated by uniform purple-blue staining across various treatments (Fig. 3.6e).

Cytotoxicity of Dox with and without hyperthermia

The cytotoxicity of Dox measured by MTT in C26 cells following 3.125-25 μM treatment demonstrated a dose-dependent decrease in the C26 viability at 37°C and 42°C compared to untreated control. Also, heating the cells with Dox treatment decreased C26 percent viability by approximately 15% compared to 37°C (Fig. 3.7).

E-LTSL & HIFU efficacy in murine colon cancer model

HIFU+E-LTSL decreased the tumor volumes by 2-fold relative to the untreated control (261±31 vs 458±66.5 mm^3). Likewise, E-LTSL alone demonstrated reduced tumor growth compared to control. For all other groups, the tumor regressions were modest (HIFU, Dox, Dox + HIFU, and E-LTSL were 354±75, 311±50.9, 347±57, and LTSL=287.4±3.3 mm^3, respectively; Fig 3.8) compared to untreated control. This was

further illustrated by survival data where both HIFU+E-LTSL and E-LTSL treated mice showed an increase in survival by an average of 4 days longer than Control and HIFU and 2-3 days longer than Dox and HIFU+Dox treated mice (Fig. 3.9.).

Expression of drug resistant marker in tumors

qRT-PCR evaluation of C26 tumors revealed changes in mRNA expression related to chemo-resistance pathways. HIFU+E-LTSL achieved >2-fold enhanced expression of Abcb1 compared to untreated control. Also, HIFU+E-LTSL showed a 5-fold greater gene expression of GATA6 than control, HIFU, Dox and HIFU+Dox (Fig 3.10). All other targets analyzed showed minimal to no change in gene expressions between the various treatment groups.

Discussion

Understanding the mechanisms of HIFU enhanced combined liposomal nanobubbles chemotherapy can help synergize the colon cancer outcomes. Our whole tumor analysis of Dox accumulation showed E-LTSL delivery can be significantly improved with HIFU compared to unheated counterparts with E-LTSLs (Fig 3.2). This is in line with prior findings where presence of nanobubbles improved drug extravasation [191] We also found that by using each tumor as its own internal control, E-LTSL precisely attained regional delivery compared to HIFU [192, 193]. This suggests that E-LTSL may overcome the current limitations of heterogeneous drug delivery of nanoparticle and conventional therapy [144, 191, 194, 195]. For example, Dox was found in peripheral regions of the tumor for all of the treatment groups. In contrast, the HIFU+E-LTSL treated regions demonstrated uniform Dox distribution in the heated region (Fig. 3.3).

Also, the mean Dox concentration was ~200 μm for HIFU+E-LTSL treated tumor region, suggesting sonoporative effects of E-LTSLs.

Dox is known to demonstrate short half-life [196]. To address this, liposomes with EPR mediated Dox accumulation have been developed [137]. By using the thermosensitive E-LTSL, we found that it was able to increase the Dox concentrations by 2-fold in the treated zones of tumors compared to respective controls, suggesting that it can improve the shortcoming of Dox's short circulatory half-life. E-LTSL benefits also include a lack of reliance on the presence of ligand rich environment (e.g. αv integrin expression) for localized therapy [197]. Incidentally, *in vitro* data showed that the C26 cells were responsive to Dox, however, the H&E and NBT staining of treated tumors showed that the E-LTSL/HIFU treatments did not kill C26 cells post-treatment, and that the higher concentrations of Dox in the tumor didn't translate into superior survival with E-LTSL and HIFU. This is in contrast to previous studies where substantial differences in therapeutic effect with Dox-based liposomes were noted [198-200]. To explore the possible mechanisms, we determined the expression of xenobiotic efflux pumps and cancer stem cell markers in the tumor samples (Fig 3.10). Xenobiotic efflux pumps are transmembrane proteins that help remove exogenous chemicals from inside to outside of the cells [201][202]. We found that xenobiotic efflux genes, abcc1 and abcg2, were mildly downregulated in the HIFU+E-LTSL groups. In contrast, abcb1 was 2-fold were greater than all other treatment groups, suggesting the likely presence of chemo-resistance phenotype. Surprisingly, these didn't correlate with the chemoresistant cancer stem cell markers, notch 2 and aldh1a1. Likewise, Gata6 was significantly upregulated in HIFU+E-LTSL compared to other groups, however, this marker has been associated with

both increased and decreased tumor progression in various tumor types[81, 203, 204]. Based on this, we hypothesize that an interaction of adaptive immune system with Dox may be needed to attain sufficient therapeutic effects. This is evidenced by prior research that showed the potential role of immune system in Dox therapeutic effects [205, 206]. Notably, in one particular study, immunocompromised mice and immunocompetent mice received similar Dox treatments [207]. Results indicated therapeutic effects in the immune competent model only. Thus, the presence of fully functioning adaptive immune system may improve immunogenic cell death and resultant T-cell response [207-211]. Future studies focusing on these mechanisms to understand therapeutic outcomes against colon cancer can shed more light on such mechanisms.

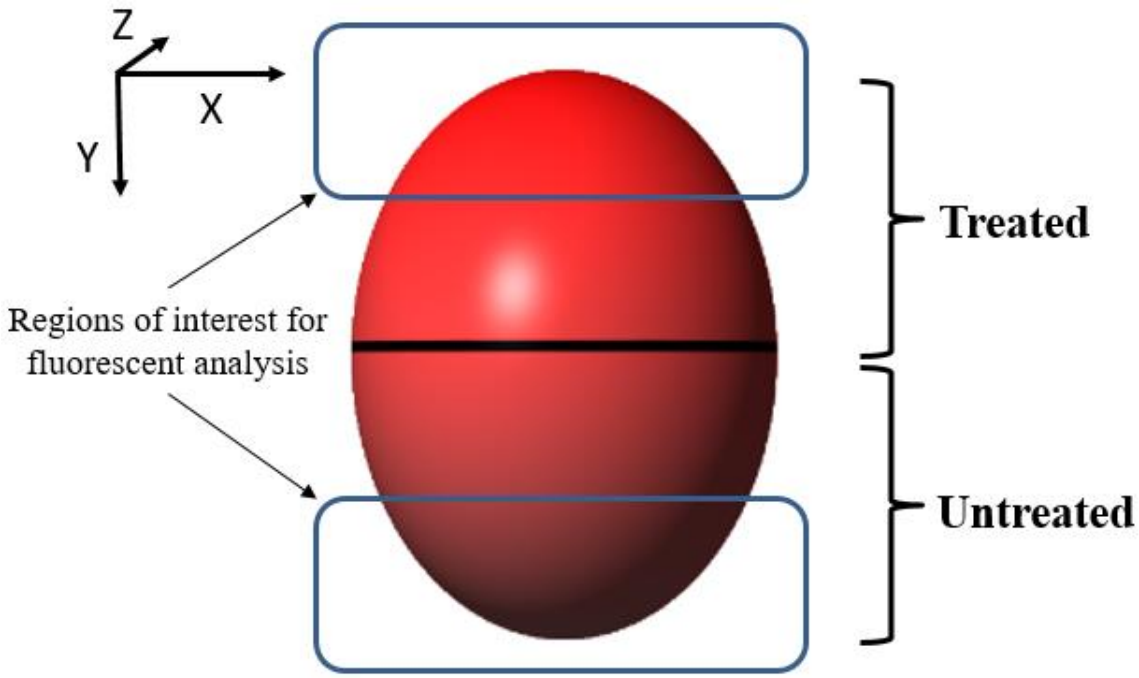

Fig. 3.1. The treated regions of the tumor received ~60 min of HIFU heating. Prior to E-LTSL and Dox injection, 3 min of preheating was performed. Fluorescence tumor imaging analysis were performed in the entire tumor.

Primer (*Mus musculus*)	Sequence
mGapdh-forward	CATCACTGCCACCCAGAAGACTG
mGapdh-reverse	ATGCCAGTGAGCTTCCCGTTCAG
mAldh1a1-forward	GGAATACCGTGGTTGTCAAGCC
mAldh1a1-reverse	CCAGGGACAATGTTTACCACGC
mNotch2-forward	CCACCTGCAATGACTTCATCGG
mNotch2-reverse	TCGATGCAGGTGCCTCCATTCT
mGata6-forward	ATGCGGTCTCTACAGCAAGATGA
mGata6-reverse	CGCCATAAGGTAGTGGTTGTGG
mAbcc1-forward	CAGTGGTTCAGGGAAGGAGTCA
mAbcc1-reverse	CACTGTGGGAAGACGAGTTGCT
mAbcg2-forward	CAGTTCTCAGCAGCTCTTCGAC
mAbcg2-reverse	TCCTCCAGAGATGCCACGGATA
mAbcb1-forward	GGTGGTGTCATTGTGGAGCAAG
mAbcb1-reverse	GCATCAGTGTCACTCTGGGATC
mGata6-forward	ATGCGGTCTCTACAGCAAGATGA
mGata6-reverse	CGCCATAAGGTAGTGGTTGTGG
mAbcc1-forward	CAGTGGTTCAGGGAAGGAGTCA

Table 3.1. PCR primers used for identification of multidrug resistance genes in C26 colon carcinomas.

Liposome	Size (nm)		Polydispersity		Zeta potential (mv)	
	Mean	SEM	mean	SEM	mean	SEM
LTSL	176.1	3.6	0.2	0.004	-42.6	0.7
E-LTSL	164.46	2.1	0.2	0.007	-28.3	1.8

Table 3.2. Size, polydispersity and zeta potential of LTSL and E-LTSL at room temperature (25 °C).

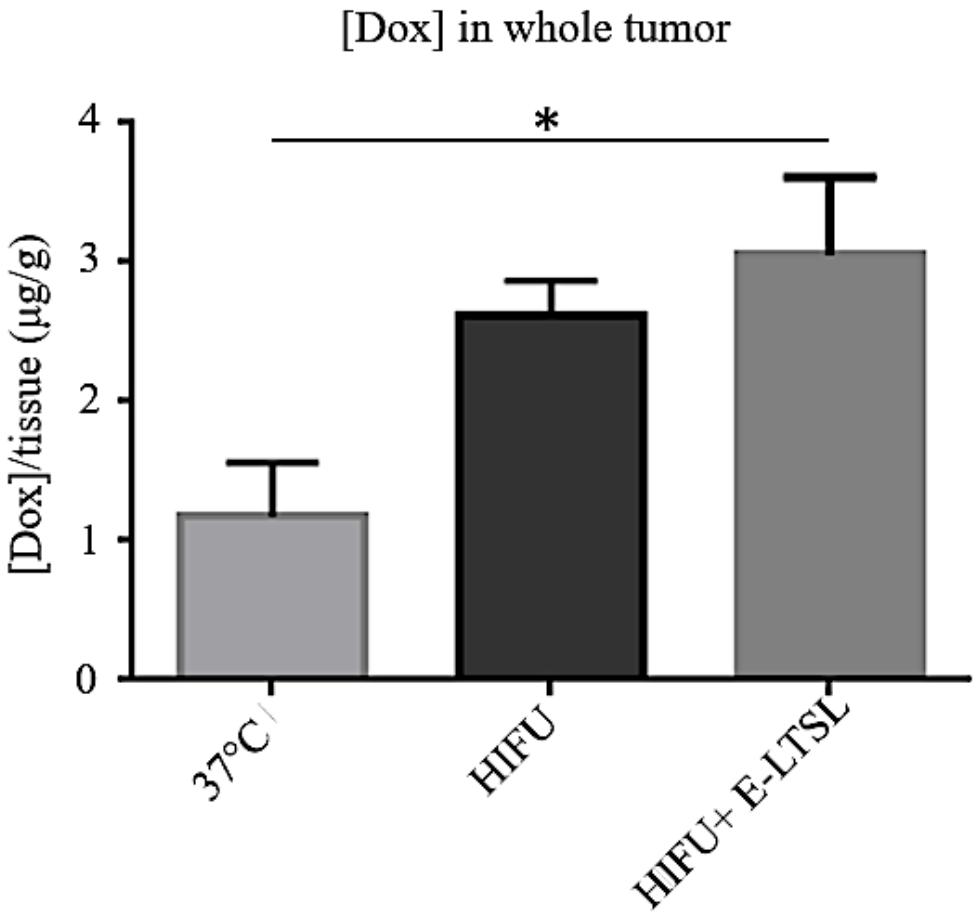

Fig. 3.2. Doxorubicin (Dox) concentrations in tumors for HIFU and HIFU + E-LTSL following 5 mg/kg Dox injection. Compared to unheated tumors (37°C), HIFU and HIFU+E-LTSL enhanced Dox delivery to tumors 1.5- to 2-fold. Data are shown as mean Dox concentration ± standard error of mean ($n = 4$, $p < 0.05$, Tukey's multiple comparison). *Indicates significant difference between groups.

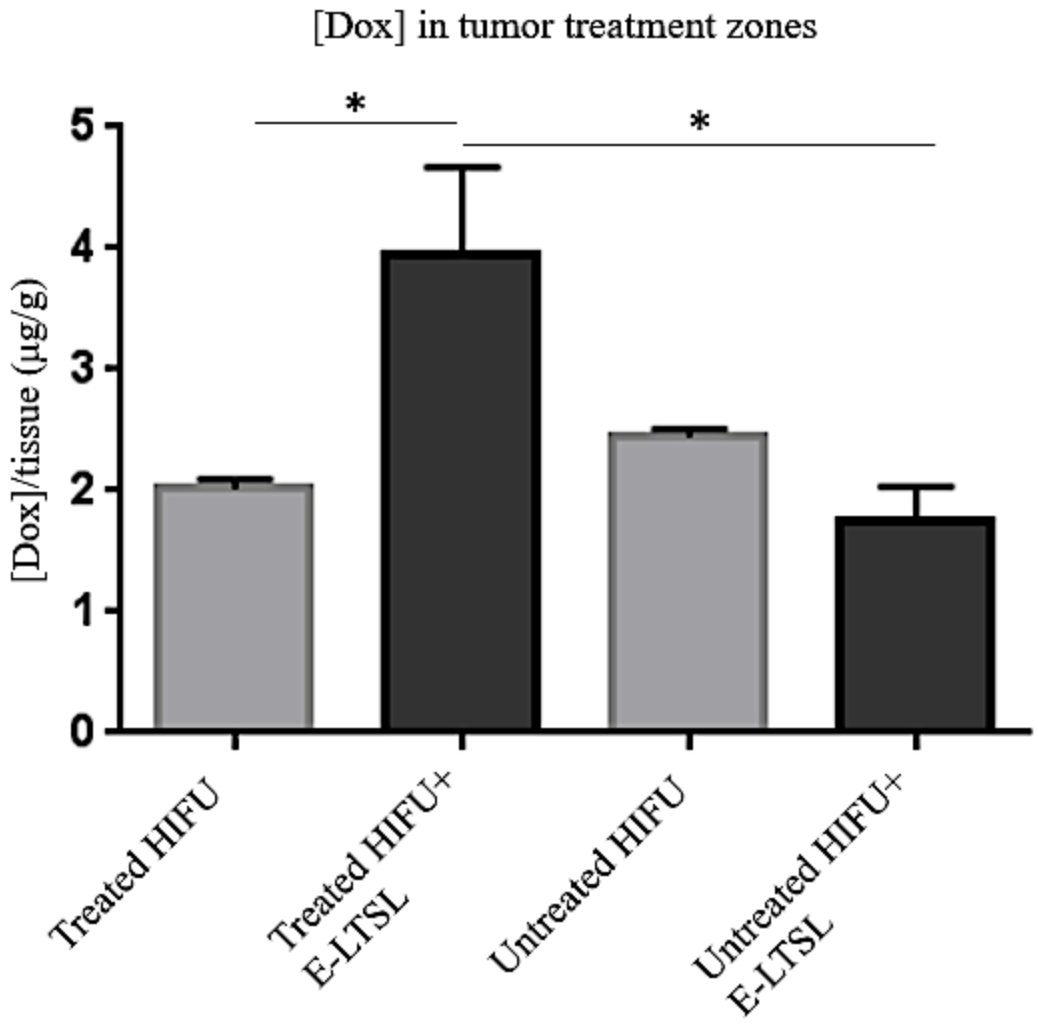

Fig. 3.3. Doxorubicin concentrations in heated regions showed significantly higher dox concentrations for HIFU + E-LTSL compared to other groups. Data are shown as mean Dox concentration ± standard error of mean (n=4; $p < 0.05$, Tukey's multiple comparison). *Indicates significant difference between groups.

HIFU Treatment	Treated		Unheated		Whole Tumor	
	mean	**SEM**	**mean**	**SEM**	**mean**	**SEM**
37ºC	NA	NA	NA	NA	1.2	0.2
HIFU	2.0	0.1	2.4	0.1	2.6	0.1
HIFU + E-LTSL	3.9	0.7	1.7	0.3	3.0	0.3

Table 3.3. Doxorubicin (Dox) concentrations in whole tumor and various treated zones for 37ºC, HIFU, and HIFU + E-LTSL tumors following a 5 mg/kg Dox injection. Data are shown as mean Dox concentration ± standard error of mean (n=4).

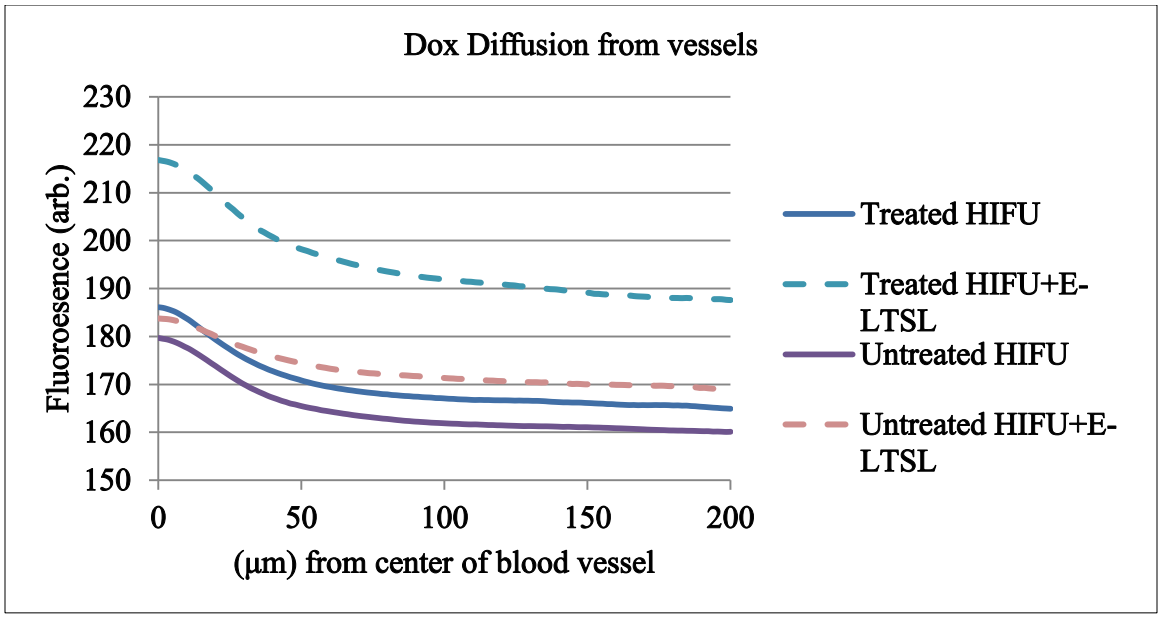

Fig. 3.4. Average fluorescence intensity of Doxorubicin starting from the center of the blood vessel in the treated and unheated regions (± E-LTSL).

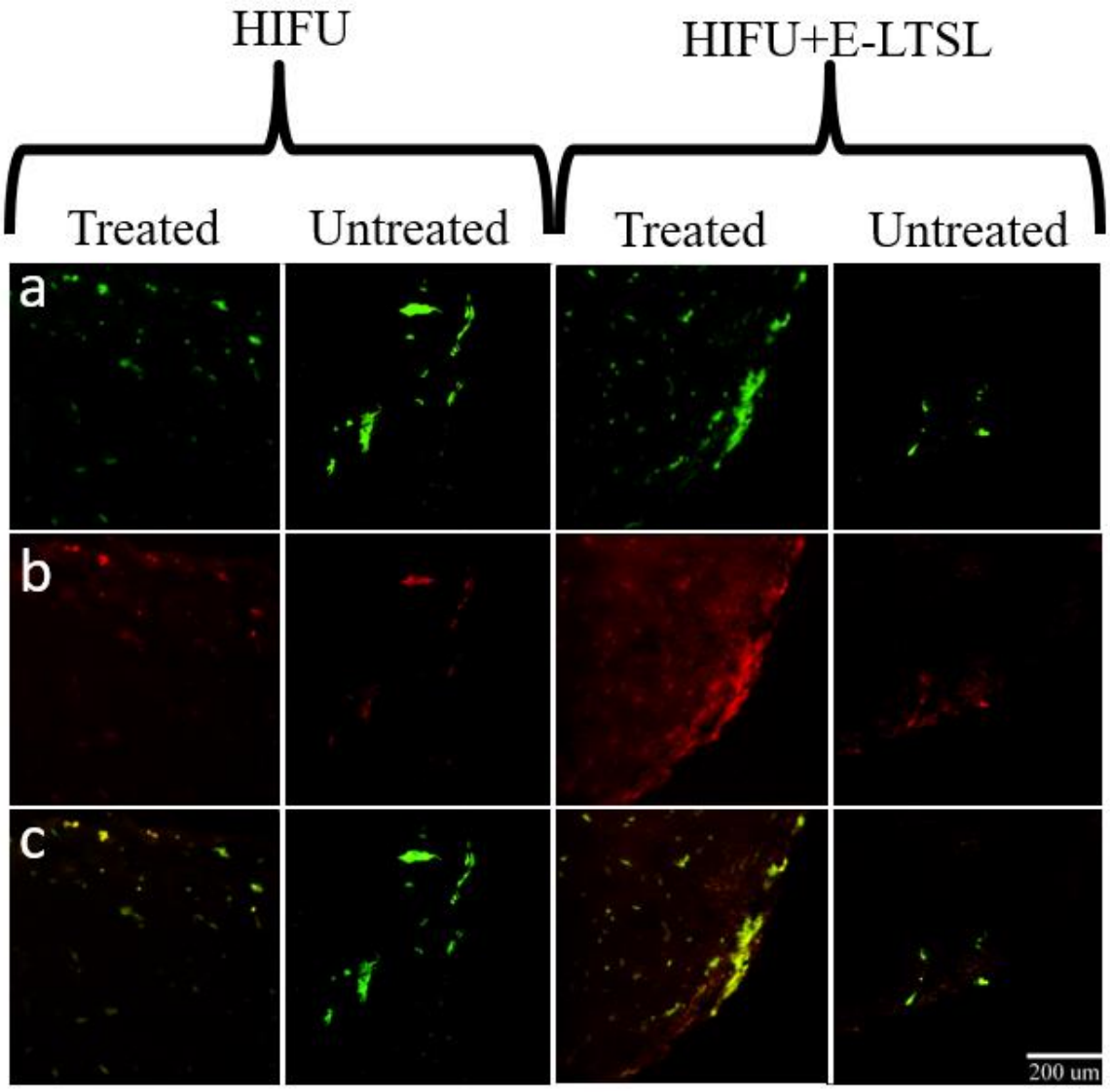

Fig. 3.5. Representative fluorescent images from tumor (±) E-LTSL in treated and untreated tumor regions: **a)** CD-31 fluorescently labeled blood vessels, **b)** Dox fluorescence (pseudo-colored red), **c)** colocalization of Dox with CD31

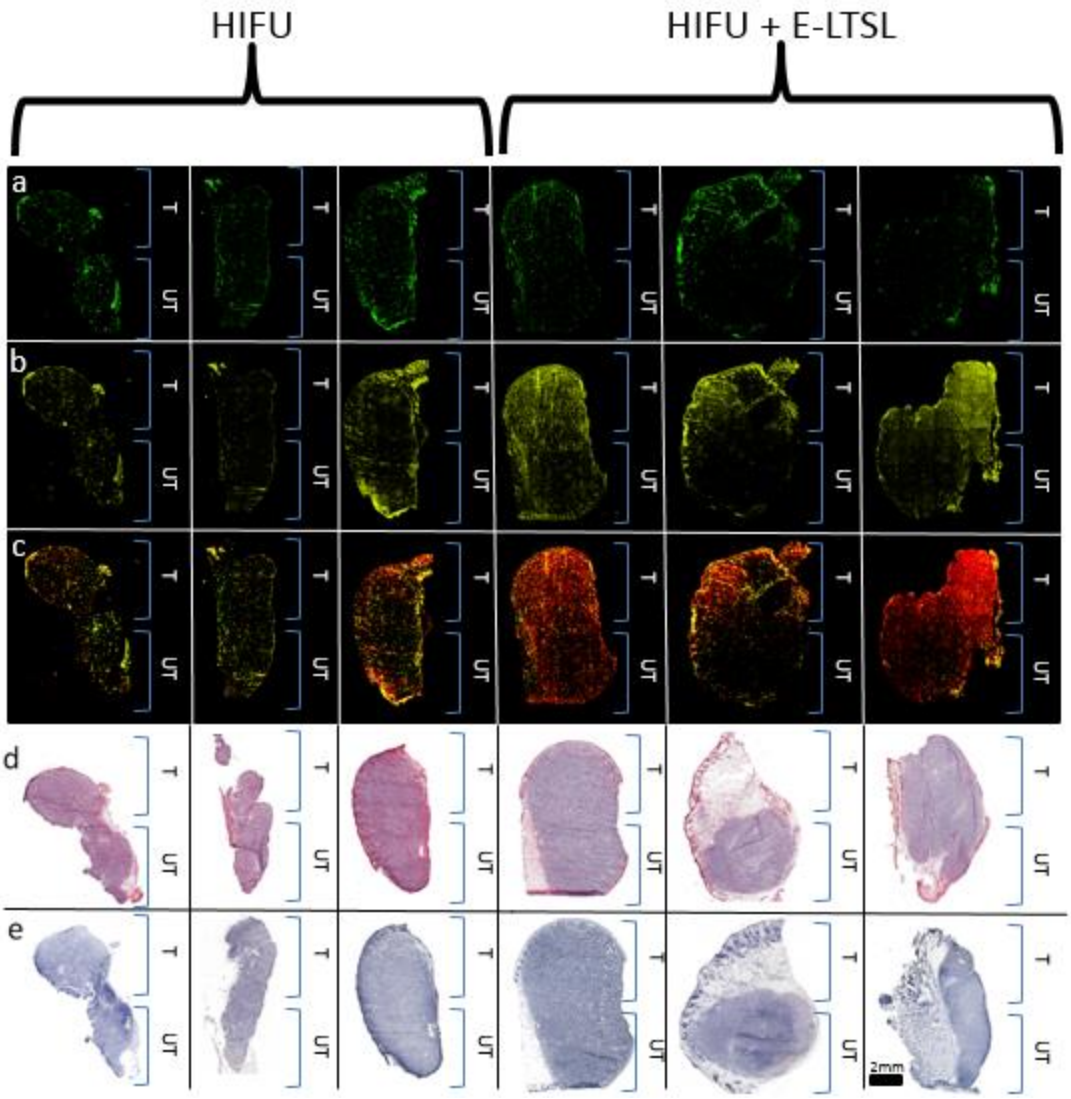

Fig. 3.6. . HIFU treated region in the tumor are labelled as T and the untreated region was labelled as UT. a) CD-31 fluorescently labeled blood vessels. b) Dox fluorescence in various tumor sections. c) colocalization images of Dox and CD31, d) H&E staining, and e) and NBT staining. Both the Treated (T) and Untreated (UT) regions are shown in all the tumor sections.

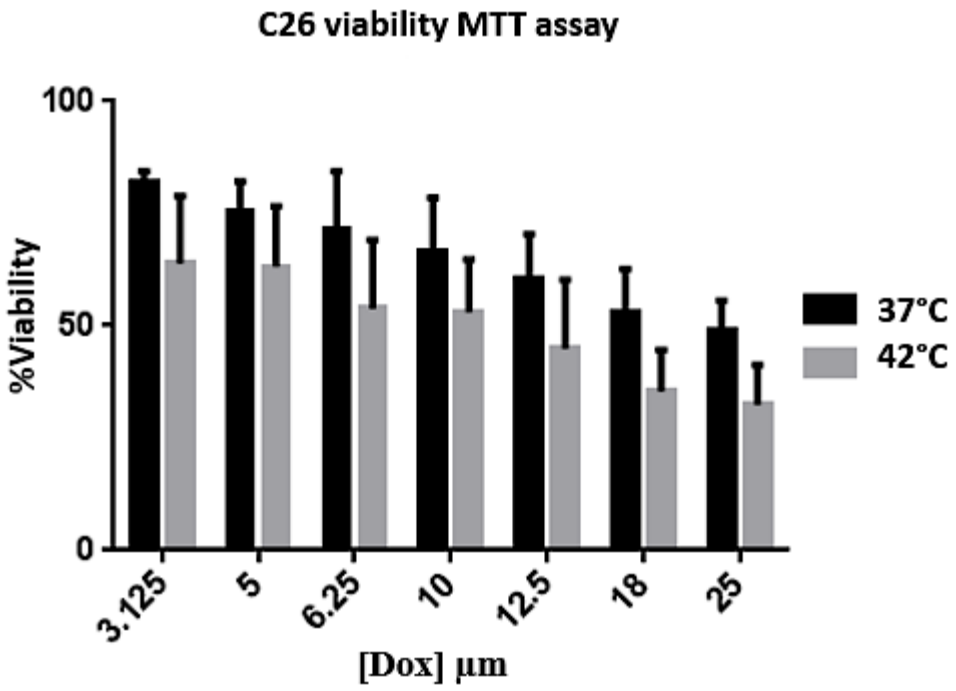

Fig 3.7. MTT was used to measure C-26 cell viability 48h post Dox incubation at 37°C and 42°C. Cells at 37°C were incubated with [Dox] in a concentration range of 3.125-25 µM at 37°C for 4 h. For hyperthermia group, cells were incubated with [Dox] from 3.125-25 µM and simultaneously heated to 42°C for 1h followed by a 3 incubation at 37°C. C26 viability was adversely effected by both increasing [Dox] and hyperthermic treatment. Data are shown as viability% ± standard error of mean (n=3).

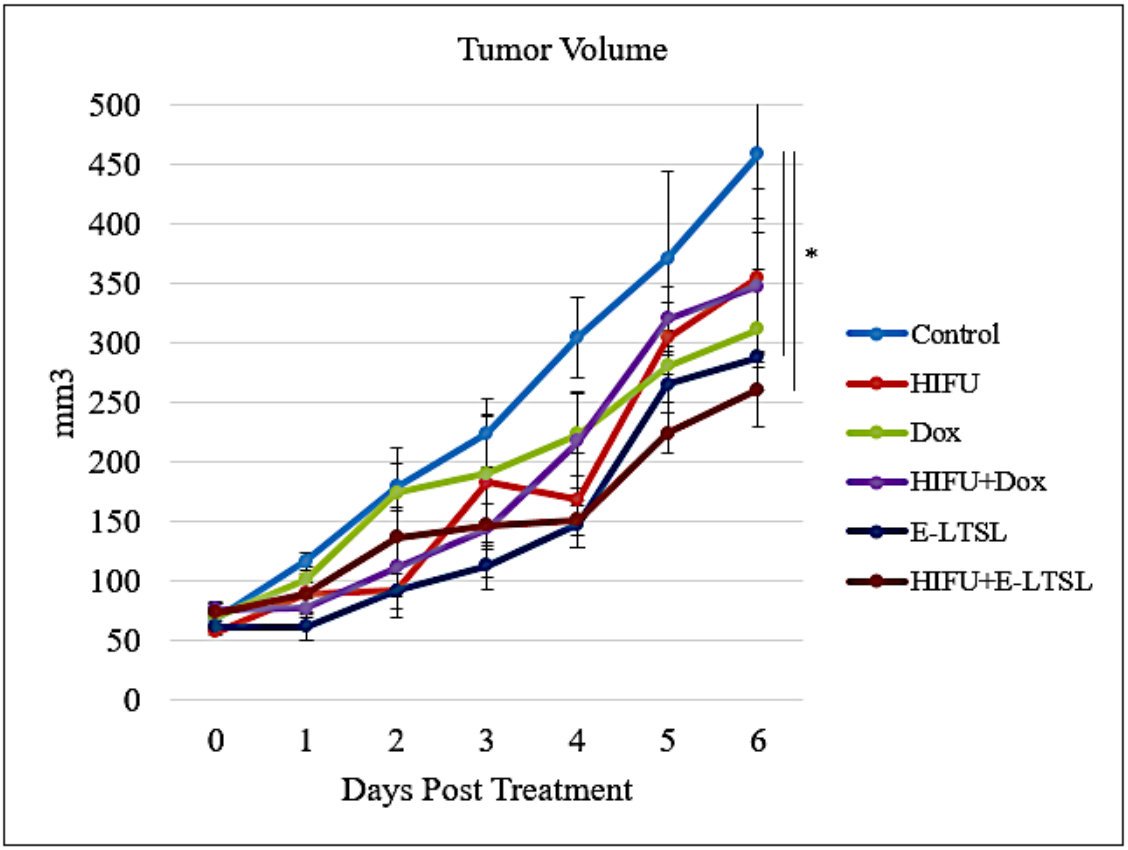

Fig. 3.8. Tumor growth rates in mice following various treatments. Mice bearing C26 tumors were treated at 5 mg/kg Dox injections on day 0, 3 and 6. Data are shown as mean tumor volumes ± standard error of mean (n=4; $p < 0.05$, Tukey's multiple comparison). *Indicates significant difference between treatment groups on Day 6.

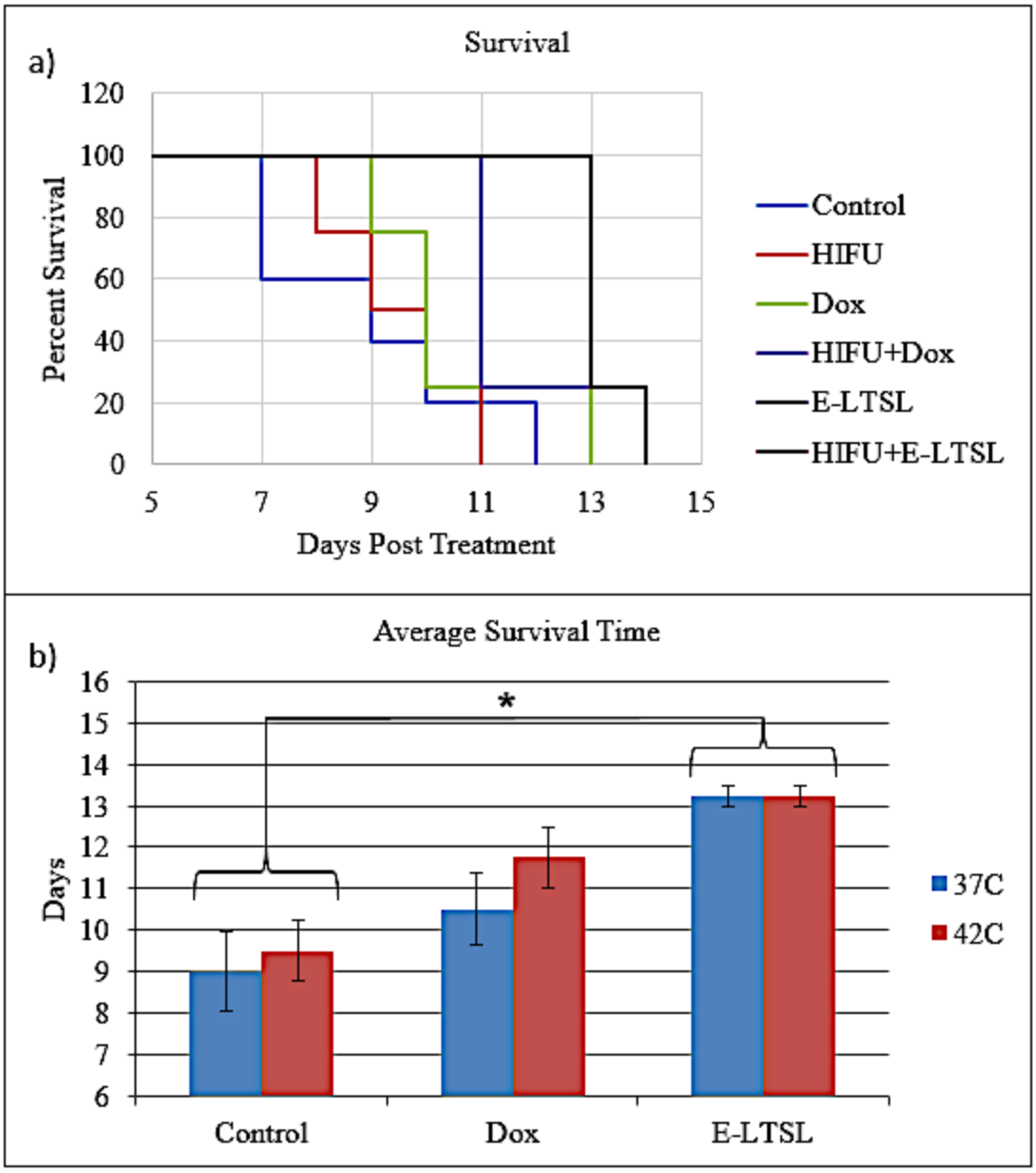

Fig. 3.9. Mean survival of tumor bearing mice following E-LTSL and HIFU treatment. Mice were treated at 5 mg/kg Dox injections on day 0, 3 and 6. a-b) HIFU+E-LTSL and E-LTSL treatments showed enhanced survival than the Control, HIFU, and HIFU+LTSL groups. Data are shown as mean tumor volumes ± standard error (n=4; $p < 0.05$, Tukey's multiple comparison). *Indicates significant difference between groups.

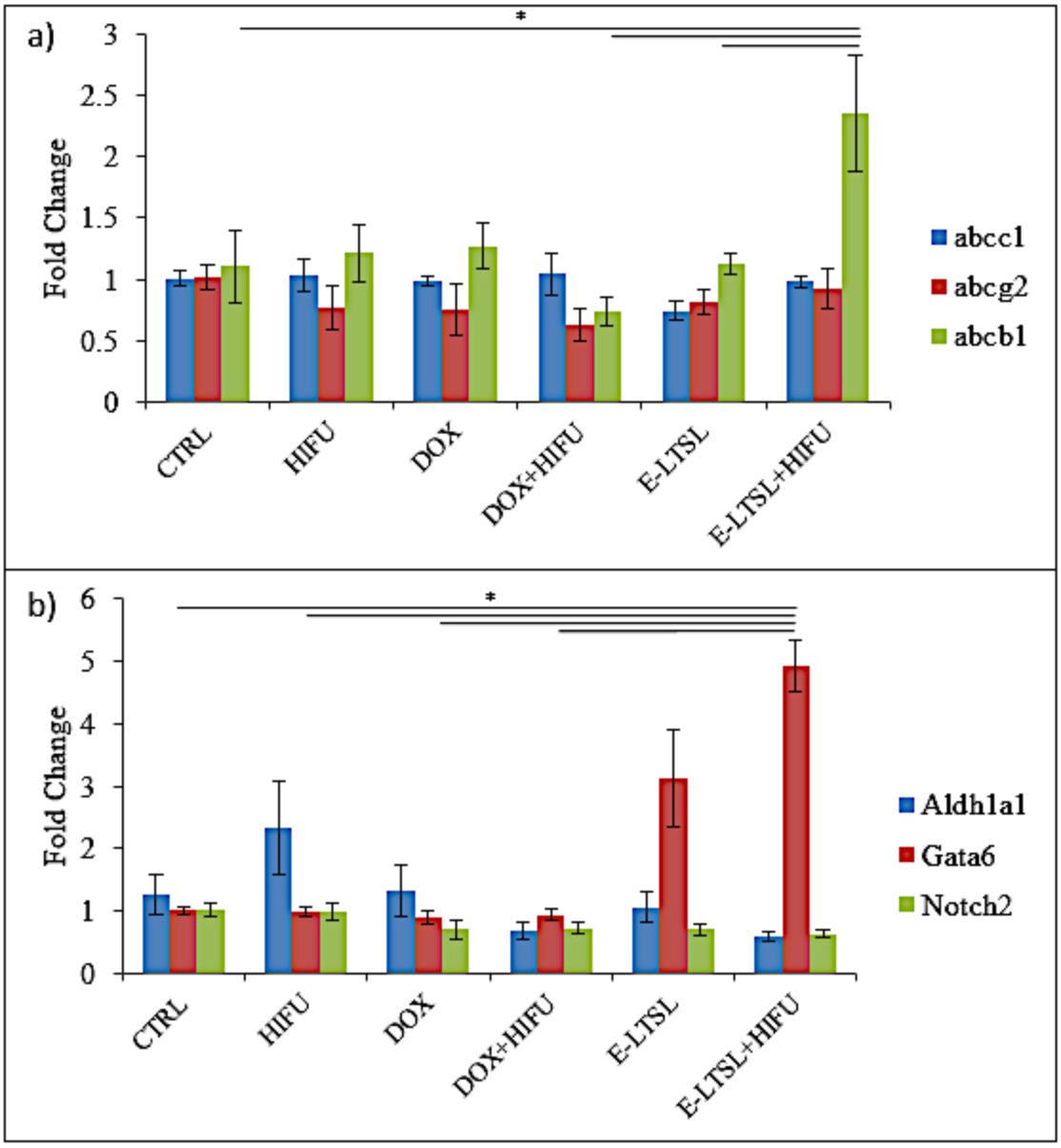

Fig. 3.10. Fold Change in mRNA expression using GAPDH as an endogenous control. **a)** Xenobiotic efflux pump controlling genes (abcg2, abcb1, and abcc1). b) Cancer stem cell markers Aldh1a1 Gata6, and Notch 2. Abcb1 fold change in HIFU+E-LTSL was significantly greater compared to E-LTSL, Dox+HIFU, and control. Gata6 fold change in HIFU+E-LTSL and E-LTSL was significantly greater than all non-liposome groups. Data are shown as mean ± standard error (n = 4). ($p < 0.05$, Tukey's multiple comparison). *Indicates significant difference between groups.

CHAPTER IV

INVESTIGATION OF ANIT-TUMOR EFFECTS OF E-LTSL AND HIFU COMBINATORIAL THERAPY IN A MURINE COLON CANCER MODEL

Abstract

Long-term survival in patients with highly aggressive cancers is dependent on countering the neoplastic growth. Recent studies have shown that the use of checkpoint inhibitors in the chemotherapeutic regimen achieve better survival outcomes. However, an optimal adaptive immune response that achieves clearance of treated and untreated tumor cells require further development. The objectives of this study in murine colon cancer model were to: 1) determine therapeutic efficacies of HIFU activated Low Temperature Sensitive Liposomes (LTSL or T-Dox) and Echogenic Low temperature Sensitive Liposome (E-LTSL) against treated and untreated tumors, 2) analyze the immune profile in treated and untreated CT26 tumors, and 3) determine and compare the immune tolerance mechanisms of the combinatorial therapies. CT26 colon carcinoma cells were implanted in the flanks of immunocompetent BALB/c mice to generate a bilateral tumor model. A single 5mg/kg Dox treatment and HIFU hyperthermia on the right flank (primary tumor) was administered. Treated primary tumors were excised one-week post treatment and the untreated tumors (abscopal tumor) were followed for one-month. Tumors and spleen were characterized for T-cell, macrophage, and dendritic cell activity

by flow cytometry and histological tumor sections were used to confirm leukocyte infiltration into tumors. Results showed that the HIFU+E-LTSL and HIFU+T-Dox treatments slowed primary and abscopal tumor growth compared to the representative controls. Flow cytometry revealed an increase in the population of dendritic cells, M1 macrophages, and functional T-cells in the untreated tumor, and splenic tissues. Furthermore, E-LTSL demonstrated significant infiltrations of leucocytes in the tumor samples with HIFU. Our in vivo data suggests that HIFU activated release of doxorubicin from T-Dox and E-LTSL, and associated bubble activity from E-LTSLs enhanced an immune competent microenvironment and clearance of colon cancer cells.

Introduction

Immunotherapy is fast emerging as the 4th modality of cancer treatment. Immunotherapeutics elicit and/or improve patient outcome by regulating key processes in both cancer cells and white blood cells, and by promoting immune mediated detection and elimination of malignant cells [212-217]. Immunotherapeutic approaches that have shown positive results include the use of immune checkpoint inhibitors such as PD-1 and CTLA-4 blockers [218, 219] and the chimeric antigen receptor T-cells which are host derived cells modified to target their cancerous cells [220, 221].

Prior research has shown that chemotherapeutic drugs within the anthracycline family such as epirubicin, idarubicin, and doxorubicin promote immunogenic cell death (ICD) of tumor cells, which can enhance the activity of CD8+ T cells. One potential mechanism that mediates this effect is the fact that Dox cytotoxicity causes translocation of calreticulin to the cancer cell surface, inducing increased tumor immunogenicity [222].

The effects of Dox and other chemo-immunotherapeutic drugs are largely dependent on their intra-tumoral concentration. For example, treatments that use nanoparticle-based drug carriers such as Doxil improve intratumoral drug concentration, markedly enhancing outcomes in mouse models relative to doxorubicin alone. Importantly, a marked change in tumor growth reduction with Doxil is now known to be dependent on the presence of T-cells, suggesting an ICD based immune effect [207].

In addition to anticancer vaccines, chemotherapy, and modified T-cells, physical treatments such as hyperthermia and the mechanical effects of focused ultrasound have also shown several beneficial effects on the adaptive immune cell population. For example, cancer cells, in response to hyperthermia produce a number of immune-stimulatory agents such as Hsp proteins that help to induce MHC II presentation on dendritic cells and activate the natural killer cells [223]. Additionally, mild hyperthermia can attract leukocytes to the tumor by releasing chemoattractant [224] and improving their adhesion due to expression of ICAM-1 on the endothelial cells [225].

The mechanical and hyperthermia effects of focused ultrasound subject tissues to intensive alternating pressure waves, resulting in cell stress and immuno-stimulatory effects [126]. Different ultrasound parameters yield varying degrees of immune responses. For example, tumor destruction by focused ultrasound ablation and histotripsy enhances white blood cell tumor infiltration and dendritic and T-cell anticancer activity [226, 227]. However, their associated tissue necrosis can reduce the release of antitumor antigen. In contrast, mild hyperthermia grade or pulsed focused ultrasound does not kill cancer cells but induces cell stress and antigen release. Thus, it may reverse tumor immunosuppression, and prime tumors prior to tumor ablation [123, 124]. Additional

methods to increase the effects of HIFU enhanced immune activation in tumors can be with the use of microbubbles or nanobubbles which potentiate associated mechanical stress [228]. Based on this premise, we hypothesized that the combination of HIFU mediated mild hyperthermia in combination with doxorubicin loaded E-LTSL would promote an enhanced immune-stimulatory response compared to conventional Dox treatments. Notably, in Chapter 2 and 3 of this dissertation, HIFU generated nanobubbles from E-LTSL and improved Dox concentration and penetration into colon tumors. However, Chapter 3 showed that the enhanced drug penetration did not translate into measurable differences in tumor growth rate in immunocompromised mice, likely due to an absence of an active T-cell population. Thus, we believe that the characterization of our proposed treatment modality in an immunogenic colon mice model can shed more light on the antitumor effects of our proposed modality. To test our hypothesis, we utilized BALB/c immunocompetent mice harboring bilateral CT26 colon cancers, and these received one of the following eight treatments: Control ± HIFU, Dox ± HIFU, Thermodox ± HIFU, and E-LTSL ± HIFU. Thermodox is a clinically available Dox loaded temperature sensitive liposome similar to LTSL from Chapter 2. Mice received a single HIFU treatment on one tumor (primary tumor), while the other tumor (abscopal tumor) remained untreated. Six days after treatment, treated tumors were surgically removed and the abscopal tumor was monitored up to day 27 post primary tumor inoculation. Flow cytometry was used to assess T-cell, dendritic cell, and macrophage populations to assess response to targeted nanobubbles therapy.

Materials and Methods

Materials

PFP (99%, Exfluor Research Corporation, Round Rock, TX, USA) was used as the US contrast agent. Monostearoyl-2-hydroxy-sn-glycero-3-phosphocholine (MSPC), 1,2-dipalmitoylsn-glycero-3-phosphocholine (DPPC), and 1,2-distearoyl-sn-glycero-3-phosphoethanolamine-N-[methoxy (Polyethylene glycol)2000] (DSPE-mPEG2000) were obtained from Corden Pharma Corporation (Boulder, CO, USA). Dox was obtained from Sigma Aldrich (St. Louis, MO, USA). Thermodox was kindly provided by Celsion Corporation (Lawrenceville, NJ, USA). The PD-10 column was obtained from GE Healthcare Life Sciences, (Buckinghamshire, United Kingdom, UK). CT26 colon cancer cells were obtained from ATCC (Mansassas, VA).

Synthesis of E-LTSLs

LTSLs (lipid composition: DPPC, MSPC, and DSPE-mPEG2000 molar ratio of 85.3:9.7:5.0) were prepared by hydration of a lipid film followed by the extrusion method as described previously [16, 153, 154]. Briefly, lipid mixtures were dissolved in chloroform. The solvent was evaporated and the resulting lipid film was hydrated in citrate buffer (pH 4.0) mixed with 1,3-propanediol (1, 3-PD) (0.65 M, for PFP emulsification) at 55 °C for 30 min and extruded five times through double stacked 200 nm polycarbonate filters to yield a final lipid concentration of 50 mg lipid/mL (80.8 mM for LTSLs). A PD-10 size-exclusion column equilibrated with 5–10 column volumes of 1 × phosphate buffered saline (PBS) was used to remove free 1,3-PD from the outside of the liposomes.

Encapsulation of Dox into the LTSLs was carried out using the pH-gradient loading protocol described by Mayer et al. [152]. Briefly, the outside of the E-LTSLs was

adjusted (by column) to about pH 7.4 using PBS, whereas the inside remained acidic at pH 4. Dox was loaded at 2 mg/100 mg lipid concentration at 37 °C for 1 h. PFP-loaded E-LTSLs were prepared using a one-step sonoporation method. Briefly, 2 mL of the liposomal formulations were incubated under continuous sonication (~ 20 kHz) in 3 mL vials along with PFP (boiling point 30 °C; 20 μL/100 mg lipid) for 1–2 min. PFP and LTSLs were kept cold prior to being combined, and the sonication bath was kept at 4 °C to minimize PFP vaporization.

Study design

All animal-related procedures were approved and carried out under the regulations and guidelines of the Oklahoma State University Animal Care and Use Committee. BALB/c mice bearing bilateral CT26 mouse adenocarcinoma cell tumors were divided into 8 treatment groups: Control, HIFU, Dox ± HIFU, Thermodox ± HIFU, and E-LTSLs ± HIFU. In all groups (n ≥3 mice), 5 mg Dox/kg body weight were administered intravenously.

Establishment of mouse model of colon cancer

CT26 cells were grown as a monolayer to 80-90% confluence in RPMI supplemented with 10% v/v fetal bovine serum (FBS) and 1% v/v streptomycin/penicillin. Confluent cells were harvested, washed, and diluted with sterile cold PBS to generate 10^6 cells/50 μL. Next, 50 μL of cell inoculum was injected per mouse in the right flank region of the mouse using a 25-gauge needle (BD, Franklin Lakes, NJ, USA). Two days later, this was repeated for the left flank similar [229]. Mice were monitored and tumor growth was measured by serial caliper measurements (General Tools Fraction + ™, New York, NY,

USA). Tumor volumes were calculated using the formula (length × width2)/2, where length is the largest dimension and width is the smallest dimension perpendicular to length. Primary tumors, or tumors initially grown on the right flank were allowed to grow to a volume of 60-70 mm3 prior to initiating studies, and treated at 5 mg Dox/kg Body weight IV.

HIFU treatment set-up and methodology

An integrated ultrasound-HIFU alpinion system was used for tumor identification, sonication, and treatment characterization. The HIFU transducer has 1.0 MHz central frequency, 45 mm radius, and 64 mm aperture diameter with a central opening 40 mm in diameter. For HIFU treatments, mice received 30 min of heating. Mice were anesthetized with 2–5% isoflurane and restrained in custom built mouse holders attached to a 3D positioning stage. The tumor bearing flank region was dipped in degassed water maintained at 37 °C for coupling with the HIFU transducer. Using real time ultrasound guidance, the tumors were positioned so that the target was in the center of the focal zone of the transducer. Prior to actual drug delivery study, we calibrated the instrument to a temperature of 42 °C in tumor bearing mice by optimizing the HIFU parameters (duty cycle, pulse repetitive frequency, total acoustic power, and time) as described previously in Chapter III. For hyperthermia treatment, the center of the tumor was aligned with the HIFU focus at a fixed focal depth for efficient coverage, and VIFU-2000 software was used to define the target boundary and slice distance in X, Y, and Z directions. HIFU treatment parameters used were as follows: HIFU treatment parameters used were as follows: 5 Hz frequency, 35% duty cycle, and 6 W acoustic power to achieve a mean target temperature of 40–42.5 °C at the focus. For all mice, blood was collected from

facial vein prior to treatment and both primary and abscopal tumor volumes were recorded for the duration of the study.

Surgical removal of primary tumors and tissue collection

On day 7 post treatment, primary tumors were surgically resected, weighed, and divided into two separate sections: one for flow cytometry, and the other for histopathology. Mice were then monitored for a 20-day period prior to euthanasia. Mice were euthanized if a >15% loss in body weight occurred, if any tumor dimension exceeded 2cm in length, or the tumor volume exceeded 2000mm^3. The abscopal tumor was processed similarly to the primary tumor. The spleen was also collected, weighed, and prepped for splenocyte stimulation. Treatment groups were compared for differences in mean tumor volume and tissue mass using ANOVA followed by pairwise comparison ($p<0.05$) with Fisher's LSD. Quantitative data was expressed as mean ± SEM. (p values < 0.05)

Flow cytometry analysis of leukocytes

Single-cell suspensions obtained from mechanical disruption of the tumors followed by enzymatic digestion (200 U/mL collagenase IV; Life Technologies, NY, USA) were filtered through a 70 μm cell strainer (Corning Inc., Corning, NY). Cells were stained with combinations of the indicated fluorochrome-conjugated anti-mouse antibodies for 30 min in the dark on ice. The antibody combinations used to determine immune profile were CD45, CD11b, CD11c, F4/80, CD86, CD3, CD4, CD8, Foxp3, Ki67, Il2, Granzyme B for dendritic cells, macrophages, and T-cells. To assess colon cancer specific antitumor immunity, splenocytes were stimulated ex-vivo with Gp70 peptide for 8h in the presence of Brefeldin. After 8h of stimulation, cells were washed with PBS and

stained with antibodies to assess T-cell, dendritic cell, and tumor associated macrophages. Treatment groups were compared for mean differences in cell populations and ANOVA followed by pairwise comparison ($p<0.05$) with Fisher's LSD. Quantitative data was expressed as mean ± SEM. (p values < 0.05)

Histopathological evaluation of immune cell infiltration in tumors

Primary and abscopal tumors were assessed for necrosis and the extent of leukocyte infiltration by H&E stained sections (n=3). Median infiltration patterns between treatment groups were compared by ANOVA followed by pairwise comparison ($p<0.05$) with Fisher's LSD by a veterinary pathologist blinded to treatments. Quantitative data was expressed as mean ± SEM. (p values < 0.05).

Results

Tumor growth for treated (primary) and untreated (abscopal) tumors

To evaluate antitumor immune effect of E-LTSL and Thermodox, mice with bilateral tumors received a single treatment in one of the flank tumors. The mean weights for treated tumors were 904.9±233.7, 920.8±252.2, 581.6±138.2, 379.3±62.5, 348.2±115.5, 232.6±24.2, 489±260.0, and 177.7±35.4 mg for Control, HIFU, Dox, HIFU+Dox, T-Dox, HIFU+T-Dox, E-LTSL, and HIFU+E-LTSL respectively. HIFU+E-LTSL and HIFU+T-Dox lowered tumor volume compared to Dox, HIFU, and Control on day 6. The mean tumor volumes for the treated tumor on day 6 for Control, HIFU, Dox, HIFU+Dox, T-Dox, HIFU+T-Dox, E-LTSL, and HIFU+E-LTSL were 407.7±73.4, 441.2±124.7, 350.1±62.4, 209.1±20.9, 199.6±34.1, 143.6±10.9, 277.4±129.9, and 121.1±35.7mm^3 respectively. It may be noted that compared to the athymic nude mice in Chapter 3,

which received three treatments over 6 days, mice in this study received only a single treatment, and still showed significant tumor regression. For example, HIFU+E-LTSL treated athymic BALB/c mice showed- a 2-fold increased volume than the immunocompetent mice. For the untreated abscopal tumors, mean weights for Control, HIFU, Dox, HIFU+Dox, T-Dox, HIFU+T-Dox, E-LTSL, and HIFU+E-LTSL were 2861±322, 2165±553, 2042±799, 1102±238, 1460±474, 764±241, 1739±768, and 729±285mg respectively. The mean abscopal tumor volumes on day 13 for Control, HIFU, Dox, HIFU+Dox, T-Dox, HIFU+T-Dox, E-LTSL, and HIFU+E-LTSL were 820.0±169.3, 747.5±239.7, 364.7±79.2, 258.0±69.9, 586.2±148.7, 194.3±55.8, 269.7±152.7, and 173.9±67.6 mm3 respectively. Both HIFU+E-LTSL and HIFU+T-Dox reduce the growth of tumors in abscopal regions compared to other groups ($p^* < 0.05$ One-way ANOVA; Fisher's LSD. (**Fig. 4.2**))

Splenic Weights

Splenic weights for Control, HIFU, Dox, HIFU+Dox, T-Dox, HIFU+T-Dox, E-LTSL, and HIFU+E-LTSL were 263.3±50.6, 214.2±26.1, 159.2±17.6, 164±14.8, 172.4±13.0, 139.6±15.1, 198.3±38.4, and 152±20.0 mg respectively (**Fig 4.4)**. Data are shown as mean mass ± standard error of mean ($n = 3$, $p < 0.05$ One-way ANOVA; Fisher's LSD).

Leukocyte activation and tumor infiltration analysis via flow cytometry

To investigate the mechanisms of local and systemic tumor regression with E-LTSL and Thermodox, T-cell, Dendritic cell, and Macrophage populations in the primary tumor, secondary tumor, and spleen were quantified using flow cytometry. HIFU+E-LTSL treatment significantly increased Ki67 proliferation marker and CD8+ T-cell populations

(~2-fold and 1.5-fold compared to the untreated control and HIFU+Dox**; Fig 4.5a**). In particular, in the abscopal tumors, the percentage of CD11c+ Dendritic cells increased across all HIFU treated mice compared to the untreated control **(Fig 4.5b)**. Likewise, the percentage of CD3+ T-cells within the abscopal tumor was significantly increased in HIFU plus Dox treatments, with the E-LTSL±HIFU being most efficacious amongst all the treatment groups **(Fig 4.5c)**. These demonstrate that local tumor treatment enhances the dendritic cell infiltration in distal untreated sites and improve the effecter T-cell activity, resulting in an abscopal effect. The activation of systemic immunity was also demonstrated by an enhancement in the population of DC and M1/M2 ratios in the spleen for various treatments compared to the untreated controls. For instance, HIFU plus Dox formulations increased the population of the MHCII+ activated DCs **(4.6 a)**. Similarly, M1 macrophages increased with a concurrent decrease in M2 macrophages for HIFU+Thermodox and HIFU+E-LTSL **(4.6 b-c).**

Histopathology

H&E (n=3) were used to confirm the presence of tumor infiltrating immune cells and type of tumor cell death. Examination of treated and abscopal tumor showed that Dox treatments induced enhanced necrosis compared to the control group. In treated tumors, HIFU+E-LTSL significantly increased the infiltration of immune cells compared to the Control and HIFU. Also, dox alone was more effective compared to HIFU alone (**Fig 4.7** and **Fig 4.8**). The H&E matched the flow cytometry analysis with regards to HIFU+E-LTSL, however, the identification of immune cell sub-types were not assessed.

Discussion

Tumor remission and reducing recurrence are the goals of cancer therapy. The objective of this study was to determine if the immunomodulatory effects of HIFU hyperthermia and E-LTSL-nanobubbles enhances the murine colon cancer regression and survival rates.

Dox's ability to induce ICD is critical to clinical success. Dox induced apoptotic cell death enhances dendritic cell recognition of cancer cells and T-cell activity [230]. In Chapter 3, immunocompromised mice showed reduced tumor growth rates upon increased drug delivery with HIFU and ELTSL, but that didn't translate into enhanced survival time. Thus, the benefits of HIFU/ bubble interaction heavily dependent on leukocyte activation and subsequent recognition of cancer cell populations in tumors [123, 231]. Here, we verified those by the tumor regressions in this study in immunocompetent models where a single treatment on Day 0 ($70mm^3$) showed similar therapeutic effects in athymic BALB/c mice that received a total of three E-LTSL treatments over a period of six days. Notably, the untreated controls demonstrated similar tumor growth rates regardless of the immune status of the mice. In general, HIFU+T-Dox/E-LTSL treated tumors (**Fig 4.2 a** and **Fig 4.3. a)** slowed growth rates compared to all other treatments, however, importantly HIFU+E-LTSL showed a superior outcome than HIFU+Dox in their CD8+T cell proliferation rates (**Fig 4.5 c**). These were also seen in the histological analysis where an increased white blood cell infiltration for E-LTSL/HIFU was noted. Thus, it appears that enhanced Dox concentration in tumor aids the CD8+-T-cell mediated colon cell cytotoxicity [232].

Changes in immune cell activity and numbers were also evident in the abscopal tumor and splenocytes of mice that received HIFU treatments with and without

Dox/nanoparticle combinations. Overall, an increased dendritic cell activity in abscopal tumors and a higher percentage of MHCII+ dendritic cells and macrophages in the spleen for HIFU+E-LTSL and HIFU+Thermodox were noted (**Fig 4.6**), and these correlated to the distant tumor growth rates (**Fig 4.2 b**).

In conclusion, E-LTSL and Thermodox enhanced chemo-immuno-therapeutic effects, antigen expressing dendritic cells and macrophages in untargeted tumor tissue and the spleen. HIFU activated E-LTSL outperformed Thermodox in tumor growth rate reduction in both treated and untreated tumors. CD8+ T-cell infiltration within the treated tumor was also supported by HIFU and E-LTSL compared to Free Dox with HIFU, suggesting a role for nanobubble based delivery modalities in colon cancer immunity.

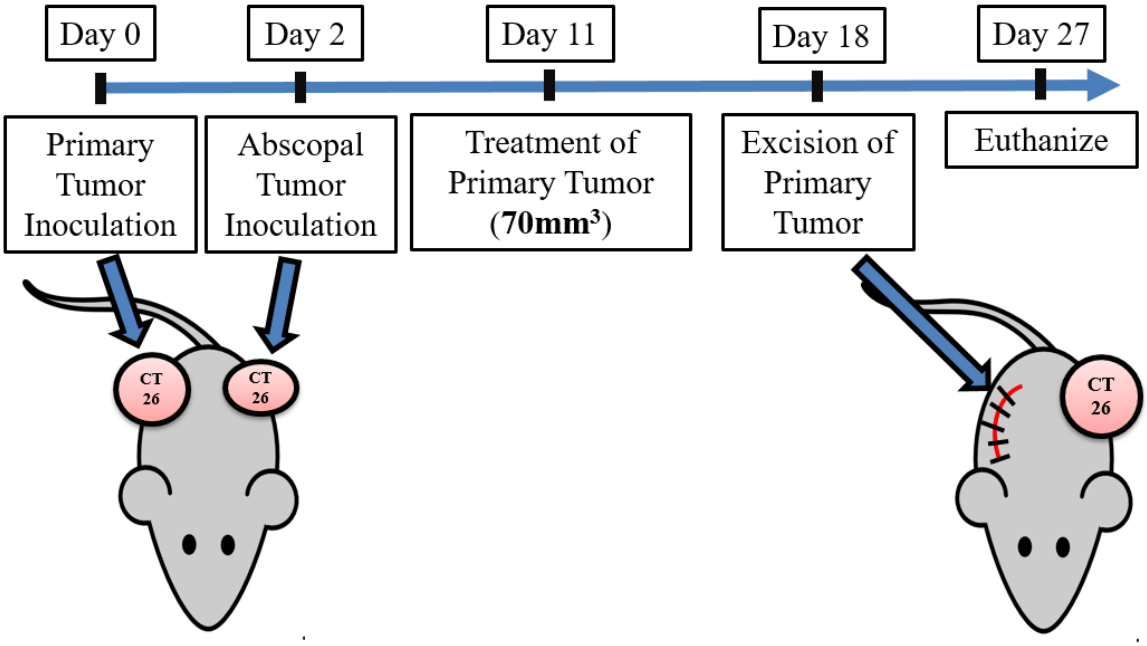

Fig. 4.1. Treatment plan for bilateral mouse model study with E-LTSL and HIFU. Mice were inoculated in the right flank and left flank on day 0 and 2. Treatments were performed when mice tumor reached ~70mm^3. Treated tumors were harvested on day 7 and the untreated flank tumors were followed for 3-4 weeks. At the end of the study, mice were euthanized, and the tumor and spleen tissues were evaluated for immune profile.

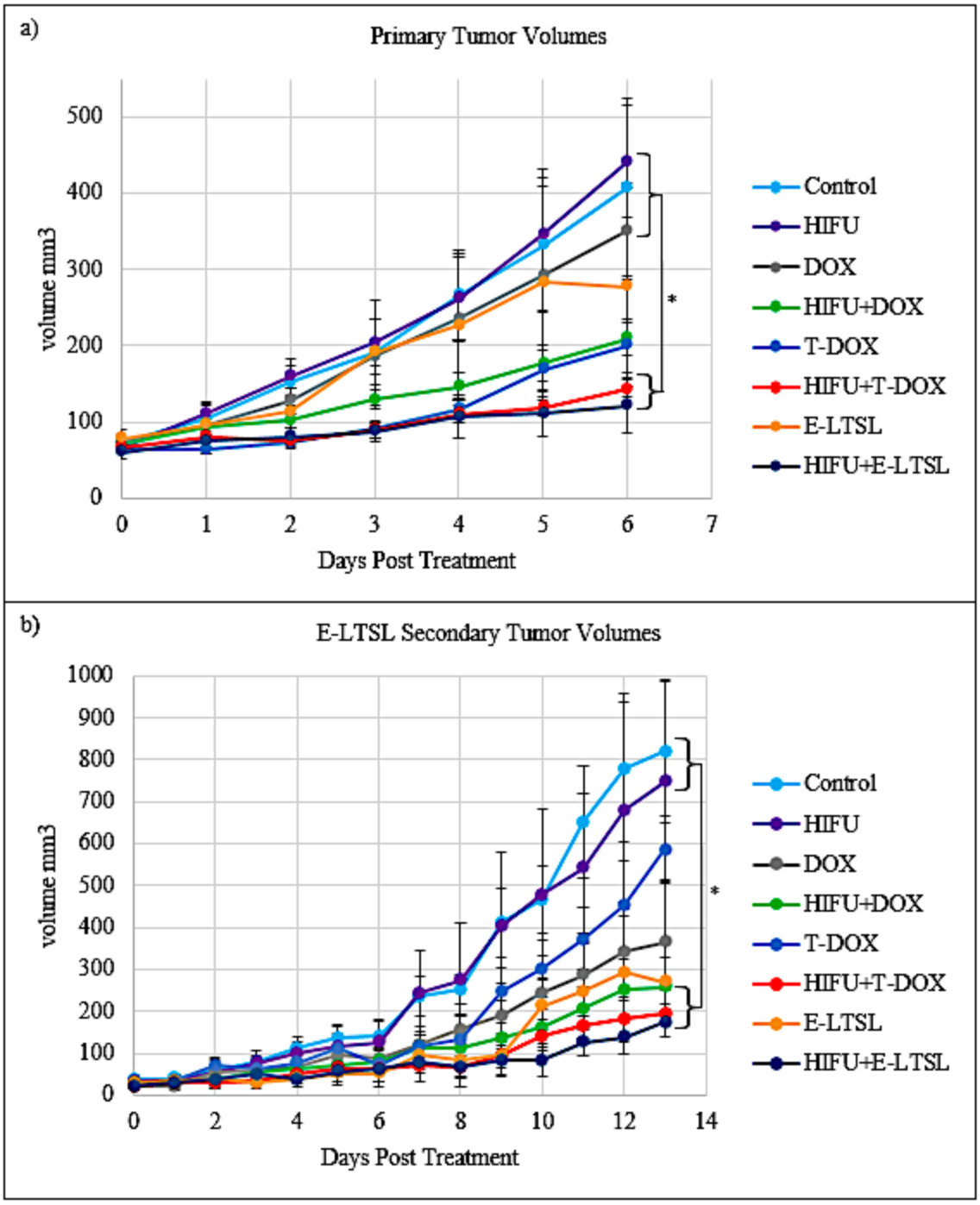

Fig. 4.2. a) CT26 primary tumor volume from day 0 to 6 (5 mg/kg Dox was administered on day 0). HIFU+E-LTSL and HIFU+T-Dox achieved significantly greater regression than Dox on day 6. **b)** HIFU+E-LTSL, HIFU+T-Dox, and HIFU+Dox achieved significantly greater regression than Dox relative to Control in the abscopal sites. Data are shown as mean ± SEM (n=3). (*$p < 0.05$, one-way ANOVA with Fisher's LSD) *Indicates significant difference between groups.

Group	Primary tumor volume day 6 post treatment (mm^3)		Abscopal tumor volume day 13 post treatment (mm^3)	
	Mean	SEM	mean	SEM
Control	407.7	73.4	820.0	169.3
HIFU	441.2	124.7	747.5	239.7
Dox	350.1	62.4	364.7	79.2
HIFU+Dox	209.1	20.9	258.0	69.9
T-Dox	199.6	34.1	586.2	148.7
HIFU+T-Dox	143.6	10.9	194.3	55.8
E-LTSL	277.4	129.9	269.7	152.7
HIFU+E-LTSL	121.1	35.7	173.9	67.6

Table 4.1. Mean volumes of treated and distant tumors for the Control, HIFU, Dox±HIFU, T-Dox±HIFU, and E-LTSL±HIFU. Data are shown as tumor weight ± SEM (n = 3).

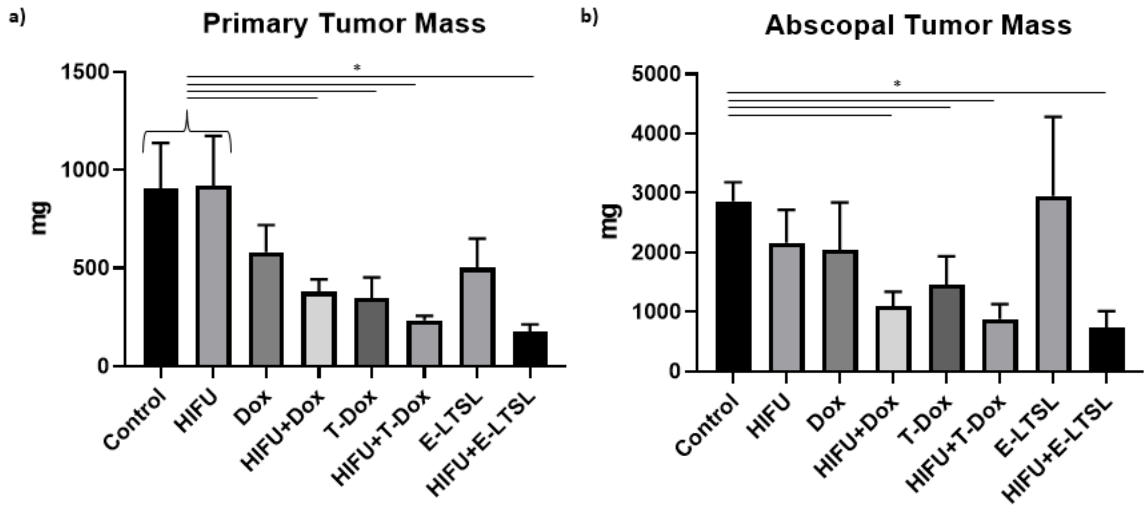

Fig. 4.3. a) HIFU+E-LTSL, HIFU+T-Dox, HIFU+Dox, and T-Dox showed significantly reduced tumor weight than control and HIFU in the treated tumor; **b)** HIFU+E-LTSL, HIFU+T-Dox, HIFU+Dox, and T-Dox demonstrated reduced tumor weights than control in the contralateral sites. Data are shown as mean ± SEM (n=3). (*$p < 0.05$, one-way ANOVA with Fisher's LSD) *Indicates significant difference compared to Control

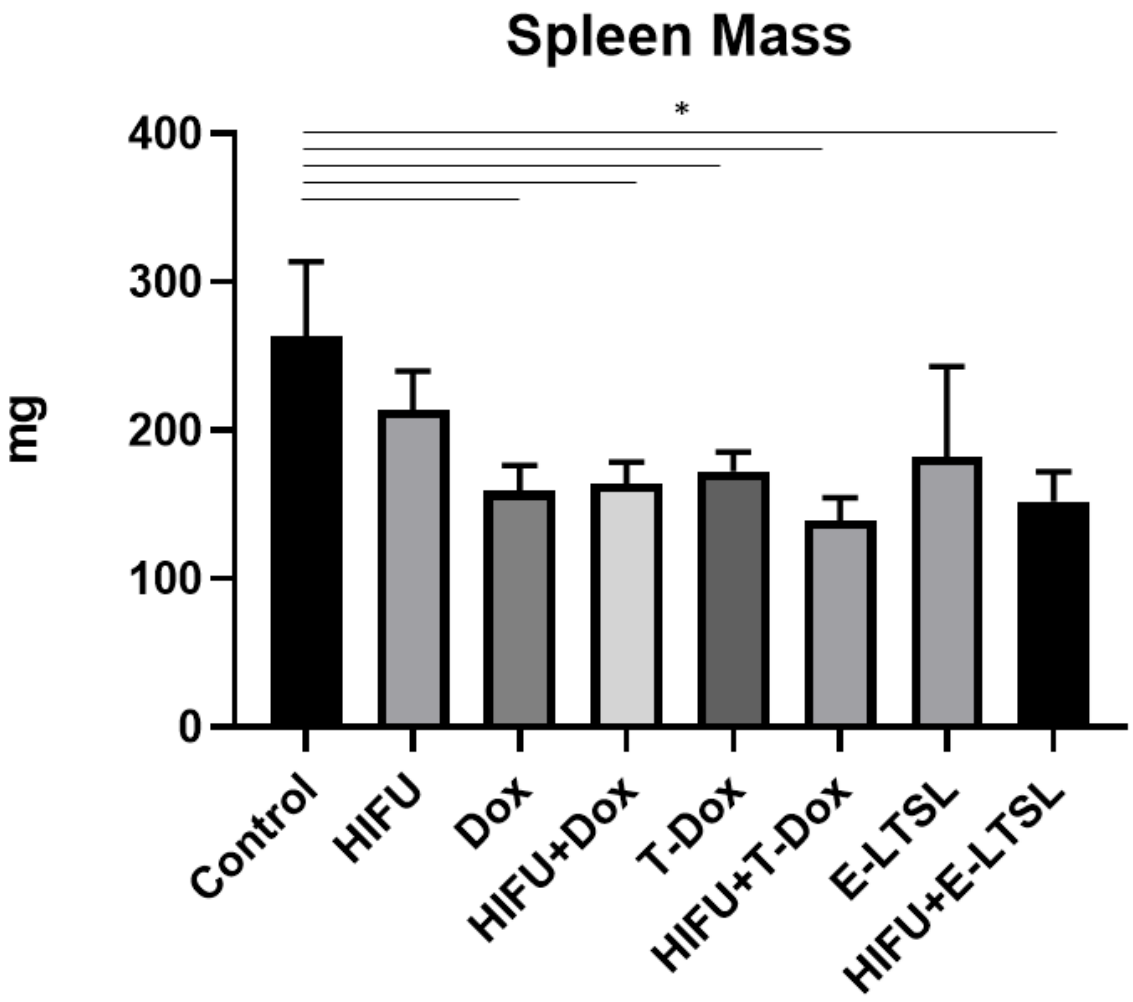

Fig. 4.4. Splenic weight for Control, HIFU, Dox±HIFU, T-Dox±HIFU, and E-LTSL±HIFU were significantly lower than the control, HIFU and E-LTSLs. Data are shown as mean mass ± standard error of mean (n = 3). $p^* < 0.05$ One-way ANOVA; Fisher's LSD. *Indicates significant difference from Control

Group	Primary tumor mass (mg)		Abscopal tumor mass (mg)		Spleen mass (mg)	
	mean	SEM	mean	SEM	mean	SEM
Control	904.9	233.7	2861	322	263.3	50.6
HIFU	920.8	252.2	2165	553	214.2	26.1
Dox	581.6	138.2	2042	799	159.2	17.6
HIFU+Dox	379.3	62.5	1102	238	164.0	14.8
T-Dox	348.2	115.5	1460	474	172.4	13.0
HIFU+T-Dox	232.6	24.2	764	241	139.6	15.1
E-LTSL	489.0	260	1739	768	198.3	38.4
HIFU+E-LTSL	177.7	35.4	729	285	152.0	20.0

Table 4.2. Spleen, primary tumor and abscopal tumor weight for Control, HIFU, Dox±HIFU, T-Dox±HIFU, and E-LTSL±HIFU. Data are shown as mean mass ± SEM (n = 3).

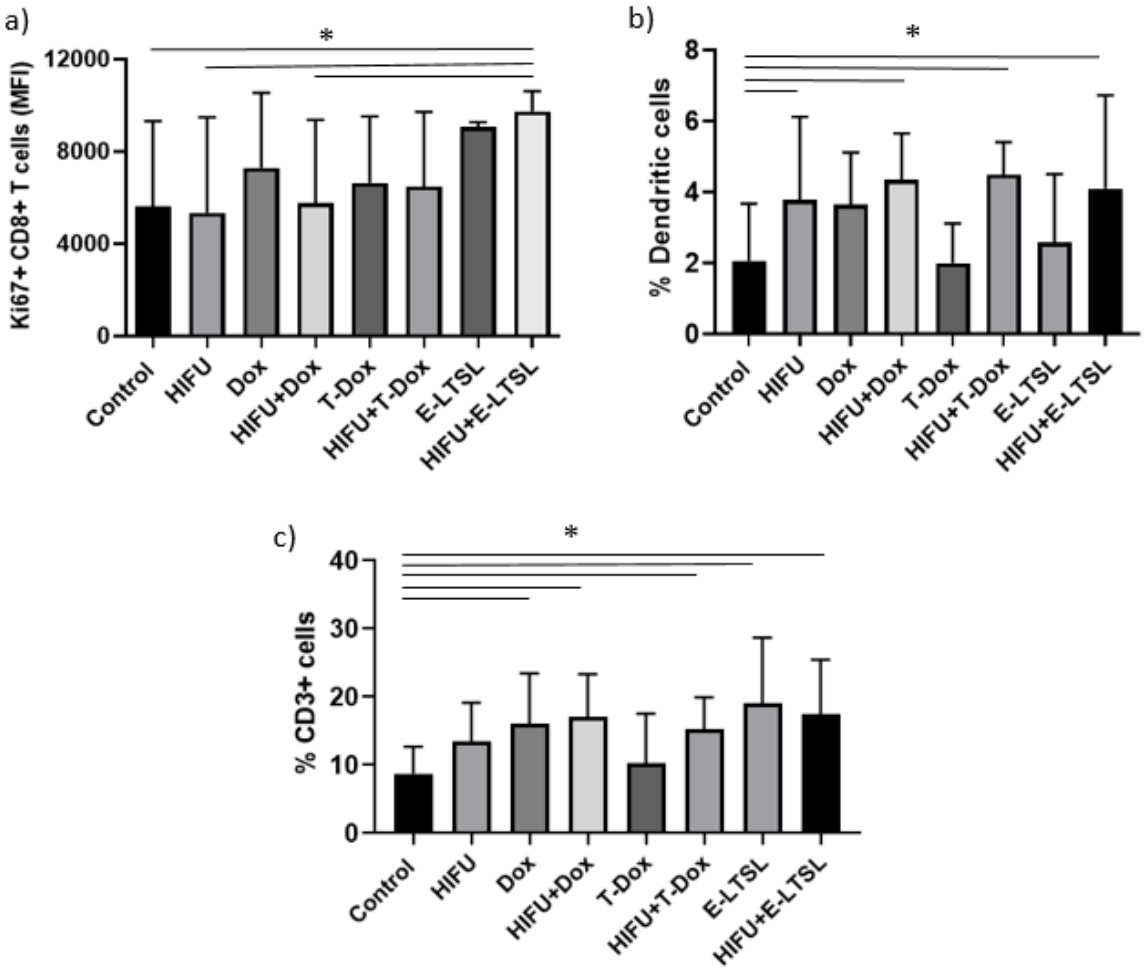

Fig 4.5. HIFU+E-LTSL activated dendritic cells and T cell response against CT26 colon carcinoma. **a)** Infiltration of Ki-67+, CD8+ T-cells in treated tumor for HIFU+E-TLSL was significantly higher than HIFU+ Dox and Control. HIFU+T-Dox was also significantly higher than Control. **b)** Percentage of dendritic cells in abscopal tumors significantly increased for all treatment groups compared to Control and TDox. **c)** Percentage of CD3+ and CD8+ T cell cells in abscopal tumors showed significant increase for the HIFU+E-LTSL treated tumors compared to the Control and HIFU+Dox. (*$p < 0.05$, one-way ANOVA with Fisher's LSD). *Indicates significant difference between groups.

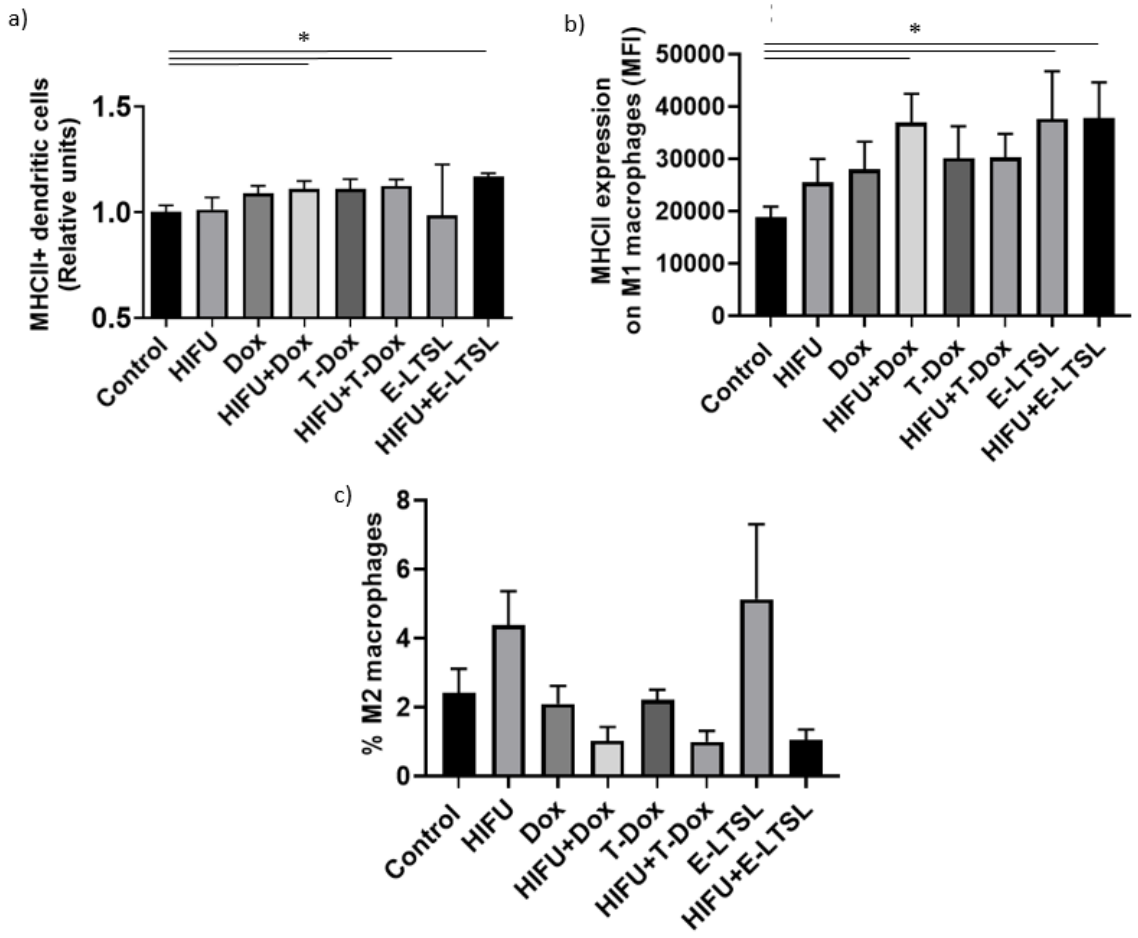

Fig 4.6. HIFU+E-LTSL activated colon cancer specific anti-tumor immunity. **a)** Percentage of activated dendritic cells in spleen. **b)** MHCII expression on M1 macrophage in the spleen expressed as mean fluorescence intensity (MFI). **c)** Percentage of M2 macrophages in spleen. HIFU+Dox, HIFU+T-Dox, and HIFU+ E-LTSL lowered M2 macrophage population and increased MHCII+ M1 macrophage population in the spleen. HIFU+E-LTSL significantly increased MHCII+ dendritic cells in the spleen compared to the Control. Data are shown as mean ± SEM (n=5). (*$p < 0.05$, one-way ANOVA with Fisher's LSD). *Indicates significant difference between groups.

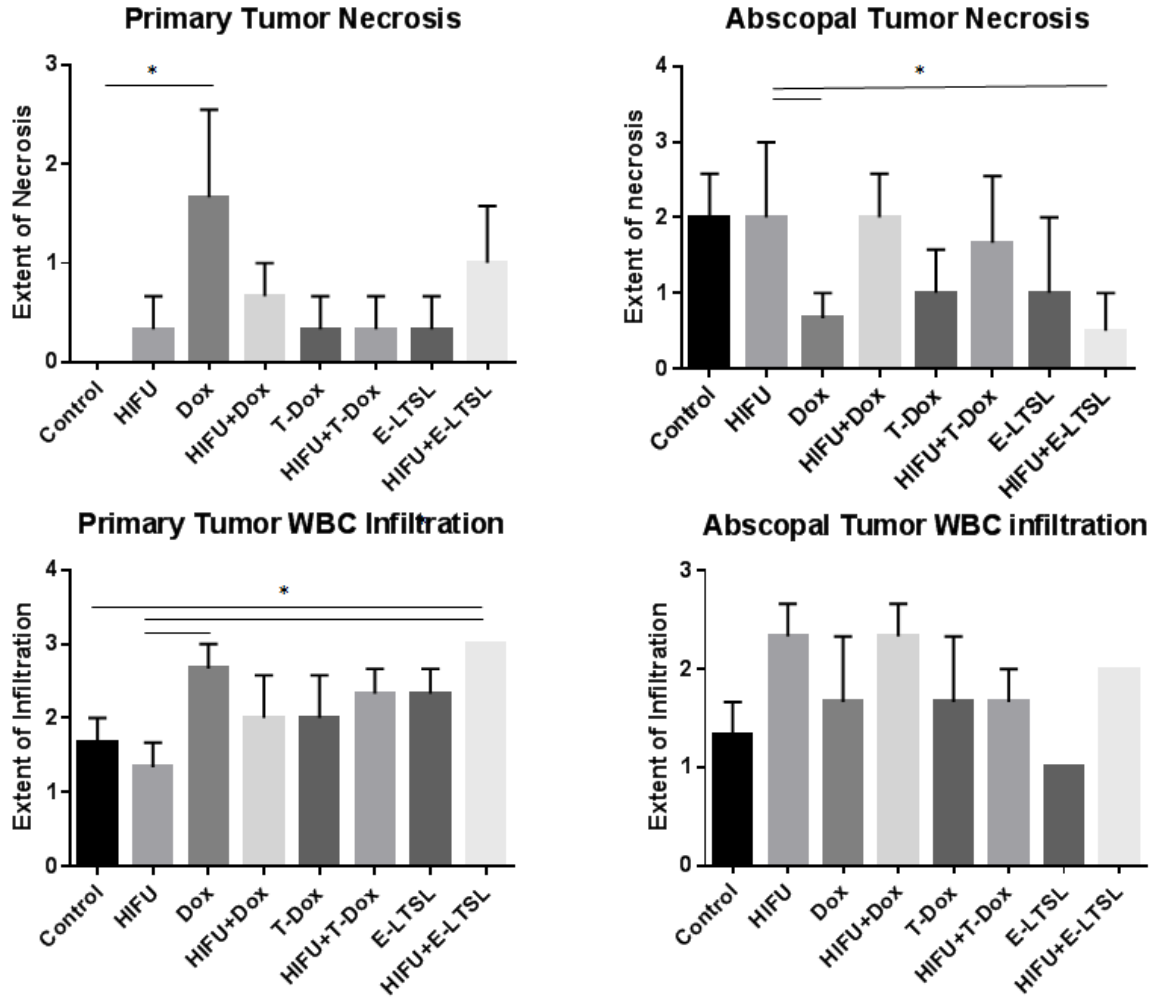

Fig 4.7. a) Mean tumor necrosis based on H&E analysis for **a)** treated primary tumor and **b)** abscopal tumor. The scoring system used was equivalent to approximate percent necrosis: a score of 0, 1, 2, 3, and 4 are equivalent to <10%, 10-25%, 25-50%, 50-75%, and >75% necrosis respectively. Mean leukocyte infiltration (inflammation) score for **c)** treated tumor and **d)** abscopal tumor. Scoring system indicative of leukocyte infiltration: The scoring system used is equivalent to degree of infiltration: a score of 0, 1, 2, 3, and 4 are equivalent to no, minimal, mild, moderate, and extensive leukocyte infiltration respectively. Data are shown as mean ± SEM (n=3). (*$p < 0.05$, one-way ANOVA with Fisher's LSD). *Indicates significant difference between groups.

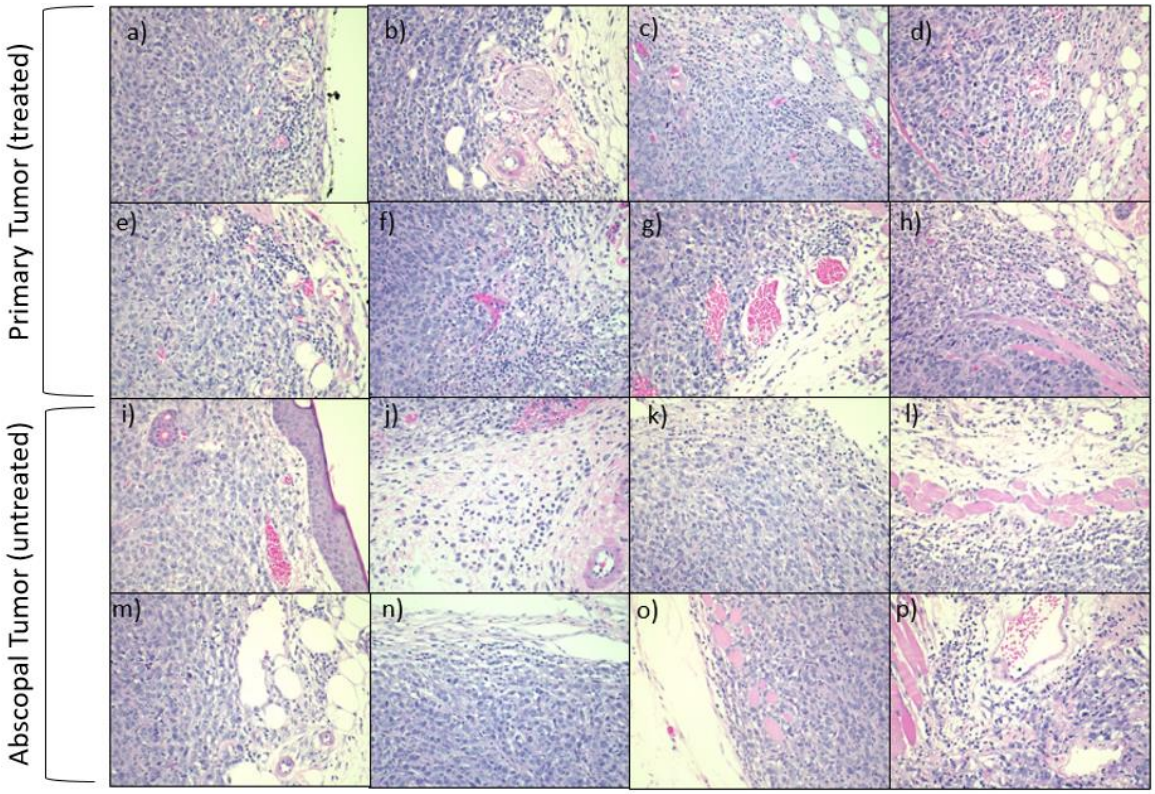

Fig 4.8. Representative H&E sections of primary tumors for **a)** Control, **b)** HIFU, **c)** Dox, **d)** HIFU+Dox, **e)** T-Dox, **f)** HIFU+T-Dox, **g)** E-LTSL, and **h)** HIFU+E-LTSL tumors**.** Representative H&E sections of abscopal tumors for **i)** Control, **j)** HIFU, **k)** Dox, **l)** HIFU+Dox, **m)** T-Dox, **n)** HIFU+T-Dox, **o)** E-LTSL, and **p)** HIFU+E-LTSL tumors**.**

CHAPTER V

DISSERTATION SUMMARY AND CONCLUSIONS

Summary & Conclusions

Colorectal cancer in the United States continues to rise. In 2019 alone, 145,000 newly diagnosed cases were expected to occur, accounting for 9% of all cancer cases [1]. Success of colon carcinoma treatment is dependent on homogeneous drug delivery to the tumors and leveraging the synergistic benefits of immune therapy. We hypothesized that E-LTSL containing Dox and bubble agents as payload would improve drug delivery and immune effects in combination with HIFU based focal treatment, and that the localized treatment would promote systemic response against untreated masses. To investigate this hypothesis, we assessed Dox distribution and penetration in tumors with HIFU/E-LTSL, evaluated efficacy in immune- compromised and -competent C26 colon cancer mouse models, and determined the immune effects in the targeted and untreated (abscopal) tumors. Our data suggested that HIFU+E-LTSL overcome the physical barriers to drug delivery and modulated tumor immune microenvironment to achieve anti-tumor effects in murine colon cancers.

Chapter II

In this chapter, we compared the Dox delivery with HIFU using a wide range of liposomal formulations in a mouse colon carcinoma model. The formulations incorporated features such as high stability in serum and mild hyperthermia (NTSL and E-NTSL), and hyperthermic (40-42.5ºC) Dox release (LTSL and E-LTSL). Additionally, the role of perfluoropentane-based bubble loaded liposomes (E-NTSL and E-LTSL) on Dox penetration in colon tumors were evaluated. Compared to all other groups, HIFU+E-LTSL achieved highest and increased the spatial distribution of Dox within the tumor, resulting in a homogenous drug delivery in the colon tumors. This study demonstrated that E-LTSL mediated Dox penetration into tumor with HIFU hyperthermia.

Chapter III

Here we correlated Dox penetration, tumor microenvironmental changes, and therapeutic efficacy in immunocompromised murine colon cancer model. Fluorescence imaging of tumor sections showed that the presence of the bubble microenvironment aided the extravasation and penetration of encapsulated and un-encapsulated Dox with HIFU. However, the enhanced Dox penetration resulted in only a modest improvement of efficacy in mice lacking T-cells. Quantification of RNA coding for cancer stem cell markers Notch2, Gata6, and Aldhah1 and xenobiotic efflux pumps within the Abc family (which can lead to downstream chemotherapeutic resistance) didn't show clear trends, suggesting that immune rich microenvironment may be hypothetically required for Dox therapeutic effects.

Chapter IV

The objective of this study was to apply HIFU + E-LTSL in an immunocompetent colon cancer mouse model and evaluate therapeutic efficacy and immune profile in treated and untreated tumors. Both E-LTSL and Thermodox, a clinically available low temperature sensitive liposome were evaluated. Immunocompetent BALB/c mice with bilateral flank colon carcinomas received intravenous treatments with the drug agents, and HIFU hyperthermia was applied unilaterally, leaving the contralateral tumor untreated. Tumor growth rate for HIFU+E-LTSL and HIFU+T-Dox showed significant reductions in the treated primary and untreated tumors compared to other groups. Dox release from the liposomes increased the population of CD8+ T-cells tumors, with the E-LTSL/HIFU showing the highest proliferation compared to other groups. Additionally, an immune competent microenvironment with enhanced populations of M1 macrophages and activated dendritic cells in the spleen and untreated tumors were noted. Overall, data from this study suggested that local treatment with heat and liposomes achieved systemic anti-tumor immunity.

Future Perspective

The role of hyperthermia and acoustically derived cell stress on Doxorubicin chemotherapy is not yet well known. We found that co-loading bubble and doxorubicin agents in thermosensitive liposomes, and combination with HIFU heating was highly potent relative to multiple dosages of chemotherapeutic alone in colon cancer treatment. Additional studies in future to understand treatment sequence, dosages, and influence of

multiple acoustic stimulations on tumor recurrence prevention can shed more light on these mechanisms.

A currently emerging field in oncology is the integration of machine learning to help determine treatment responses in cancer. MRI and CT scans of tumors taken following chemotherapy can show subtle tumor features that can be leveraged to predict therapeutic outcomes. In general, ultrasound imaging, while less expensive and widely available typically demonstrates poor image resolutions. Our E-LTSL provides real-time therapeutic imaging, thus it can be hypothetically coupled with machine-learning algorithms to asses real-time tumor drug delivery [233]. These can also be extrapolated to assess tumor inflammation. Thus, E-LTSL can truly serve theranostic agent to guide personalized regimens. We propose that these approaches be developed further in future studies in clinically relevant scenarios.

REFERENCES

1. Siegel, R.L., K.D. Miller, and A. Jemal, *Cancer statistics, 2019.* CA Cancer J Clin, 2019. **69**(1): p. 7-34.
2. Bray, F., et al., *Global cancer statistics 2018: GLOBOCAN estimates of incidence and mortality worldwide for 36 cancers in 185 countries.* CA Cancer J Clin, 2018. **68**(6): p. 394-424.
3. Deckers, R. and C.T.W. Moonen, *Ultrasound triggered, image guided, local drug delivery.* J Control Release, 2010. **148**(1): p. 25-33.
4. Escoffre, J.M., et al., *Focused ultrasound mediated drug delivery from temperature-sensitive liposomes: in-vitro characterization and validation.* Phys Med Biol, 2013. **58**(22): p. 8135-51.
5. Dromi, S., et al., *Pulsed-high intensity focused ultrasound and low temperature-sensitive liposomes for enhanced targeted drug delivery and antitumor effect.* Clin Cancer Res, 2007. **13**(9): p. 2722-7.
6. de Smet, M., et al., *SPECT/CT imaging of temperature-sensitive liposomes for MR-image guided drug delivery with high intensity focused ultrasound.* J Control Release, 2013. **169**(1-2): p. 82-90.
7. Staruch, R.M., et al., *Enhanced drug delivery in rabbit VX2 tumours using thermosensitive liposomes and MRI-controlled focused ultrasound hyperthermia.* Int J Hyperthermia, 2012. **28**(8): p. 776-87.
8. Sutton, J.T., et al., *Pulsed ultrasound enhances the delivery of nitric oxide from bubble liposomes to ex vivo porcine carotid tissue.* Int J Nanomedicine, 2014. **9**: p. 4671-83.
9. Stapleton, S., et al., *Radiation and Heat Improve the Delivery and Efficacy of Nanotherapeutics by Modulating Intratumoral Fluid Dynamics.* ACS Nano, 2018. **12**(8): p. 7583-7600.
10. Grull, H. and S. Langereis, *Hyperthermia-triggered drug delivery from temperature-sensitive liposomes using MRI-guided high intensity focused ultrasound.* J Control Release, 2012. **161**(2): p. 317-27.
11. Kircher, M.F. and J.K. Willmann, *Molecular body imaging: MR imaging, CT, and US. Part II. Applications.* Radiology, 2012. **264**(2): p. 349-68.
12. Kircher, M.F. and J.K. Willmann, *Molecular body imaging: MR imaging, CT, and US. part I. principles.* Radiology, 2012. **263**(3): p. 633-43.
13. Fernando, R., et al., *MRI-Guided Monitoring of Thermal Dose and Targeted Drug Delivery for Cancer Therapy.* Pharm Res, 2013.
14. Deckers, R., et al., *Absolute MR thermometry using nanocarriers.* Contrast Media & Molecular Imaging, 2014(4): p. 283-290

15. Hijnen, N.M., et al., *The magnetic susceptibility effect of gadolinium-based contrast agents on PRFS-based MR thermometry during thermal interventions.* J Ther Ultrasound, 2013. **1**: p. 8.
16. Maples, D., et al., *Synthesis and characterisation of ultrasound imageable heat-sensitive liposomes for HIFU therapy.* Int J Hyperthermia, 2015. **31**(6): p. 674-85.
17. Kandadai, M.A., et al., *Comparison of surfactants used to prepare aqueous perfluoropentane emulsions for pharmaceutical applications.* Langmuir, 2010. **26**(7): p. 4655-60.
18. Multhoff, G., et al., *Heat shock protein 72 on tumor cells: a recognition structure for natural killer cells.* J Immunol, 1997. **158**(9): p. 4341-50.
19. Botzler, C., et al., *Definition of extracellular localized epitopes of Hsp70 involved in an NK immune response.* Cell Stress Chaperones, 1998. **3**(1): p. 6-11.
20. Multhoff, G., et al., *Heat shock protein 70 (Hsp70) stimulates proliferation and cytolytic activity of natural killer cells.* Exp Hematol, 1999. **27**(11): p. 1627-36.
21. Ostberg, J.R., et al., *Enhancement of natural killer (NK) cell cytotoxicity by fever-range thermal stress is dependent on NKG2D function and is associated with plasma membrane NKG2D clustering and increased expression of MICA on target cells.* J Leukoc Biol, 2007. **82**(5): p. 1322-31.
22. Zheng, H., et al., *Heat shock factor 1-independent activation of dendritic cells by heat shock: implication for the uncoupling of heat-mediated immunoregulation from the heat shock response.* Eur J Immunol, 2003. **33**(6): p. 1754-62.
23. Basu, S. and P.K. Srivastava, *Fever-like temperature induces maturation of dendritic cells through induction of hsp90.* Int Immunol, 2003. **15**(9): p. 1053-61.
24. Yoshioka, H., et al., *The influence of hyperthermia in vitro on the functions of peritoneal macrophages in mice.* Jpn J Surg, 1990. **20**(1): p. 119-22.
25. van Bruggen, I., T.A. Robertson, and J.M. Papadimitriou, *The effect of mild hyperthermia on the morphology and function of murine resident peritoneal macrophages.* Exp Mol Pathol, 1991. **55**(2): p. 119-34.
26. Mace, T.A., et al., *Effector CD8+ T cell IFN-gamma production and cytotoxicity are enhanced by mild hyperthermia.* Int J Hyperthermia, 2012. **28**(1): p. 9-18.
27. Dodd, G.D., 3rd, et al., *Minimally invasive treatment of malignant hepatic tumors: at the threshold of a major breakthrough.* Radiographics, 2000. **20**(1): p. 9-27.
28. den Brok, M.H., et al., *In situ tumor ablation creates an antigen source for the generation of antitumor immunity.* Cancer Res, 2004. **64**(11): p. 4024-9.
29. Liu, F., et al., *Boosting high-intensity focused ultrasound-induced anti-tumor immunity using a sparse-scan strategy that can more effectively promote dendritic cell maturation.* J Transl Med, 2010. **8**: p. 7.
30. Xing, Y., et al., *The effect of high intensity focused ultrasound treatment on metastases in a murine melanoma model.* Biochem Biophys Res Commun, 2008. **375**(4): p. 645-50.
31. Cooper, E.L., *From Darwin and Metchnikoff to Burnet and beyond.* Contrib Microbiol, 2008. **15**: p. 1-11.
32. Ehrlich, P., *Address in Pathology, ON CHEMIOTHERAPY: Delivered before the Seventeenth International Congress of Medicine.* Br Med J, 1913. **2**(2746): p. 353-9.
33. Bangham, A.D., *Lipid bilayers and biomembranes.* Annu Rev Biochem, 1972. **41**: p. 753-76.

34. Matsumura, Y. and H. Maeda, *A new concept for macromolecular therapeutics in cancer chemotherapy: mechanism of tumoritropic accumulation of proteins and the antitumor agent smancs.* Cancer Res, 1986. **46**(12 Pt 1): p. 6387-92.
35. Muggia, F.M., *Doxorubicin-polymer conjugates: further demonstration of the concept of enhanced permeability and retention.* Clin Cancer Res, 1999. **5**(1): p. 7-8.
36. Vasey, P.A., et al., *Phase I clinical and pharmacokinetic study of PK1 [N-(2-hydroxypropyl)methacrylamide copolymer doxorubicin]: first member of a new class of chemotherapeutic agents-drug-polymer conjugates. Cancer Research Campaign Phase I/II Committee.* Clin Cancer Res, 1999. **5**(1): p. 83-94.
37. Iwai, K., et al., *Tumor targeting by arterial administration of lipids: rabbit model with VX2 carcinoma in the liver.* Anticancer Res, 1987. **7**(3 Pt B): p. 321-7.
38. Hanahan, D. and R.A. Weinberg, *The hallmarks of cancer.* Cell, 2000. **100**(1): p. 57-70.
39. Bouck, N., V. Stellmach, and S.C. Hsu, *How tumors become angiogenic.* Adv Cancer Res, 1996. **69**: p. 135-74.
40. Barenholz, Y., *Doxil(R)--the first FDA-approved nano-drug: lessons learned.* J Control Release, 2012. **160**(2): p. 117-34.
41. Gabizon, A., et al., *Prolonged circulation time and enhanced accumulation in malignant exudates of doxorubicin encapsulated in polyethylene-glycol coated liposomes.* Cancer Res, 1994. **54**(4): p. 987-92.
42. Gabizon, A., H. Shmeeda, and Y. Barenholz, *Pharmacokinetics of pegylated liposomal Doxorubicin: review of animal and human studies.* Clin Pharmacokinet, 2003. **42**(5): p. 419-36.
43. Aftab, S., et al., *Nanomedicine: An effective tool in cancer therapy.* Int J Pharm, 2018. **540**(1-2): p. 132-149.
44. Bardania, H., S. Tarvirdipour, and F. Dorkoosh, *Liposome-targeted delivery for highly potent drugs.* Artif Cells Nanomed Biotechnol, 2017. **45**(8): p. 1478-1489.
45. Jain, A. and Jain, *Advances in Tumor Targeted Liposomes.* Curr Mol Med, 2018. **18**(1): p. 44-57.
46. Kalmouni, M., S. Al-Hosani, and M. Magzoub, *Cancer targeting peptides.* Cell Mol Life Sci, 2019. **76**(11): p. 2171-2183.
47. Lu, Z.R. and P. Qiao, *Drug Delivery in Cancer Therapy, Quo Vadis?* Mol Pharm, 2018. **15**(9): p. 3603-3616.
48. Maslov, M., S. Foianini, and M. Lovich, *Delivery of drugs, growth factors, genes and stem cells via intrapericardial, epicardial and intramyocardial routes for sustained local targeted therapy of myocardial disease.* Expert Opin Drug Deliv, 2017. **14**(10): p. 1227-1239.
49. Mozar, F.S. and E.H. Chowdhury, *Impact of PEGylated Nanoparticles on Tumor Targeted Drug Delivery.* Curr Pharm Des, 2018. **24**(28): p. 3283-3296.
50. James, J.S., *DOXIL approved for KS.* AIDS Treat News, 1995(no 236): p. 6.
51. Fokas, E., W.G. McKenna, and R.J. Muschel, *The impact of tumor microenvironment on cancer treatment and its modulation by direct and indirect antivascular strategies.* Cancer Metastasis Rev, 2012. **31**(3-4): p. 823-42.
52. Galizia, G., et al., *First-line chemotherapy vs bowel tumor resection plus chemotherapy for patients with unresectable synchronous colorectal hepatic metastases.* Arch Surg, 2008. **143**(4): p. 352-8; discussion 358.

53. Nash, G.M., et al., *Radical resection of rectal cancer primary tumor provides effective local therapy in patients with stage IV disease.* Ann Surg Oncol, 2002. **9**(10): p. 954-60.
54. Stillwell, A.P., P.G. Buettner, and Y.H. Ho, *Meta-analysis of survival of patients with stage IV colorectal cancer managed with surgical resection versus chemotherapy alone.* World J Surg, 2010. **34**(4): p. 797-807.
55. Lin, C.S., et al., *Managements of locally advanced unresectable thymic epithelial tumors.* J Chin Med Assoc, 2004. **67**(4): p. 172-8.
56. Bilici, A., *Advances in the management of unresectable or metastatic pancreatic neuroendocrine tumors: chemotherapy, targeted therapy, hormonal treatment, and future directions.* Asian Pac J Cancer Prev, 2015. **16**(6): p. 2151-9.
57. Huang, C.Y., et al., *A review on the effects of current chemotherapy drugs and natural agents in treating non-small cell lung cancer.* Biomedicine (Taipei), 2017. **7**(4): p. 23.
58. Park, S.M., et al., *Novel temperature-triggered liposome with high stability: formulation, in vitro evaluation, and in vivo study combined with high-intensity focused ultrasound (HIFU).* J Control Release, 2013. **170**(3): p. 373-9.
59. Santos, M.A., D.E. Goertz, and K. Hynynen, *Focused Ultrasound Hyperthermia Mediated Drug Delivery Using Thermosensitive Liposomes and Visualized With in vivo Two-Photon Microscopy.* Theranostics, 2017. **7**(10): p. 2718-2731.
60. Ta, T., et al., *Localized delivery of doxorubicin in vivo from polymer-modified thermosensitive liposomes with MR-guided focused ultrasound-mediated heating.* J Control Release, 2014. **194**: p. 71-81.
61. Ranjan, A., et al., *Image-guided drug delivery with magnetic resonance guided high intensity focused ultrasound and temperature sensitive liposomes in a rabbit Vx2 tumor model.* J Control Release, 2012. **158**(3): p. 487-94.
62. Graham, S.M., et al., *Inertial cavitation to non-invasively trigger and monitor intratumoral release of drug from intravenously delivered liposomes.* J Control Release, 2014. **178**: p. 101-7.
63. Maruyama, K., et al., *[Drug and gene delivery by "bubble liposomes" and ultrasound].* Yakugaku Zasshi, 2007. **127**(5): p. 781-7.
64. Afshar-Kharghan, V., *The role of the complement system in cancer.* J Clin Invest, 2017. **127**(3): p. 780-789.
65. Gonzalez, H., C. Hagerling, and Z. Werb, *Roles of the immune system in cancer: from tumor initiation to metastatic progression.* Genes Dev, 2018. **32**(19-20): p. 1267-1284.
66. Lisovska, N. and N. Shanazarov, *Tumor progression mechanisms: Insights from the central immune regulation of tissue homeostasis.* Oncol Lett, 2019. **17**(6): p. 5311-5318.
67. Wu, D., *Innate and Adaptive Immune Cell Metabolism in Tumor Microenvironment.* Adv Exp Med Biol, 2017. **1011**: p. 211-223.
68. Ektate, K., et al., *Chemo-immunotherapy of colon cancer with focused ultrasound and Salmonella-laden temperature sensitive liposomes (thermobots).* Sci Rep, 2018. **8**(1): p. 13062.
69. Lamsam, L., et al., *A review of potential applications of MR-guided focused ultrasound for targeting brain tumor therapy.* Neurosurg Focus, 2018. **44**(2): p. E10.
70. Unga, J. and M. Hashida, *Ultrasound induced cancer immunotherapy.* Adv Drug Deliv Rev, 2014. **72**: p. 144-53.
71. Housman, G., et al., *Drug resistance in cancer: an overview.* Cancers (Basel), 2014. **6**(3): p. 1769-92.

72. Fic, M., et al., *The Impact of Melatonin on Colon Cancer Cells' Resistance to Doxorubicin in an in Vitro Study.* Int J Mol Sci, 2017. **18**(7).
73. Michieli, M., et al., *P-glycoprotein, lung resistance-related protein and multidrug resistance associated protein in de novo acute non-lymphocytic leukaemias: biological and clinical implications.* Br J Haematol, 1999. **104**(2): p. 328-35.
74. van der Zee, A.G., et al., *Value of P-glycoprotein, glutathione S-transferase pi, c-erbB-2, and p53 as prognostic factors in ovarian carcinomas.* J Clin Oncol, 1995. **13**(1): p. 70-8.
75. Duan, Z., E. Choy, and F.J. Hornicek, *NSC23925, identified in a high-throughput cell-based screen, reverses multidrug resistance.* PLoS One, 2009. **4**(10): p. e7415.
76. Allen, J.D. and A.H. Schinkel, *Multidrug resistance and pharmacological protection mediated by the breast cancer resistance protein (BCRP/ABCG2).* Mol Cancer Ther, 2002. **1**(6): p. 427-34.
77. Diestra, J.E., et al., *Frequent expression of the multi-drug resistance-associated protein BCRP/MXR/ABCP/ABCG2 in human tumours detected by the BXP-21 monoclonal antibody in paraffin-embedded material.* J Pathol, 2002. **198**(2): p. 213-9.
78. Cole, S.P. and R.G. Deeley, *Multidrug resistance mediated by the ATP-binding cassette transporter protein MRP.* Bioessays, 1998. **20**(11): p. 931-40.
79. van der Waals, L.M., I.H.M. Borel Rinkes, and O. Kranenburg, *ALDH1A1 expression is associated with poor differentiation, 'right-sidedness' and poor survival in human colorectal cancer.* PLoS One, 2018. **13**(10): p. e0205536.
80. Rodriguez-Torres, M. and A.L. Allan, *Aldehyde dehydrogenase as a marker and functional mediator of metastasis in solid tumors.* Clin Exp Metastasis, 2016. **33**(1): p. 97-113.
81. Belaguli, N.S., et al., *GATA6 promotes colon cancer cell invasion by regulating urokinase plasminogen activator gene expression.* Neoplasia, 2010. **12**(11): p. 856-65.
82. Capo-chichi, C.D., et al., *Anomalous expression of epithelial differentiation-determining GATA factors in ovarian tumorigenesis.* Cancer Res, 2003. **63**(16): p. 4967-77.
83. Kamnasaran, D., et al., *GATA6 is an astrocytoma tumor suppressor gene identified by gene trapping of mouse glioma model.* Proc Natl Acad Sci U S A, 2007. **104**(19): p. 8053-8.
84. Becker, J.C., et al., *Immune-suppressive properties of the tumor microenvironment.* Cancer Immunol Immunother, 2013. **62**(7): p. 1137-48.
85. Dunn, G.P., et al., *Cancer immunoediting: from immunosurveillance to tumor escape.* Nat Immunol, 2002. **3**(11): p. 991-8.
86. Garrido, F., et al., *Implications for immunosurveillance of altered HLA class I phenotypes in human tumours.* Immunol Today, 1997. **18**(2): p. 89-95.
87. Tevis, K.M., et al., *Mimicking the tumor microenvironment to regulate macrophage phenotype and assessing chemotherapeutic efficacy in embedded cancer cell/macrophage spheroid models.* Acta Biomater, 2017. **50**: p. 271-279.
88. De Palma, M. and C.E. Lewis, *Macrophage regulation of tumor responses to anticancer therapies.* Cancer Cell, 2013. **23**(3): p. 277-86.
89. Amit, M. and Z. Gil, *Macrophages increase the resistance of pancreatic adenocarcinoma cells to gemcitabine by upregulating cytidine deaminase.* Oncoimmunology, 2013. **2**(12): p. e27231.
90. Sica, A., et al., *Macrophage polarization in tumour progression.* Semin Cancer Biol, 2008. **18**(5): p. 349-55.

91. van Kempen, L.C., et al., *The tumor microenvironment: a critical determinant of neoplastic evolution.* Eur J Cell Biol, 2003. **82**(11): p. 539-48.
92. Shree, T., et al., *Macrophages and cathepsin proteases blunt chemotherapeutic response in breast cancer.* Genes Dev, 2011. **25**(23): p. 2465-79.
93. Mielgo, A. and M.C. Schmid, *Impact of tumour associated macrophages in pancreatic cancer.* BMB Rep, 2013. **46**(3): p. 131-8.
94. Beatty, G.L., et al., *CD40 agonists alter tumor stroma and show efficacy against pancreatic carcinoma in mice and humans.* Science, 2011. **331**(6024): p. 1612-6.
95. Yokokawa, J., et al., *Enhanced functionality of CD4+CD25(high)FoxP3+ regulatory T cells in the peripheral blood of patients with prostate cancer.* Clin Cancer Res, 2008. **14**(4): p. 1032-40.
96. Gasparoto, T.H., et al., *Patients with oral squamous cell carcinoma are characterized by increased frequency of suppressive regulatory T cells in the blood and tumor microenvironment.* Cancer Immunol Immunother, 2010. **59**(6): p. 819-28.
97. Munn, D.H., et al., *Potential regulatory function of human dendritic cells expressing indoleamine 2,3-dioxygenase.* Science, 2002. **297**(5588): p. 1867-70.
98. Grinstaff, M.W. and K.S. Suslick, *Air-filled proteinaceous microbubbles: synthesis of an echo-contrast agent.* Proc Natl Acad Sci U S A, 1991. **88**(17): p. 7708-10.
99. Lee, M., et al., *Stabilization and fabrication of microbubbles: applications for medical purposes and functional materials.* Soft Matter, 2015. **11**(11): p. 2067-79.
100. !!! INVALID CITATION !!! [80-82].
101. Apfel, R.E. and C.K. Holland, *Gauging the likelihood of cavitation from short-pulse, low-duty cycle diagnostic ultrasound.* Ultrasound Med Biol, 1991. **17**(2): p. 179-85.
102. Fan, Z., D. Chen, and C.X. Deng, *Characterization of the dynamic activities of a population of microbubbles driven by pulsed ultrasound exposure in sonoporation.* Ultrasound Med Biol, 2014. **40**(6): p. 1260-72.
103. He, C. and J. Chen, *Study of interactions between cells and microbubbles in high speed centrifugation field for biomolecule delivery.* Conf Proc IEEE Eng Med Biol Soc, 2014. **2014**: p. 2932-5.
104. Fan, Z., R.E. Kumon, and C.X. Deng, *Mechanisms of microbubble-facilitated sonoporation for drug and gene delivery.* Ther Deliv, 2014. **5**(4): p. 467-86.
105. Yoon, Y.I., et al., *Ultrasound-mediated gene and drug delivery using a microbubble-liposome particle system.* Theranostics, 2014. **4**(11): p. 1133-44.
106. Liu, H.L., et al., *Low-pressure pulsed focused ultrasound with microbubbles promotes an anticancer immunological response.* J Transl Med, 2012. **10**: p. 221.
107. Yu, F.T., et al., *Low Intensity Ultrasound Mediated Liposomal Doxorubicin Delivery Using Polymer Microbubbles.* Mol Pharm, 2016. **13**(1): p. 55-64.
108. Li, S.D. and L. Huang, *Nanoparticles evading the reticuloendothelial system: role of the supported bilayer.* Biochim Biophys Acta, 2009. **1788**(10): p. 2259-66.
109. Oerlemans, C., et al., *Evidence for a new mechanism behind HIFU-triggered release from liposomes.* J Control Release, 2013. **168**(3): p. 327-33.
110. Wallace, N. and S.P. Wrenn, *Ultrasound triggered drug delivery with liposomal nested microbubbles.* Ultrasonics, 2015. **63**: p. 31-8.
111. Choi, J.J., et al., *Non-invasive and real-time passive acoustic mapping of ultrasound-mediated drug delivery.* Phys Med Biol, 2014. **59**(17): p. 4861-77.

112. Radhakrishnan, K., et al., *Relationship between cavitation and loss of echogenicity from ultrasound contrast agents.* Phys Med Biol, 2013. **58**(18): p. 6541-63.
113. Domenici, F., et al., *Ultrasound well below the intensity threshold of cavitation can promote efficient uptake of small drug model molecules in fibroblast cells.* Drug Deliv, 2013. **20**(7): p. 285-95.
114. Tachibana, K., et al., *Induction of cell-membrane porosity by ultrasound.* Lancet, 1999. **353**(9162): p. 1409.
115. Lorelius, L.E., et al., *Enhanced drug retention in VX2 tumors by use of degradable starch microspheres.* Invest Radiol, 1984. **19**(3): p. 212-5.
116. Sirsi, S. and M. Borden, *Microbubble Compositions, Properties and Biomedical Applications.* Bubble Sci Eng Technol, 2009. **1**(1-2): p. 3-17.
117. Chapelon, J.Y., et al., *In vivo effects of high-intensity ultrasound on prostatic adenocarcinoma Dunning R3327.* Cancer Res, 1992. **52**(22): p. 6353-7.
118. Hu, Z., et al., *Investigation of HIFU-induced anti-tumor immunity in a murine tumor model.* J Transl Med, 2007. **5**: p. 34.
119. Chida, S., et al., *Infiltration by macrophages and lymphocytes in transplantable mouse sarcoma after irradiation with high-intensity focused ultrasound.* Anticancer Res, 2009. **29**(10): p. 3877-82.
120. Deng, J., et al., *Dendritic cells loaded with ultrasound-ablated tumour induce in vivo specific antitumour immune responses.* Ultrasound Med Biol, 2010. **36**(3): p. 441-8.
121. Huang, X., et al., *M-HIFU inhibits tumor growth, suppresses STAT3 activity and enhances tumor specific immunity in a transplant tumor model of prostate cancer.* PLoS One, 2012. **7**(7): p. e41632.
122. Xia, J.Z., et al., *High-intensity focused ultrasound tumor ablation activates autologous tumor-specific cytotoxic T lymphocytes.* Ultrasound Med Biol, 2012. **38**(8): p. 1363-71.
123. Bandyopadhyay, S., et al., *Low-Intensity Focused Ultrasound Induces Reversal of Tumor-Induced T Cell Tolerance and Prevents Immune Escape.* J Immunol, 2016. **196**(4): p. 1964-76.
124. Skalina, K.A., et al., *Low Intensity Focused Ultrasound (LOFU)-mediated Acoustic Immune Priming and Ablative Radiation Therapy for in situ Tumor Vaccines.* Sci Rep, 2019. **9**(1): p. 15516.
125. Aydin, O., et al., *The Proteomic Effects of Pulsed Focused Ultrasound on Tumor Microenvironments of Murine Melanoma and Breast Cancer Models.* Ultrasound Med Biol, 2019. **45**(12): p. 3232-3245.
126. Cohen, G., et al., *The Impact of Focused Ultrasound in Two Tumor Models: Temporal Alterations in the Natural History on Tumor Microenvironment and Immune Cell Response.* Cancers (Basel), 2020. **12**(2).
127. Xu, J.S., et al., *Synthesizing and binding dual-mode poly (lactic-co-glycolic acid) (PLGA) nanobubbles for cancer targeting and imaging.* Biomaterials, 2010. **31**(7): p. 1716-22.
128. Lin, C.Y., et al., *Effects of focused ultrasound and microbubbles on the vascular permeability of nanoparticles delivered into mouse tumors.* Ultrasound Med Biol, 2010. **36**(9): p. 1460-9.
129. Lin, C.Y., et al., *Enhancement of focused ultrasound with microbubbles on the treatments of anticancer nanodrug in mouse tumors.* Nanomedicine, 2012. **8**(6): p. 900-7.
130. Wu, H., et al., *Acoustic characterization and pharmacokinetic analyses of new nanobubble ultrasound contrast agents.* Ultrasound Med Biol, 2013. **39**(11): p. 2137-46.

131. Zhang, X., et al., *An experimental research into endostatin microbubble combined with focused ultrasound for anti-tumor angiogenesis in colon cancer.* Gastroenterol Rep (Oxf), 2014. **2**(1): p. 44-53.
132. Sta Maria, N.S., et al., *Low Dose Focused Ultrasound Induces Enhanced Tumor Accumulation of Natural Killer Cells.* PLoS One, 2015. **10**(11): p. e0142767.
133. Perera, R.H., et al., *Improving performance of nanoscale ultrasound contrast agents using N,N-diethylacrylamide stabilization.* Nanomedicine, 2017. **13**(1): p. 59-67.
134. Bulner, S., et al., *Enhancing Checkpoint Inhibitor Therapy with Ultrasound Stimulated Microbubbles.* Ultrasound Med Biol, 2019. **45**(2): p. 500-512.
135. Fernando, R., et al., *MRI-guided monitoring of thermal dose and targeted drug delivery for cancer therapy.* Pharm Res, 2013. **30**(11): p. 2709-17.
136. Sha, X., et al., *Effect of phospholipid composition on pharmacokinetics and biodistribution of epirubicin liposomes.* J Liposome Res, 2012. **22**(1): p. 80-8.
137. Soloman, R. and A.A. Gabizon, *Clinical pharmacology of liposomal anthracyclines: focus on pegylated liposomal Doxorubicin.* Clin Lymphoma Myeloma, 2008. **8**(1): p. 21-32.
138. Chen, H. and J.H. Hwang, *Ultrasound-targeted microbubble destruction for chemotherapeutic drug delivery to solid tumors.* J Ther Ultrasound, 2013. **1**: p. 10.
139. de Smet, M., et al., *Magnetic resonance imaging of high intensity focused ultrasound mediated drug delivery from temperature-sensitive liposomes: an in vivo proof-of-concept study.* J Control Release, 2011. **150**(1): p. 102-10.
140. Frenkel, V., et al., *Delivery of liposomal doxorubicin (Doxil) in a breast cancer tumor model: investigation of potential enhancement by pulsed-high intensity focused ultrasound exposure.* Acad Radiol, 2006. **13**(4): p. 469-79.
141. Staruch, R., R. Chopra, and K. Hynynen, *Localised drug release using MRI-controlled focused ultrasound hyperthermia.* Int J Hyperthermia, 2011. **27**(2): p. 156-71.
142. Ibsen, S., C.E. Schutt, and S. Esener, *Microbubble-mediated ultrasound therapy: a review of its potential in cancer treatment.* Drug Des Devel Ther, 2013. **7**: p. 375-88.
143. Lin, P.S., et al., *Effect of tumour necrosis factor, heat, and radiation on the viability and microfilament organization in cultured endothelial cells.* Int J Hyperthermia, 1992. **8**(5): p. 667-77.
144. Tillander, M., et al., *High intensity focused ultrasound induced in vivo large volume hyperthermia under 3D MRI temperature control.* Med Phys, 2016. **43**(3): p. 1539-49.
145. Rapoport, N., et al., *Ultrasound-mediated tumor imaging and nanotherapy using drug loaded, block copolymer stabilized perfluorocarbon nanoemulsions.* J Control Release, 2011. **153**(1): p. 4-15.
146. Lin, C.Y. and W.G. Pitt, *Acoustic droplet vaporization in biology and medicine.* Biomed Res Int, 2013. **2013**: p. 404361.
147. Chen, C.C. and M.A. Borden, *The role of poly(ethylene glycol) brush architecture in complement activation on targeted microbubble surfaces.* Biomaterials, 2011. **32**(27): p. 6579-87.
148. Ibsen, S., et al., *A novel nested liposome drug delivery vehicle capable of ultrasound triggered release of its payload.* J Control Release, 2011. **155**(3): p. 358-66.
149. Radhakrishnan, K., et al., *Stability of echogenic liposomes as a blood pool ultrasound contrast agent in a physiologic flow phantom.* Ultrasound Med Biol, 2012. **38**(11): p. 1970-81.

150. Sen, A., et al., *Mild elevation of body temperature reduces tumor interstitial fluid pressure and hypoxia and enhances efficacy of radiotherapy in murine tumor models.* Cancer Res, 2011. **71**(11): p. 3872-80.
151. Chen, Q., et al., *Targeting tumor microvessels using doxorubicin encapsulated in a novel thermosensitive liposome.* Mol Cancer Ther, 2004. **3**(10): p. 1311-7.
152. Gasselhuber, A., et al., *Mathematical spatio-temporal model of drug delivery from low temperature sensitive liposomes during radiofrequency tumour ablation.* Int J Hyperthermia, 2010. **26**(5): p. 499-513.
153. Fernando, R., et al., *Hyperthermia sensitization and proton beam triggered liposomal drug release for targeted tumor therapy.* Pharm Res, 2014. **31**(11): p. 3120-6.
154. Senavirathna, L.K., et al., *Tumor Spheroids as an in vitro model for determining the therapeutic response to proton beam radiotherapy and thermally sensitive nanocarriers.* Theranostics, 2013. **3**(9): p. 687-91.
155. Yuh, E.L., et al., *Delivery of systemic chemotherapeutic agent to tumors by using focused ultrasound: study in a murine model.* Radiology, 2005. **234**(2): p. 431-7.
156. Fokong, S., et al., *Image-guided, targeted and triggered drug delivery to tumors using polymer-based microbubbles.* J Control Release, 2012. **163**(1): p. 75-81.
157. Hernot, S. and A.L. Klibanov, *Microbubbles in ultrasound-triggered drug and gene delivery.* Adv Drug Deliv Rev, 2008. **60**(10): p. 1153-66.
158. Javadi, M., et al., *Encapsulating nanoemulsions inside eLiposomes for ultrasonic drug delivery.* Langmuir, 2012. **28**(41): p. 14720-9.
159. Theek, B., et al., *Sonoporation enhances liposome accumulation and penetration in tumors with low EPR.* J Control Release, 2016. **231**: p. 77-85.
160. Koning, G.A., et al., *Hyperthermia and thermosensitive liposomes for improved delivery of chemotherapeutic drugs to solid tumors.* Pharm Res, 2010. **27**(8): p. 1750-4.
161. Landon, C.D., et al., *Nanoscale Drug Delivery and Hyperthermia: The Materials Design and Preclinical and Clinical Testing of Low Temperature-Sensitive Liposomes Used in Combination with Mild Hyperthermia in the Treatment of Local Cancer.* Open Nanomed J, 2011. **3**: p. 38-64.
162. Zhu, M., et al., *Treatment of murine tumors using acoustic droplet vaporization-enhanced high intensity focused ultrasound.* Phys Med Biol, 2013. **58**(17): p. 6179-91.
163. Giustetto, P., et al., *Heat enhances gas delivery and acoustic attenuation in CO(2) filled microbubbles.* Conf Proc IEEE Eng Med Biol Soc, 2008. **2008**: p. 2306-9.
164. Ektate, K., et al., *Motion Compensated Ultrasound Imaging Allows Thermometry and Image Guided Drug Delivery Monitoring from Echogenic Liposomes.* Theranostics, 2016. **6**(11): p. 1963-74.
165. Eetezadi, S., et al., *Effects of Doxorubicin Delivery Systems and Mild Hyperthermia on Tissue Penetration in 3D Cell Culture Models of Ovarian Cancer Residual Disease.* Mol Pharm, 2015. **12**(11): p. 3973-85.
166. Endo-Takahashi, Y., et al., *pDNA-loaded Bubble liposomes as potential ultrasound imaging and gene delivery agents.* Biomaterials, 2013. **34**(11): p. 2807-13.
167. Endo-Takahashi, Y., et al., *Systemic delivery of miR-126 by miRNA-loaded Bubble liposomes for the treatment of hindlimb ischemia.* Sci Rep, 2014. **4**: p. 3883.
168. Suzuki, R., et al., *Effective gene delivery with liposomal bubbles and ultrasound as novel non-viral system.* J Drug Target, 2007. **15**(7-8): p. 531-7.

169. Kato, S., S. Mori, and T. Kodama, *A Novel Treatment Method for Lymph Node Metastasis Using a Lymphatic Drug Delivery System with Nano/Microbubbles and Ultrasound.* J Cancer, 2015. **6**(12): p. 1282-94.
170. Ho, Y.J., Y.C. Chang, and C.K. Yeh, *Improving Nanoparticle Penetration in Tumors by Vascular Disruption with Acoustic Droplet Vaporization.* Theranostics, 2016. **6**(3): p. 392-403.
171. Bae, Y.H. and K. Park, *Targeted drug delivery to tumors: myths, reality and possibility.* J Control Release, 2011. **153**(3): p. 198-205.
172. Yuan, F., et al., *Vascular permeability in a human tumor xenograft: molecular size dependence and cutoff size.* Cancer Res, 1995. **55**(17): p. 3752-6.
173. Yuan, F., et al., *Microvascular permeability and interstitial penetration of sterically stabilized (stealth) liposomes in a human tumor xenograft.* Cancer Res, 1994. **54**(13): p. 3352-6.
174. Prabhakar, U., et al., *Challenges and key considerations of the enhanced permeability and retention effect for nanomedicine drug delivery in oncology.* Cancer Res, 2013. **73**(8): p. 2412-7.
175. Sciani, J.M., et al., *An unexpected cell-penetrating peptide from Bothrops jararaca venom identified through a novel size exclusion chromatography screening.* J Pept Sci, 2017. **23**(1): p. 68-76.
176. Sugahara, K.N., et al., *Coadministration of a tumor-penetrating peptide enhances the efficacy of cancer drugs.* Science, 2010. **328**(5981): p. 1031-5.
177. Schmithals, C., et al., *Improving Drug Penetrability with iRGD Leverages the Therapeutic Response to Sorafenib and Doxorubicin in Hepatocellular Carcinoma.* Cancer Res, 2015. **75**(15): p. 3147-54.
178. Wang, K., et al., *Tumor penetrability and anti-angiogenesis using iRGD-mediated delivery of doxorubicin-polymer conjugates.* Biomaterials, 2014. **35**(30): p. 8735-47.
179. Zhou, W., et al., *Cancer-secreted miR-105 destroys vascular endothelial barriers to promote metastasis.* Cancer Cell, 2014. **25**(4): p. 501-15.
180. Lum, B.L., et al., *Molecular targets in oncology: implications of the multidrug resistance gene.* Pharmacotherapy, 1993. **13**(2): p. 88-109.
181. To, K.K., et al., *Vatalanib sensitizes ABCB1 and ABCG2-overexpressing multidrug resistant colon cancer cells to chemotherapy under hypoxia.* Biochem Pharmacol, 2015. **97**(1): p. 27-37.
182. Brangi, M., et al., *Camptothecin resistance: role of the ATP-binding cassette (ABC), mitoxantrone-resistance half-transporter (MXR), and potential for glucuronidation in MXR-expressing cells.* Cancer Res, 1999. **59**(23): p. 5938-46.
183. Hsu, H.H., et al., *Oxaliplatin resistance in colorectal cancer cells is mediated via activation of ABCG2 to alleviate ER stress induced apoptosis.* J Cell Physiol, 2018. **233**(7): p. 5458-5467.
184. Wahab, S.M.R., et al., *The Identifications and Clinical Implications of Cancer Stem Cells in Colorectal Cancer.* Clin Colorectal Cancer, 2017. **16**(2): p. 93-102.
185. Deng, Y., et al., *ALDH1 is an independent prognostic factor for patients with stages II-III rectal cancer after receiving radiochemotherapy.* Br J Cancer, 2014. **110**(2): p. 430-4.
186. Chu, D., et al., *Notch2 expression is decreased in colorectal cancer and related to tumor differentiation status.* Ann Surg Oncol, 2009. **16**(12): p. 3259-66.

187. Manzoor, A.A., et al., *Overcoming limitations in nanoparticle drug delivery: triggered, intravascular release to improve drug penetration into tumors.* Cancer Res, 2012. **72**(21): p. 5566-75.
188. Wu, N.Z., et al., *Simultaneous measurement of liposome extravasation and content release in tumors.* Microcirculation, 1997. **4**(1): p. 83-101.
189. Zhan, W. and X.Y. Xu, *A mathematical model for thermosensitive liposomal delivery of Doxorubicin to solid tumour.* J Drug Deliv, 2013. **2013**: p. 172529.
190. Kopechek, J.A., et al., *The impact of bubbles on measurement of drug release from echogenic liposomes.* Ultrason Sonochem, 2013. **20**(4): p. 1121-30.
191. VanOsdol, J., et al., *Sequential HIFU heating and nanobubble encapsulation provide efficient drug penetration from stealth and temperature sensitive liposomes in colon cancer.* J Control Release, 2017. **247**: p. 55-63.
192. Muller-Klieser, W. and P. Vaupel, *Effect of hyperthermia on tumor blood flow.* Biorheology, 1984. **21**(4): p. 529-38.
193. Song, C.W., et al., *Implications of increased tumor blood flow and oxygenation caused by mild temperature hyperthermia in tumor treatment.* Int J Hyperthermia, 2005. **21**(8): p. 761-7.
194. Parker, K.J., *Effects of heat conduction and sample size on ultrasonic absorption measurements.* J Acoust Soc Am, 1985. **77**(2): p. 719-25.
195. Salomir, R., et al., *Local hyperthermia with MR-guided focused ultrasound: spiral trajectory of the focal point optimized for temperature uniformity in the target region.* J Magn Reson Imaging, 2000. **12**(4): p. 571-83.
196. Speth, P.A., Q.G. van Hoesel, and C. Haanen, *Clinical pharmacokinetics of doxorubicin.* Clin Pharmacokinet, 1988. **15**(1): p. 15-31.
197. Akashi, Y., et al., *Anticancer effects of gemcitabine are enhanced by co-administered iRGD peptide in murine pancreatic cancer models that overexpressed neuropilin-1.* Br J Cancer, 2014. **110**(6): p. 1481-7.
198. Chen, K.J., et al., *Hyperthermia-mediated local drug delivery by a bubble-generating liposomal system for tumor-specific chemotherapy.* ACS Nano, 2014. **8**(5): p. 5105-15.
199. Yang, W., et al., *Thermosensitive liposomal doxorubicin plus radiofrequency ablation increased tumor destruction and improved survival in patients with medium and large hepatocellular carcinoma: A randomized, double-blinded, dummy-controlled clinical trial in a single center.* J Cancer Res Ther, 2019. **15**(4): p. 773-783.
200. Li, L., et al., *Mild hyperthermia triggered doxorubicin release from optimized stealth thermosensitive liposomes improves intratumoral drug delivery and efficacy.* J Control Release, 2013. **168**(2): p. 142-50.
201. Zhang, H. and L.W. Fu, *[Multidrug resistance-associated proteins and their roles in multidrug resistance].* Yao Xue Xue Bao, 2011. **46**(5): p. 479-86.
202. Li, W., et al., *Overcoming ABC transporter-mediated multidrug resistance: Molecular mechanisms and novel therapeutic drug strategies.* Drug Resist Updat, 2016. **27**: p. 14-29.
203. Lai, H.T., et al., *GATA6 enhances the stemness of human colon cancer cells by creating a metabolic symbiosis through upregulating LRH-1 expression.* Mol Oncol, 2020.
204. Liu, H., et al., *GATA6 suppresses migration and metastasis by regulating the miR-520b/CREB1 axis in gastric cancer.* Cell Death Dis, 2019. **10**(2): p. 35.

205. Mosley, R.L., D. Styre, and J.R. Klein, *Immune recognition by cytotoxic T lymphocytes of minor histocompatibility antigens expressed on a murine colon carcinoma line.* Cell Immunol, 1989. **122**(1): p. 200-7.
206. Gri, G., et al., *Antitumor effect of interleukin (IL)-12 in the absence of endogenous IFN-gamma: a role for intrinsic tumor immunogenicity and IL-15.* Cancer Res, 2002. **62**(15): p. 4390-7.
207. Rios-Doria, J., et al., *Doxil synergizes with cancer immunotherapies to enhance antitumor responses in syngeneic mouse models.* Neoplasia, 2015. **17**(8): p. 661-70.
208. Mattarollo, S.R., et al., *Pivotal role of innate and adaptive immunity in anthracycline chemotherapy of established tumors.* Cancer Res, 2011. **71**(14): p. 4809-20.
209. Zhu, S., et al., *Doxorubicin directs the accumulation of interleukin-12 induced IFN gamma into tumors for enhancing STAT1 dependent antitumor effect.* Clin Cancer Res, 2007. **13**(14): p. 4252-60.
210. Ma, Y., et al., *Contribution of IL-17-producing gamma delta T cells to the efficacy of anticancer chemotherapy.* J Exp Med, 2011. **208**(3): p. 491-503.
211. Apetoh, L., et al., *Immunogenicity of anthracyclines: moving towards more personalized medicine.* Trends Mol Med, 2008. **14**(4): p. 141-51.
212. Slovin, S., *Chemotherapy and immunotherapy combination in advanced prostate cancer.* Clin Adv Hematol Oncol, 2012. **10**(2): p. 90-100.
213. Proietti, E., et al., *Exploitation of the propulsive force of chemotherapy for improving the response to cancer immunotherapy.* Mol Oncol, 2012. **6**(1): p. 1-14.
214. Berdeja, J.G., *Immunotherapy of lymphoma: update and review of the literature.* Curr Opin Oncol, 2003. **15**(5): p. 363-70.
215. Adams, S., et al., *Current Landscape of Immunotherapy in Breast Cancer: A Review.* JAMA Oncol, 2019.
216. Bellmunt, J., T. Powles, and N.J. Vogelzang, *A review on the evolution of PD-1/PD-L1 immunotherapy for bladder cancer: The future is now.* Cancer Treat Rev, 2017. **54**: p. 58-67.
217. Montie, J.E., et al., *A critical review of immunotherapy of disseminated renal adenocarcinoma.* J Surg Oncol, 1982. **21**(1): p. 5-8.
218. Panagi, M., et al., *TGF-beta inhibition combined with cytotoxic nanomedicine normalizes triple negative breast cancer microenvironment towards anti-tumor immunity.* Theranostics, 2020. **10**(4): p. 1910-1922.
219. Makkouk, A., et al., *Three steps to breaking immune tolerance to lymphoma: a microparticle approach.* Cancer Immunol Res, 2015. **3**(4): p. 389-98.
220. Wang, W., *Preclinical Evaluation of Chimeric Antigen Receptor-Modified T Cells Specific to Epithelial Cell Adhesion Molecule for Treating Colorectal Cancer.* Hum Gene Ther, 2019.
221. Chmielewski, M., et al., *IL-12 release by engineered T cells expressing chimeric antigen receptors can effectively Muster an antigen-independent macrophage response on tumor cells that have shut down tumor antigen expression.* Cancer Res, 2011. **71**(17): p. 5697-706.
222. Obeid, M., et al., *Calreticulin exposure dictates the immunogenicity of cancer cell death.* Nat Med, 2007. **13**(1): p. 54-61.

223. Chen, T., et al., *Heat shock protein 70, released from heat-stressed tumor cells, initiates antitumor immunity by inducing tumor cell chemokine production and activating dendritic cells via TLR4 pathway.* J Immunol, 2009. **182**(3): p. 1449-59.
224. Nagarsekar, A., J.D. Hasday, and I.S. Singh, *CXC chemokines: a new family of heat-shock proteins?* Immunol Invest, 2005. **34**(3): p. 381-98.
225. Chen, Q., et al., *Fever-range thermal stress promotes lymphocyte trafficking across high endothelial venules via an interleukin 6 trans-signaling mechanism.* Nat Immunol, 2006. **7**(12): p. 1299-308.
226. Hu, Z., et al., *Release of endogenous danger signals from HIFU-treated tumor cells and their stimulatory effects on APCs.* Biochem Biophys Res Commun, 2005. **335**(1): p. 124-31.
227. Wu, F., L. Zhou, and W.R. Chen, *Host antitumour immune responses to HIFU ablation.* Int J Hyperthermia, 2007. **23**(2): p. 165-71.
228. Huang, F.Y., et al., *Induction of enhanced immunogenic cell death through ultrasound-controlled release of doxorubicin by liposome-microbubble complexes.* Oncoimmunology, 2018. **7**(7): p. e1446720.
229. Zamarin, D., et al., *Localized oncolytic virotherapy overcomes systemic tumor resistance to immune checkpoint blockade immunotherapy.* Sci Transl Med, 2014. **6**(226): p. 226ra32.
230. Casares, N., et al., *Caspase-dependent immunogenicity of doxorubicin-induced tumor cell death.* J Exp Med, 2005. **202**(12): p. 1691-701.
231. Jang, H.J., et al., *Current and Future Clinical Applications of High-Intensity Focused Ultrasound (HIFU) for Pancreatic Cancer.* Gut Liver, 2010. **4 Suppl 1**: p. S57-61.
232. Zhou, Q., et al., *Changes in circulating immunosuppressive cytokine levels of cancer patients after high intensity focused ultrasound treatment.* Ultrasound Med Biol, 2008. **34**(1): p. 81-7.
233. Liu, C., et al., *A Spectral Fiedler Field-based Contrast Platform for Imaging of Nanoparticles in Colon Tumor.* Sci Rep, 2018. **8**(1): p. 11390.

VITA

Joshua Paul VanOsdol

Candidate for the Degree of

Doctor of Philosophy/Education

Thesis: ROLE OF BUBBLE-BASED NANOSYSTEMS IN CHEMO-IMMUNOTHERAPY OF COLON CANCER

Major Field: Comparative Biomedical Sciences: Oncology

Biographical:

Education:

Completed the requirements for the Doctor of Philosophy in Comparative Biomedical Sciences at Oklahoma State University, Stillwater, Oklahoma in May, 2020.

Completed the requirements for the Bachelor of Science at Fairmont State University, Fairmont, West Virginia/United States in 2012.

Experience:

Intern/part time researcher at Fairmont State University (2012-2013) and Oklahoma State University (2013-2014)

Graduate teaching associate for Infectious Diseases I, Infectious Diseases II, and Immunology (Aug 2014-May2019)

Professional Memberships:

Society for Thermal Oncology